The role of a disintegrin and metalloprotease 10 in the liver

Dissertation

zur Erlangung des Doktorgrades

der Mathematisch-Naturwissenschaftlichen Fakultät

der Christian-Albrechts-Universität

zu Kiel

vorgelegt von

Miryam Müller

Kiel 2015

Erster Gutachter:	Prof. Dr. Stefan Rose-John
Zweiter Gutachter:	Prof. Dr. Thomas Roeder
Tag der mündlichen Prüfung:	14.09.2015
Zum Druck genehmigt:	14.09.2015

gez. Prof. Dr. Wolfgang J. Duschl, Dekan

Eidesstattliche Erklärung

Ich erkläre hiermit, dass die nachfolgende Abhandlung eigenständig und unter Einhaltung der Regeln der guten wissenschaftlichen Praxis der Deutschen Forschungsgemeinschaft verfasst wurde. Nur die angegeben Quellen und Hilfen wurden verwendet. Zitate, wörtlich oder sinngemäß, wurden als solche gekennzeichnet.

Die Arbeit wurde weder ganz noch zum Teil im Rahmen eines Prüfungsverfahrens vorgelegt.

Ich versichere, dass ich bis zum heutigen Tage weder an dieser, noch an einer anderen Hochschule ein Promotionsverfahren endgültig nicht bestanden habe oder mir ein akademischer Titel aberkannt wurde.

Kiel, Juni 2015 Miryam Müller

Abstract

Proteolytic release of ectodomains at the cell membrane, termed ectodomain shedding, is an irreversible post-translational mechanism to regulate protein function. Members of the a disintegrin and metalloprotease (ADAM) family are key enzymes in shedding of receptors and ligands and, hence, influence cell signaling.

Conditional deletion of ADAM10 in murine tissues, such as brain or skin, indicates an essential role for the protease in both organ development and tissue integrity. However, the function of ADAM10 in liver physiology *in vivo* is largely unknown.

We show that in mice with a liver specific deletion of ADAM10 tissue homeostasis in the liver is impaired.

Development of the biliary tree, which is dependent on the ADAM10 substrate Notch, was not altered in our mice. Still, mice lacking ADAM10 in the liver developed spontaneous necrosis to various degrees. Interestingly, the liver injury did not cause an increase in pro-inflammatory cytokines. Despite regeneration of the necrotic areas, we observed an accumulation of proliferating liver progenitor cells and a persistent activation of hepatic stellate cells leading to a striking liver fibrosis. We detected, in accordance with these findings, enhanced liver progenitor cell mitogen signaling in a liver progenitor cell line in the absence of ADAM10 activity.

Our results demonstrate that ADAM10-mediated proteolytic processing seems to be essential in the termination of liver progenitor cell-driven regenerative processes that, if deregulated, lead to chronic liver disease. They furthermore underline the importance of irreversible post-translational modifications for the maintenance of tissue homeostasis.

Zusammenfassung

Die proteolytische Abspaltung von extrazellulären Domänen an der Zelloberfläche, auch als *Ectodomain-Shedding* bezeichnet, ist ein unumkehrbarer post-translationeller Mechanismus zur Regulation der Proteinfunktion. Mitglieder der "A disintegrin and metalloprotease" (ADAM) Familie sind für das *Ectodomain-Shedding* von vielen Rezeptoren und Liganden verantwortlich und beeinflussen so die zelluläre Kommunikation.

Durch gewebsspezifische Knock-Outs von ADAM10, in Gehirn oder Haut von Mäusen, konnte der Protease bereits eine wichtige Funktion sowohl in der Organentwicklung als auch in der Gewebsintegrität zugeordnet werden. Die *in vivo* Funktion von ADAM10 in der Leber ist jedoch größtenteils unbekannt.

Wir zeigen in dieser Studie, dass in Mäusen mit einem leberspezifischen Knock-Out von ADAM10 die Gewebsintegrität der Leber beeinträchtigt ist.

Die Entwicklung des Gallengangsystems, für die das ADAM10 Substrat Notch benötigt wird, war in unseren Mäusen nicht beeinträchtigt. Jedoch entwickelten Mäuse mit einem leberspezifischen ADAM10 Knock-Out spontane Nekrosen, die unterschiedlich stark ausgeprägt waren. Interessanterweise bewirkte der Leberschaden keine Erhöhung von entzündungsfördernden Zytokinen. Trotz Reparatur der nekrotischen Gebiete beobachteten wir eine Anhäufung von sich vermehrenden Lebervorläuferzellen und eine damit einhergehende andauernde Aktivierung von Ito-Zellen, die zu einer markanten Leberfibrose führten. In Übereinstimmung mit diesen Beobachtungen konnten wir in einer Zelllinie von Lebervorläuferzellen zeigen, dass die Hemmung der ADAM10 Aktivität zu einem erhöhten Mitogensignal führt.

Unsere Ergebnisse weisen darauf hin, dass die proteolytische Spaltung durch ADAM10 wichtig ist für die Beendung von Lebervorläuferzell-abhängiger Regeneration, die unreguliert zu chronischen Lebererkrankungen führt. Sie betonen außerdem die Bedeutung von unumkehrbaren post-translationellen Modifizierungen für die Aufrechterhaltung der Gewebsintegrität.

Index

1 Introduction

1.1 Liver

The liver has always held a fascination for mankind. In ancient Mesopotamia hepatoscopy, the art of liver augury, was practiced to get signs of the gods' intentions. The Greeks even believed the liver to be the seat of life and passion. However, since the end of the nineteenth century the liver has been in the focus of scientists for a different reason: it's enormous potential to regenerate [1]. After loss of 2/3 of the liver, regrowth of the liver to its original mass takes only 5-7 days in rodents and 8-15 days in humans. The underlying mechanisms will be discussed in more detail in chapter 1.1.2.

The liver is the largest internal organ, both in mice and men. It executes essential functions including bile production, metabolism of dietary compounds, detoxification, regulating glucose levels via glycogen storage, and contributing to blood homeostasis by secreting serum proteins and clotting factors. The liver, through regulating levels of plasma glucose and ammonia, is essential for brain function. Liver failure can therefore lead to hepatic encephalopathy and ultimately to coma [2].

1.1.1 Development, cellular architecture and function

Five cell types are predominantly found in the adult liver. Firstly, the hepatocytes that form the liver parenchymal tissue and make up the main mass of the liver. Secondly, the biliary epithelial cells also known as cholangiocytes that line the bile ducts. Furthermore there are the liver-resident macrophages, the Kupffer cells, and the hepatic stellate cells. Finally, the endothelial cells that line the blood vessels. The sinusoidal endothelial lining has a specific fenestration pattern and is separated from the hepatocytes by the space of Disse (Figure 1.3) [3].

Through fate mapping experiments the embryonic development of the liver was shown to proceed in several steps [4]. At embryonic day of gestation 9 the hepatic diverticulum is formed out of the ventral foregut endoderm. The anterior portion of the hepatic diverticulum gives rise to the hepatoblasts, bipotential progenitors that can develop into hepatocytes and cholangiocytes. Hepatoblasts express genes found in mature hepatocytes (*alb*, coding for Albumin) and genes found in mature cholangiocytes (*krt19*, coding for cytokeratin 19) as well as fetal liver genes (*afp*, coding for alpha-fetoprotein). The posterior part of

the hepatic diverticulum later on develops into the gall bladder and the extrahepatic bile ducts. At embryonic day of gestation 9.5 the liver bud is formed by hepatoblasts (see Figure 1.1).

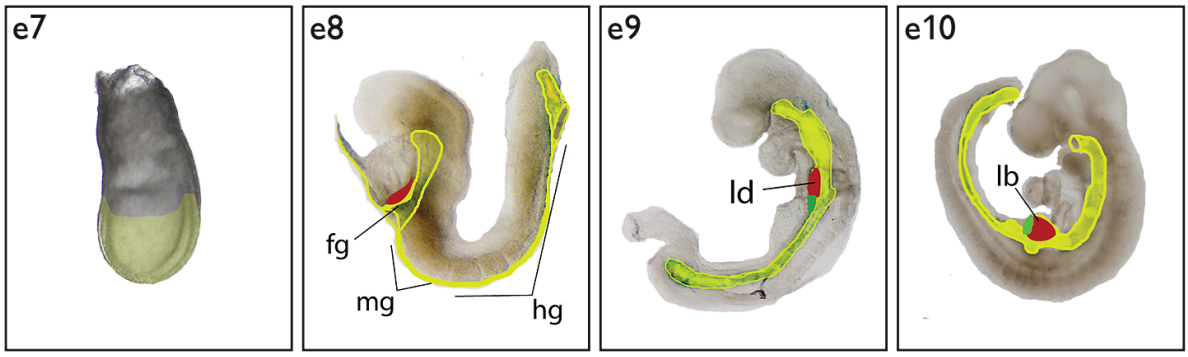

Figure 1.1: Early liver development

Depicted are early stages of murine embryo development. The endoderm is formed during gastrulation between embryonic day of gestation 6.5 - embryonic day of gestation 7.5 and starts developing into foregut (fg), midgut (mg), and hindgut (hg). At embryonic day of gestation 9 the liver diverticulum (ld) is formed from the ventral foregut and expands into the liverbud (lb) by embryonic day of gestation 10. Endoderm tissue is highlighted in yellow, the liver in red, and the gallbladder in green. e= embryonic day of gestation

Modified from [3] (reprint permitted with citation)

From embryonic day of gestation 10 to embryonic day of gestation 15 the liver experiences a growth spurt due to vascularization and colonialization by hematopoietic cells, turning the liver into the major fetal hematopoietic organ.

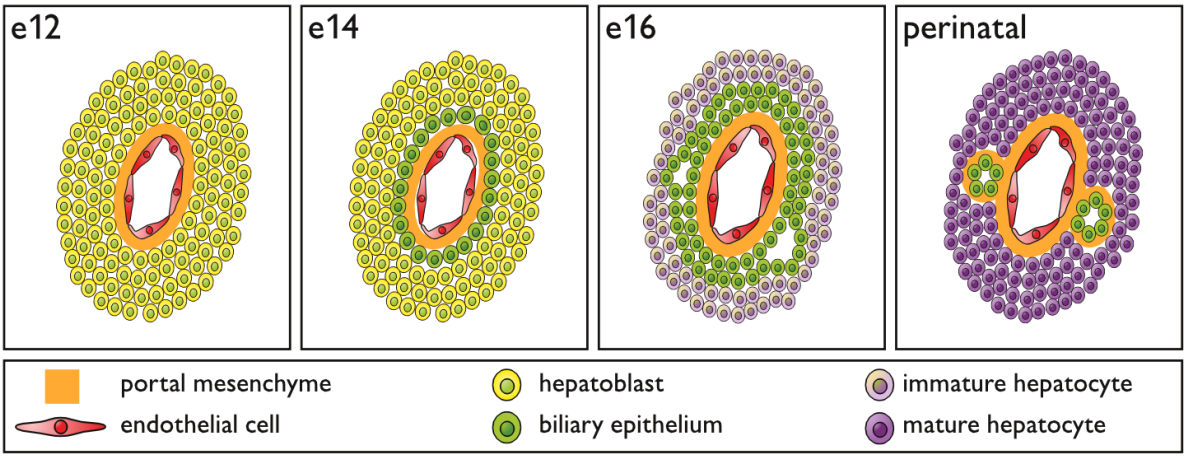

Figure 1.2: Late liver development

The schematic shows the steps of bile duct formation during development. Around embryonic day of gestation 13 hepatoblasts surrounding the portal vein mesenchyme adopt a biliary fate. This layer duplicates and by ductal plate remodeling focal dilations in the bi-layer arise. From embryonic day of gestation 17 to the perinatal period the focal dilations develop into bile ducts, that are surrounded by portal mesenchyme. The rest of the bi-layer regresses and hepatocytes in the parenchyma mature. e= embryonic day of gestation

Around embryonic day of gestation 13 gradual differentiation of the hepatoblasts begins. Hepatoblasts that are in proximity to the portal vein start transitioning into cholangiocytes whereas the majority of hepatoblasts differentiates into hepatocytes forming the parenchymal tissue. This process is also referred to as ductal plate remodeling (see Figure 1.2) [5].

Signals from the periportal mesenchyme induce this development. Evidently, expression of Notch and the Notch ligand Jagged-1 are important for proper bile duct formation. Activation of Notch2 on hepatoblasts through Jagged-1, expressed on mesenchymal cells, is required for cholangiocyte differentiation [6]. Mice deficient for Notch2 or Notch1 and Notch2 show an altered three-dimensional structure of the biliary tree with diminished bile ducts. Over-expression of Notch1 intracellular domain leads to a hyper-branching of the biliary network and to formation of cholangiocarcinoma [7, 8]. Paucity of bile ducts can also be observed in human patients suffering from Alagille syndrome. These patients have autosomal dominant mutations in either *notch* or *jag1* and therefore fail to correctly resolve the ductal plate during development [9].

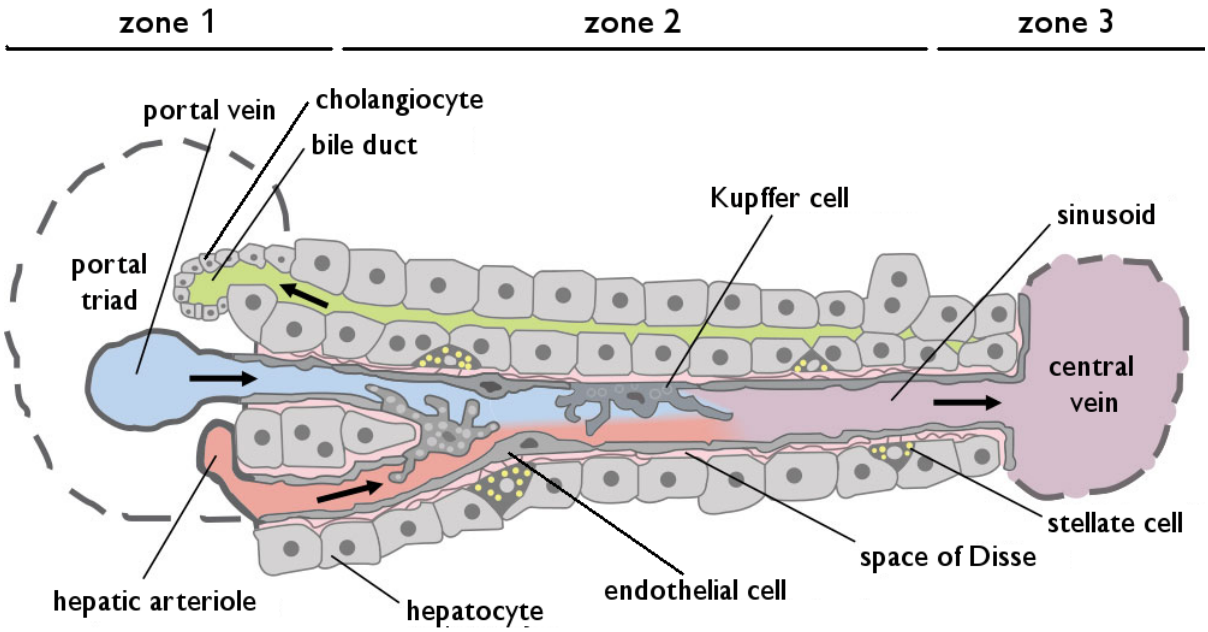

Figure 1.3: Schematic of adult liver structure and zoning

Depicted are all 5 major liver cell types: hepatocytes, cholangiocytes, Kupffer cells, stellate cells, and endothelial cells. Additionally, central features like portal triad, central vein, or space of Disse are indicated. Division in zones is based on a metabolic perspective.

Modified from [10] (open source)

Stellate cells, Kupffer cells and the endothelial cells derive from the mesoderm and will not be discussed here in detail [3].

The liver can be separated in three zones. Zone 1 contains the portal triad consisting of portal vein, hepatic artery and bile duct. The central vein lies in zone 3. The liver parenchyma in between zone 1 and 3 is denominated zone 2 (Figure 1.3). The portal triad is located in the middle of hepatic plates, cell sheets of hepatocytes, that are divided by sinusoid spaces connected to blood vessels. Via the basal side the hepatocytes take up metabolites and toxins from the blood in the sinusoids. On the apical side the hepatocytes secrete primary bile acids into bile canaliculi, small grooves in the cell surface, from which it flows into the canals of Hering and finally via the bile ducts to the gall bladder [3].

1.1.2 Liver cell death and liver tissue homeostasis

The liver, like most organs, has a steady turnover of cells which is, however, comparably low. Only 0.05% of hepatocytes in healthy individuals are, at any given time, undergoing apoptosis. Apoptosis is mainly occurring in zone 3, indicating an aging of hepatocytes from zone 1 to zone 3 [11]. However, cell death in the liver can occur massively through toxin-induced injury or bacterial or parasitic infections. Liver damage is also mediated through lifestyle-dependent chronic diseases like alcoholic liver disease or non-alcoholic fatty liver disease. Classically, cell death is divided into necrosis and apoptosis, but also other forms of cell death are found like necroptosis and autophagy [12]. Necrotic cell death in the liver is found mostly following toxic-induced liver injury [13]. But often necrosis and apoptosis occur side by side in liver disease as described for alcoholic liver disease [14].

Several serum proteins serve as biomarkers to detect liver damage and cell death. The most common biomarker for diagnosis of liver disease is alanine transaminase (formerly known as glutamate-pyruvate transaminase). Alanine transaminase is highly specific for hepatocellular damage. Alanine transaminase levels in the blood are upregulated upon acute (500 – 20 000 U/l, mice and men) or chronic (120 – 500 U/l, mice and men) liver damage and can be correlated to chronic disease progression. However, in cirrhotic patients alanine transaminases are not necessarily upregulated. Aspartate aminotransferase (formerly known as glutamic oxaloacetic transaminase) can be used as a serum marker for liver injury but lacks specificity due to expression in other tissues like heart and kidney. [15]. Levels of

alkaline phosphatase can be used to detect cholestatic liver damage found for example in patients with primary biliary cirrhosis [16].

For liver regeneration to progress smoothly a coordinated response of immune cells, including macrophages, T-cells, and eosinophils, is required. Macrophages are recruited to injured hepatocytes and initiate the inflammatory response through release of pro-inflammatory cytokines like tumor necrosis factor α or interleukin-6. Macrophages can act pro-fibrotically by activating hepatic stellate cells but also help resolve fibrosis by inducing apoptosis in hepatic stellate cells and secreting matrix metalloproteases that degrade the extracellular matrix [17, 18]. Liver regeneration is strongly disabled in diseases like advanced cirrhosis or hepatitis leading to liver failure with fatal consequences. The only lasting clinical treatment is organ transplantation. Due to donor sparsity and procedural complication alternatives to transplantation are desperately needed.

Mechanisms of liver regeneration are dependent on the damage and are considered mutually exclusive. The primary mode is through replication of existing mature hepatocytes by inducing mitosis and increasing cell volume of present hepatocytes. In animal models this situation can be mimicked by partial hepatectomy. This process is tightly regulated and leads to restoration of the original liver mass [19]. However, in cases of severe fibrosis in chronic sickness, when the regenerative potential of hepatocytes is impaired or depleted, or if hepatocyte proliferation is inhibited by toxins, another mechanism is initiated. Liver progenitor cells (also known as hepatic progenitor cells or oval cells) are activated, proliferate, and differentiate to mature liver cells [20].

1.1.3 Liver progenitor cells

Due to their bipotential capacity it is suggested that liver progenitor cells derive from fetal hepatocytes and reside in very small numbers in a niche close to the canals of Hering until they are activated [21]. It has been shown that the cells responsible for regeneration after chronic liver injury are leucine-rich repeat-containing G-protein coupled receptor 5 (Lgr5) positive, as are stem cells in the intestine that drive constitutive self-renewal, underlining their progenitor status. However, $Lgr5^+$ cells are not detectable under non-diseased conditions [22]. Despite many studies describing liver progenitor cells, they are not acknowledged by all and alternative theories imply a dedifferentiation of either cholangiocytes or hepatocytes that then differentiate into hepatocytes or cholangiocytes, respectively [2].

For appropriate differentiation of liver progenitor cells an interplay of Notch and Wnt signaling is necessary. Wnt signaling drives differentiation of liver progenitor cells towards a hepatocytic fate whereas Notch signaling leads to differentiation into cholangiocytes. It could be shown that through phagocytosis of hepatocyte debris macrophages upregulate *wnt* expression and activate Wnt-signaling in nearby liver progenitor cells. Furthermore, the Notch pathway inhibiting ubiquitin ligase Numb is activated by β-catenin presenting a decisive cross-section of both lineage specifying pathways [23].

Known mitogens of liver progenitor cells are hepatocyte growth factor and tumor necrosis factor superfamily member 12 (also known as tumor necrosis factor-like weak inducer of apoptosis).

Hepatocyte growth factor binds to its receptor c-Met and induces c-Met autophosphorylation on tyrosine residues [24]. In a murine model inducing liver progenitor cell-driven regeneration it was shown that mice with a Met deficiency died from liver failure. Liver failure was proposed to result from ineffective progenitor cell mediated regeneration, since it was demonstrated that loss of c-Met leads to a decreased oval cell pool and also affects migration and differentiation abilities of oval cells [25].

Tumor necrosis factor superfamily member 12 is released by macrophages in chronic liver injury. Tumor necrosis factor superfamily member 12 activates the NFκB pathway through its receptor tumor necrosis factor receptor superfamily member 12a (also Fn14) leading to liver progenitor cell activation and proliferation [26].

But also the microenvironment and, within it, interactions with other cells are essential for liver progenitor cell-driven regeneration [20]. Especially the cross-talk between liver progenitor cells and hepatic stellate cells is of interest since it can either lead to wound healing or progressive chronic liver injury. One key regulator of the hepatic stellate cell/ liver progenitor cell cross-talk is lymphotoxin-β, a member of the tumor necrosis factor family. Lymphotoxin-β is expressed on activated liver progenitor cells in chronic liver injury. Lymphotoxin-β binds to the lymphotoxin-β receptor, which is expressed on hepatic stellate cells. This interaction leads to side-by-side migration of liver progenitor cells and hepatic stellate cells to sites of injury and might increase fibrogenesis [27].

Due to their plasticity and differentiation potential liver progenitor cells are considered interesting therapeutic targets as an alternative to orthopic liver transplantation. However,

despite all recent advances in liver progenitor cell research, knowledge about the complex regulatory mechanisms of liver progenitor cells is still limited and needs to be expanded.

Although liver progenitor cells are known to contribute to liver regeneration, a prolonged liver progenitor cell response leads to fibrosis. Additionally, deregulation of differentiation and proliferation of liver progenitor cells can cause malignant transformation to tumor-initiating cells [28]. It has been reported that progenitor cells can progress to a malignant status, dependent on autocrine interleukin-6 signaling [29].

1.1.4 Liver fibrosis

During liver repair extracellular matrix is deposited. This is a transient and reversible process in acute or limited injuries. However in chronic liver diseases extracellular matrix accumulates and progressively substitutes liver parenchyma leading to fibrosis. Several patterns of fibrosis can be distinguished and depend on the underlying disease.

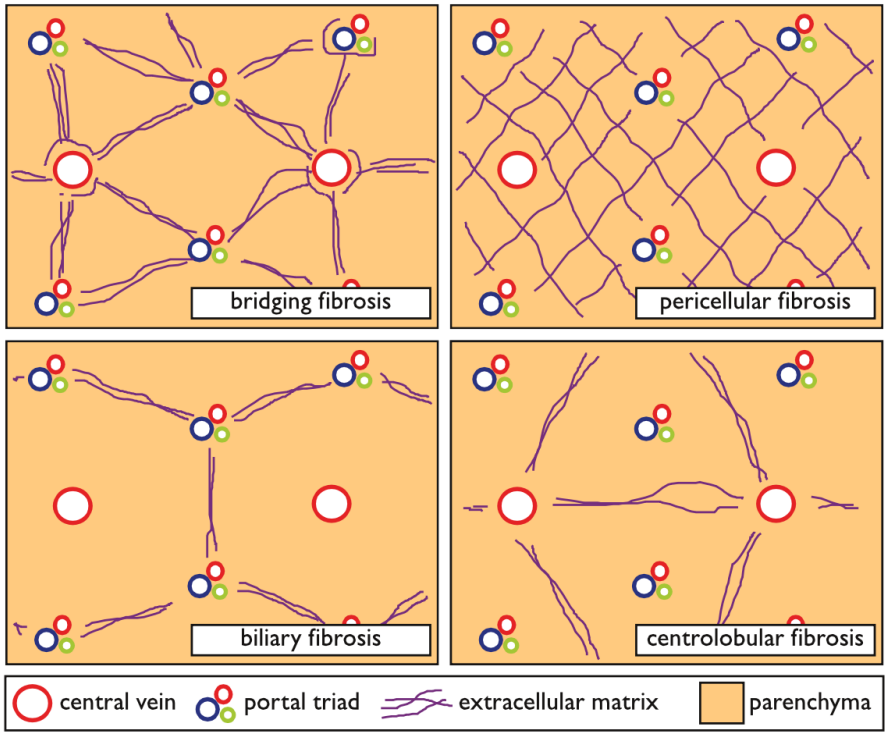

Figure 1.4: Fibrotic patterns

Bridging fibrosis is characterized by fibrotic septa spanning from portal regions to central regions. The typical "chicken-wire" pattern from extracellular matrix deposition around hepatocytes is found in pericellular fibrosis. In biliary fibrosis septa connect the portal regions whereas in centrolobular fibrosis the central regions are connected by fibrotic septa.

Formation of portal central fibrotic septa is classified as bridging fibrosis. Infection with hepatitis B or C virus lead to bridging fibrosis. Perisinusoidal or pericellular fibrosis can be

distinguished by a typical "chicken-wire" pattern that results from extracellular matrix deposition in the space of Disse around sinusoids or hepatocytes. Typical triggers are alcoholic liver disease and non-alcoholic fatty liver disease. Lastly, there are biliary fibrosis, consisting of fibrotic septa spanning from portal region to portal region, and centrolobular fibrosis with fibrotic septa from central area to central area (see Figure 1.4) [30].

Even though advancement of liver fibrosis to liver cirrhosis can be slow, it leads to a high risk of mortality. On top of being already a high risk in itself, cirrhosis can trigger development of hepatocellular carcinoma (Figure 1.5) [31].

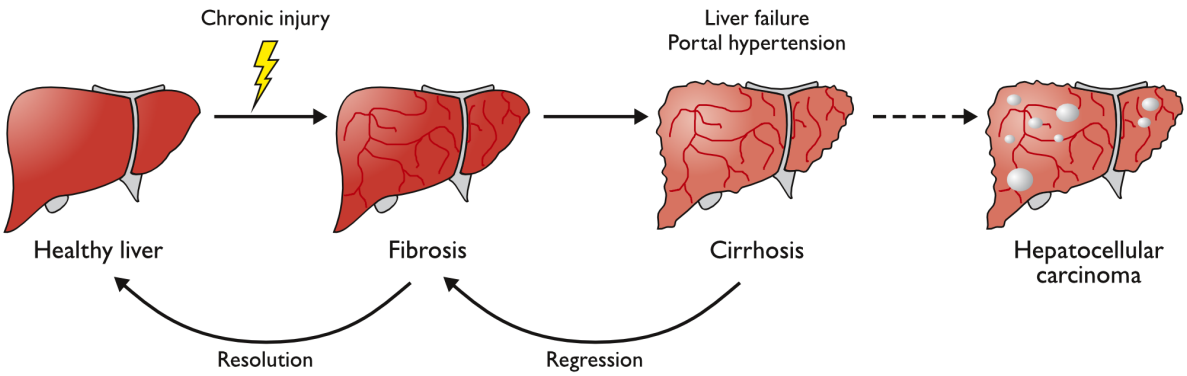

Figure 1.5: Progressive liver disease

Chronic injuries like viral infections or alcohol abuse cause inflammation and parenchymal cell death. In the process of tissue repair extracellular matrix is deposited. If damage persists the extracellular matrix accumulates leading to fibrosis and consequently to cirrhosis, at which step liver failure and portal hypertension occur. Although fibrosis can be rapidly resolved if the cause is eliminated this is not the case for cirrhosis. Once cirrhosis is established only regression but not resolution is possible. Transplantation is currently the only long-term treatment option for liver failure. Although liver cirrhosis in itself is a cause of mortality, it can additionally contribute to development of hepatocellular carcinoma.

The primary effector cells in fibrosis are hepatic stellate cells. They usually reside in an inactive or quiescent state in the space of Disse. Upon liver injury hepatic stellate become activated. Activation takes place in two phases: initiation and perpetuation. The first phase starts shortly after injury occurs. It is driven by signals from Kupffer cells and endothelial cells as well as exposure to debris from damaged hepatocytes. This leads to altered gene expression and altered responsiveness to cytokines. Proteins affected through transcriptional changes are collagen I, α-smooth muscle actin, transforming growth factor β 1, transforming growth factor β-receptor, matrix metalloprotease-2, and tissue inhibitor of metalloprotease 1 and 2 [32]. After the first priming phase a second phase finalizes activation. Hepatic stellate cells lose their vitamin-A rich lipid droplets completely, proliferate, show greater contractility and produce great amounts of extracellular matrix (Figure 1.6)

[26]. Composition of the extracellular matrix is different compared to healthy livers. The normally present collagens IV and VI are replaced by collagens I and III as well as fibronectin [30]. Proliferation of hepatic stellate cells is driven mainly by transforming growth factor β and epidermal growth factor. These growth factors are also proteolytically released for paracrine stimulation of regenerative hepatocyte proliferation [33, 34].

Fibrosis is part of the wound healing process in the liver. It has been shown that fibrosis leads to more resistance to subsequent acute injury and that collagen I protects hepatocytes against toxic damage. Only if resolution of fibrosis is dysregulated and excessive amounts of extracellular matrix are deposited tissue function is altered and becomes pathologic [18].

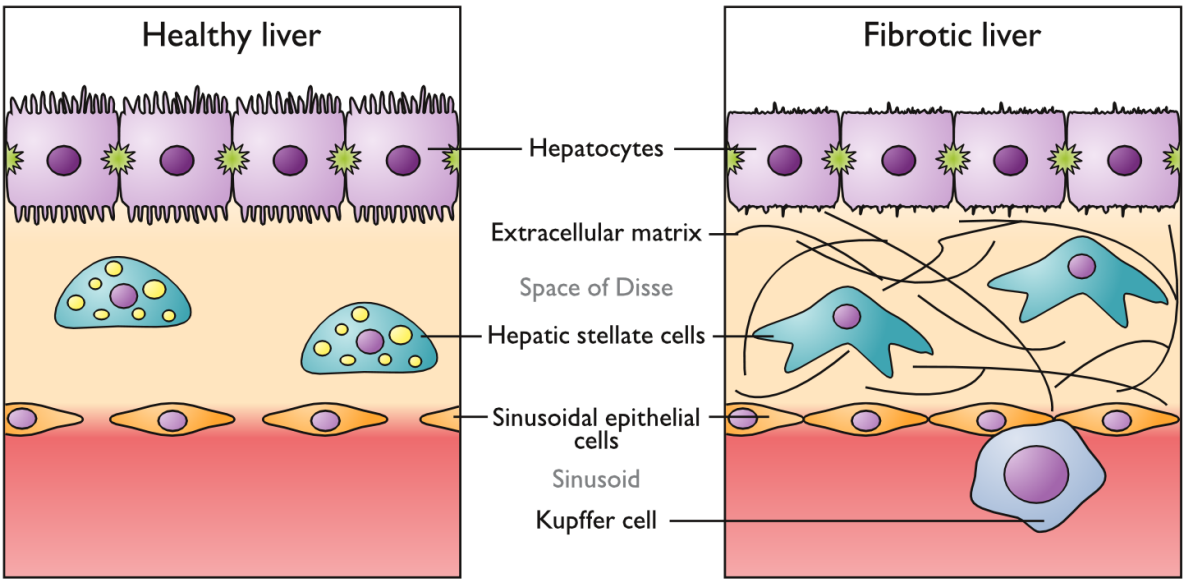

Figure 1.6: Schematic of cellular events in liver fibrosis

In case of chronic injury in the liver hepatic stellate cells, residing in the space of Disse, get activated through signals from Kupffer cells and endothelial cells. This leads to loss of their lipid droplets, changes in morphology, and deposition of extracellular matrix. In addition hepatocytic microvilli are lost as well as endothelial fenestration.

1.2 A disintegrin and metalloproteases (ADAMs)

Proteins are known to be tightly regulated at the transcriptional and translational level. However, they can also be modified post-translationally, affecting protein stability or function. One post-translational modification is proteolytic processing. The release of membrane-bound proteins by proteolytic cleavage is termed ectodomain shedding. Members of the a disintegrin and metalloprotease (ADAM) family are key enzymes in ectodomain shedding.

ADAMs belong to the metzincins, a superfamily of zinc-based proteinases [35]. Within this superfamily the ADAMs are found in the adamalysin subfamily (http://http://merops.sanger.ac.uk/; [36]). ADAMs are either secreted or type I single-pass transmembrane proteins of approximately 750 amino acids (aa) length. ADAMs have been detected in many species ranging from nematodes (*C. elegans*) to vertebrates (*M. musculus, H sapiens*) [37].

1.2.1 Domain structure of ADAMs

ADAMs have a very conserved modular layout as shown in the schematic in Figure 1.7. All ADAMs are synthesized in the endoplasmic reticulum with an N-terminal signal peptide regulating transit through the secretory pathway. ADAMs are glycosylated co-translationally [38]. C-terminal to the signal peptide is a pro-domain which acts as an intramolecular chaperone [39, 40]. The pro-domain further inhibits activity of the metalloprotease domain via a cysteine-switch mechanism. It is removed intracellularly by pro-protein convertases like furin during maturation in the trans-Golgi compartment [41, 42]. Several studies have shown that recombinant pro-domains of ADAMs can very selectively inhibit the active

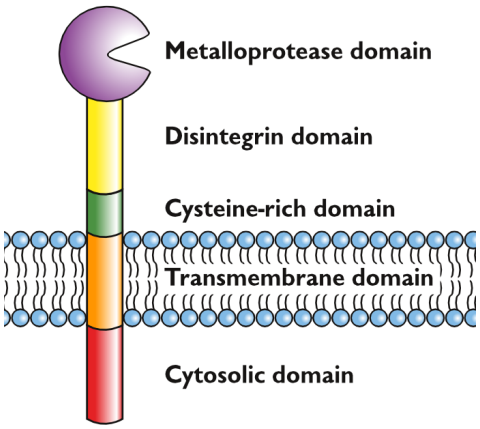

Figure 1.7: Domain structure of an ADAM (based on ADAM10)

ADAMs are secreted or, as depicted here, type I transmembrane proteins consisting of a cytosolic, a transmembrane, a cysteine-rich, a disintegrin, in some cases an epidermal growth factor-like (not shown), and a metalloprotease domain. ADAMs are synthesized as zymogens with a pro-domain (not shown), that serves both as an intramolecular chaperone and as inhibitor of the protease.

mature form [43, 44]. Subsequent to the pro-domain ADAMs have a metalloprotease domain succeeded by a disintegrin-like domain that is considered to mediate interactions between ADAMs and integrins through a 14 aa stretch named "disintegrin loop" [45]. Following those domains are a cysteine-rich domain and an epidermal growth factor-like domain that is not found in ADAM10 or ADAM17 [46]. Structural analysis of the metalloprotease/disintegrin/cysteine-rich domains implies a C-shaped form with the cysteine-rich domain facing the catalytic site of the metalloprotease domain [47]. Next is the transmembrane and finally the cytoplasmic domain which differs strongly in length (11-231 aa) and sequence between various ADAM family members [48].

1.2.2 Biological functions of ADAMs

There are 21 ADAMs in humans that are considered functional. Functionality can be achieved by having a characteristic active site in the metalloprotease domain (HEXGHXXGXXHD) implying proteolytic activity. But also non-proteolytic ADAMs can be considered functional, with a role in protein folding and protein-protein interaction [49]. A classification based on functionality and tissue expression is shown in Figure 1.8.

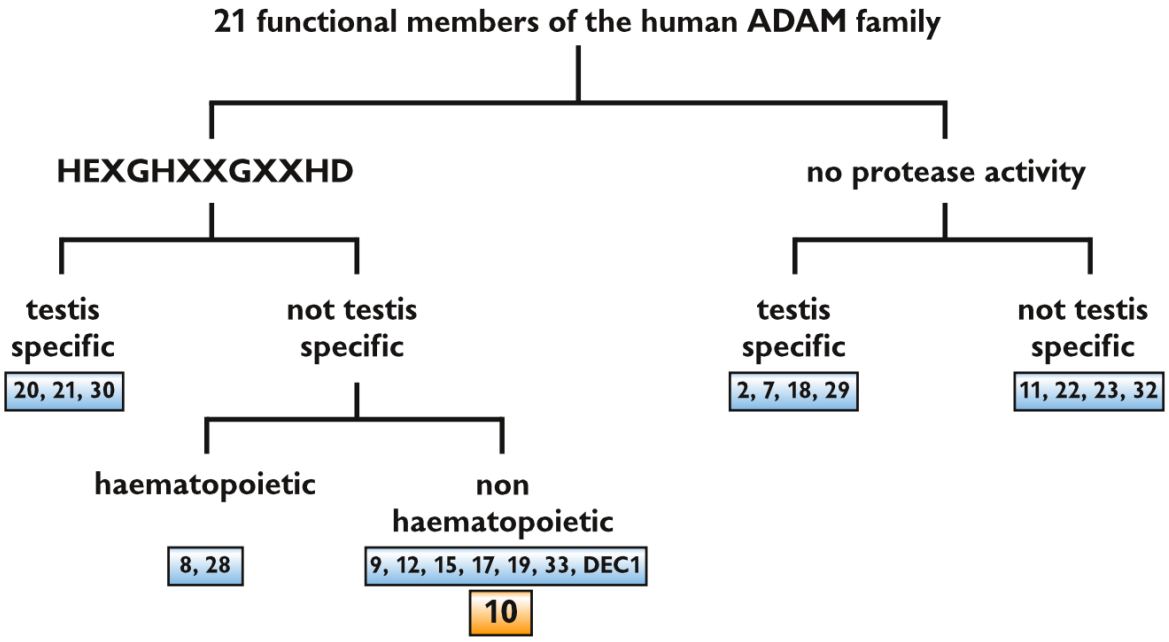

Figure 1.8: Classification of the human ADAMs based on their functionality and tissue expression

The 21 functional members of the human ADAM family are grouped depending on proteolytic or non-proteolytic function as well as tissue specificity. The numbers of the respective ADAMs are listed below each group in the blue boxes. The for this study relevant protease ADAM10 is highlighted in orange.

Reprinted with permission from [50]

Although all ADAMs share the described modular layout, a phylogentic analysis of the metalloprotease domain sequence shows a clear separation of ADAM10 and ADAM17 from the other ADAMs but not from each other [50].

ADAMs have diverse functions e.g. in sperm-egg binding, ectodomain shedding, and as part of regulated intramembrane proteolysis. Only the two latter functions will be discussed here as these are the main functions for the investigated ADAM10. A graphic summary is shown in Figure 1.9.

Ectodomain shedding has several functions, the first of which is releasing a ligand from the cell surface, enabling it to engage to its receptor either on the same cell (autocrine signaling) or on other cells (paracrine signaling). Examples are epidermal growth factor receptor ligands like transforming growth factor α and betacellulin [51]. A second mechanism is shedding of receptors or ligands to abrogate juxtacrine cell-cell signaling [52]. Thirdly, receptors can be shed to act as decoy for soluble ligands, as reported for interleukin-1 receptor 2 [53]. Shed receptors can also form complexes with ligands and induce signaling in cells only expressing the signal-transducing subunit, but not the receptor itself. A prime example for this mechanism is interleukin-6 trans-signaling where it also has been shown that signal quality differs depending on whether the receptor is membrane-bound or soluble [54].

Ectodomain shedding is also a prerequisite for regulated intramembrane proteolysis. Proteolytic cleavage of the ectodomain leads to the creation of a truncated substrate that can then be further processed by intramembrane-cleaving proteases. Four families of the intramembrane-cleaving proteases are known: S2P metalloproteases, presenilin aspartyl proteases, SPP aspartyl proteases, and rhomboid serine proteases [55]. The intramembrane-cleaving proteases release the intracellular domain of the substrate protein. The intracellular domain can then translocate to the nucleus, bind to a transcription regulating complex, and affect gene transcription. Prominent proteins known to undergo regulated intramembrane proteolysis are Notch, amyloid precursor protein, and CD44 [56–58].

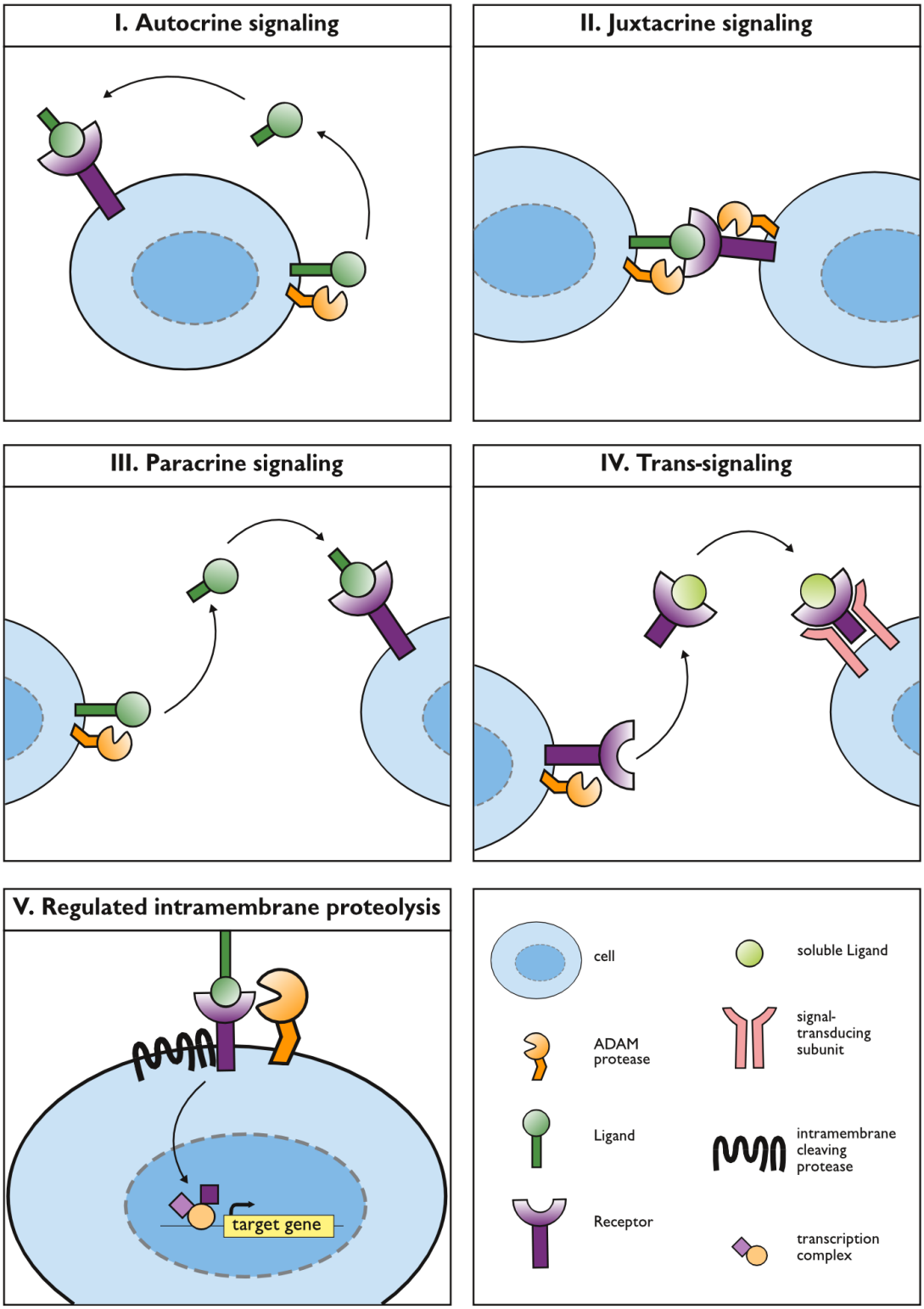

Figure 1.9: ADAMs play a role in different signaling mechanisms

The schematic shows a selection of signaling processes that can be influenced by proteolytic activity of ADAMs. Mechanisms include shedding of ligands for autocrine (I) or paracrine (III) signaling, abolition of juxtacrine signaling by cleaving either ligand or receptor (II), proteolytic release of a receptor to either act as a decoy for a soluble ligand or to induce signaling at cells that express the signal-transducing subunit but not the receptor (IV), and triggering a sequential proteolytic cascade releasing an intracellular domain that induces gene transcription (V).

1.3 A disintegrin and metalloprotease 10

ADAM10, also known as CD156c, kuzbanian protein homolog, or mammalian disintegrin metalloprotease, is a 748 aa long type I transmembrane protein that was first identified in myelin membrane preparations from the bovine brain [59]. ADAM10 is encoded in the gene loci 15q21.3 in humans and 9:D in mice [60, 61]. The murine and the human ADAM10 gene locus shows a highly conserved region upstream of the transcription initiation site starting at -500 bp. Gene expression of ADAM10 can be repressed by its GC-rich 5' untranslated region [62] or, specifically in the liver, by microRNA-122 [63].

1.3.1 Regulation of ADAM10

The domain structure of ADAM10 is as shown in Figure 1.7. Of special interest is the cytoplasmic tail of ADAM10 that influences trafficking to selected areas, maturation, protein stability and activity. The C-terminus of ADAM10 contains two proline-rich putative src homolog 3 binding sites. In neurons it was shown that, by binding of synapse-associated protein 97 via the src homolog 3 domain, ADAM10 was transported to the post-synaptic membrane [64]. Furthermore, the src homolg 3 binding sites lead to a sorting of ADAM10 to basolateral tight-junctions in epithelial cells [65]. The cytoplasmic domain of ADAM10 has additionally an endoplasmic reticulum retention motif as well as an isoleucine-glutamine (IQ) consensus site for calcium-independent binding of calmodulin that both influence protein trafficking to the cell surface and maturation [66, 67]. Several glycosylation sites for N-glycans are found in the extracellular domain of ADAM10. Glycosylated ADAM10 is protected from proteolytic degradation [38].

The C-terminus of ADAM10 is also a substrate for phosphorylation either by Protein kinase C α or via a not completely unraveled mechanism, downstream of G-protein coupled receptors [68, 69].

Further regulatory processes affecting ADAM10 activity include proprotein convertases [42] as discussed earlier or natural inhibitors tissue inhibitor of metalloprotease 1 and 3 [70]. ADAM10 itself can also be proteolytically processed by its own substrate meprin β leading to a soluble form of ADAM10 that is still enzymatically active and might have a different substrate spectrum [71, 72]. Other proteases shown to cleave ADAM10 are ADAM9 and ADAM15 leading to regulated intramembrane proteolysis and resulting in an ADAM10 C-terminal fragment. The C-terminal fragment translocates to speckles in the

nucleus closely associated with two known nuclear speckle subtypes that are shown to localize to active transcription sites. This implies a role for ADAM10 in transcriptional control of genes [72, 73].

ADAM10 activity can also be regulated by localization to different membrane domains. Several groups demonstrated that ADAM10 is active after cholesterol depletion and activity is inhibited upon anchoring ADAM10 to cholesterol-rich domains [74, 75]. These findings even led to clinical trials with cholesterol lowering statins in patients with Alzheimer's disease that were, however, inconsistent in their results and showed either a protective effect [76] or no protective effect [77].

Membrane compartment localization of ADAM10 is yet interesting for another reason. It has been shown in several studies that ADAM10 interacts with multiple members of the tetraspanin family. Tetraspanin 12 and Tetraspanin 15 were both reported to regulate cellular trafficking and increase ADAM10 maturation [78, 79]. In addition to that, it was demonstrated that tetraspanins influence ADAM10 localization to tetraspanin-enriched microdomains and thereby regulate the activity of ADAM10 towards several substrates [80].

1.3.2 Biological functions of ADAM10

ADAM10 has until now more than 40 identified substrates [81]. The two most prominent targets of ADAM10 are amyloid precursor protein, making ADAM10 an interesting target in Alzheimer's disease, and the Notch receptors, that play important roles in development [82, 83]. ADAM10 also plays a role in other cell functions ranging from cell migration (N-cadherin [68]) to immunity (CD23 [84]) to proliferation and apoptosis (CXCL16 [85] and FasL [86]).

This multitude of functions indicate that a tight regulation of ADAM10 is important and that deregulation of ADAM10 activity can lead to pathogenesis. In Alzheimer's disease amyloid precursor protein is cleaved by the beta-secretase BACE causing a specific truncated C-terminal fragment of the amyloid precursor protein that forms the toxic Aβ plaques. ADAM10 is competing with the beta-secretase BACE for amyloid precursor protein and proteolytic processing by ADAM10 instead of BACE leads to the formation of a fragment that does not form toxic plaques [87].

Notch is target of ADAM10, that, upon ligand binding, undergoes regulated intramembrane proteolysis. The released intracellular domain of Notch translocates to the nucleus where it forms a ternary complex with DNA binding proteins and regulates gene expression [88]. Target genes regulated by Notch include hairy and enhancer of split-1, a transcriptional repressor that regulates proliferation and differentiation in embryogenesis, and Snail, a transcription factor inducing epithelial to mesenchymal transition [89, 90]. Although ADAM17 is also reported to cleave Notch, it is not necessarily redundant to cleavage by ADAM10 and it has been proposed that ADAM10 Notch cleavage is ligand dependent and that ADAM17 cleaves Notch independent of ligand activation [91].

ADAM10 is, mainly through Notch-mediated functions, important for maintaining cell and tissue homeostasis as reported for B cells, intestinal stem cells, and skin [92-94]. Besides regulation of epidermal homeostasis via modulation of epidermal growth factor receptor signaling, ADAM10 also controls keratinocyte adhesion and migration through cleavage of E-cadherin and β-catenin signaling which, when deregulated, leads to eczematous dermatits [95, 96].

ADAM10 has also been shown *in vitro* to cleave c-Met and abrogate hepatocyte growth factor-signaling [97]. However, the implication in liver physiology and pathology is greatly unknown.

Finally, ADAM10 overexpression has been described in many types of adenocarcinoma: breast cancer [98], colon carcinoma [99], gastric cancer [100], hepatocellular carcinoma [63], leukaemia [101], prostate cancer [102], oral squamous cell carcinoma [103], and uterus and ovarian cancer [104].

The many physiological roles of ADAM10 show that not only must ADAM10 be tightly regulated but it underlines the difficulty of developing therapeutic strategies that only target a certain aspect of ADAM10-mediated ectodomain shedding without deleterious side-effects. Cell biological and biochemical studies already contributed greatly to knowledge of candidate substrates and effects on cell characteristics. But these approaches are limited and a more physiologic setting is needed to better understand the role of ADAM10 in development and disease and to develop efficient drugs [105].

1.3.3 ADAM10 deficient mice

Thus, to study the function of ADAM10 more comprehensively in a physiological and pathological setting a mouse model lacking the protease was created. However these mice died early at embryonic day of gestation 9.5. The early lethality can be contributed to the ADAM10 target Notch since animals deficient in Notch1 and 2 show a similar phenotype [106].

To circumvent the early lethality, conditional knock-out mice were generated using the Cre/loxP site-specific recombination technology. The Cre/loxP system originates from the P1 phage and enables the targeted excision of DNA-sequences. The target sequence is flanked by parallel oriented DNA recognition site, called loxP. A Cre-recombinase recognizes those sites and excises the sequence in-between leading to a deletion. Strands are then rejoined by DNA ligase. [107]

Mice were generated with loxP sites flanking exon 2 of the ADAM10 gene (see Figure 1.10). By breeding these mice with mice expressing tissue-specific Cre-recombinase ADAM10 deletion is limited to the targeted cells and embryonic lethality is avoided [108].

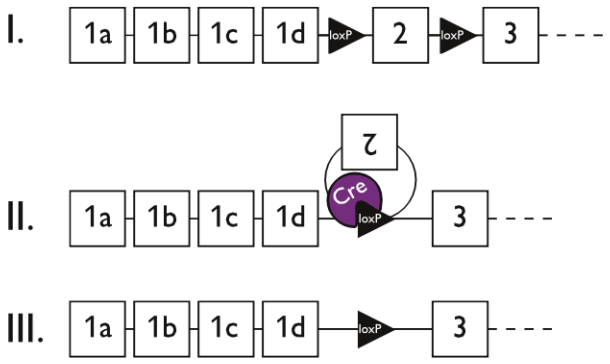

Figure 1.10: Recombination of ADAM10 with the Cre/loxP system

Exon 2 of ADAM10 is flanked by loxP sites (I). In the presence of a Cre-recombinase the parallel oriented loxP sites are recognized and bound (II). The sequence in between the two loxP sites is excised and the remaining loxP sites are ligated (III).

1.4 Aim

ADAM10 was shown to be essential for organ development and tissue homeostasis but also to lead to pathologies if deregulated. Yet, little is known about ADAM10 in liver physiology and pathology. We therefore want to investigate the role of ADAM10 and its regulation in the liver.

To this aim we will generate mice deficient for ADAM10 in hepatoblasts and subsequently in hepatocytes, cholangiocytes and adult liver progenitor cells. We will examine these mice by histological, molecular biological, and biochemical analysis. Data from the murine model will be complemented with *in vitro* experiments using the liver progenitor cell line BMOL.

We hope to contribute to a better understanding of the consequences of proteolytic processing by ADAM10 in the liver with the ultimate goal of providing new approaches to therapeutic interventions.

2 Material & Methods

2.1 Material

2.1.1 Chemicals and recombinant proteins

William's E medium	Sigma-Aldrich, Steinheim, Germany
Glutamine	Sigma-Aldrich, Steinheim, Germany
FCS	PAN Biotech, Aidenbach, Germany
Matrigel	Corning, Bedford (MA), USA
GI254023X	Iris Biotech, Marktredwitz, Germany
GW208264X	Iris Biotech, Marktredwitz, Germany

Basic chemicals were purchased from Carl Roth (Karlsruhe, Germany), Sigma-Aldrich (Steinheim, Germany), or AppliChem (Darmstadt, Germany), unless otherwise stated.

Table 1. Recombinant proteins

Name	Supplier	Product#
recombinant human insulin like growth factor-II (rhIGF-II)	Immunotools, Friesoythe, Germany	11343573
recombinant murine epidermal growth factor (rmEGF)	Immunotools, Friesoythe, Germany	12343406
recombinant human Insulin	Sigma-Aldrich, Steinheim, Germany	I2643
recombinant human Tnfsf12 (rmTWEAK)	Peprotech, Hamburg, Germany	310-06
recombinant murine hepatocyte growth factor (rmHGF)	Peprotech, Hamburg, Germany	315-23
recombinant human transforming growth factor β 2 (rhTGFβ2)	Immunotools, Friesoythe, Germany	11344751

2.1.2 Primer

All oligonucleotides were synthesized by Sigma-Aldrich.

Table 2. Primers for genotyping and genomic DNA

Target	Forward Primer (5'-3')	Reverse Primer (5'-3')	Expected bandsize
Adam10	ATGGATTGCCCTTTTATGTATTTA	GCCGATGTGCCAGATGAGTG	262 bp (wt) 420 bp (flox)
ΔAdam10	TACAACCATGCCCAGCTTTTTAGT	GCCGATGTGCCAGATGAGTG	700 bp
Cre	CGAGTGATGAGGTTCGCAAG	TGAGTGAACGAACCTGGTCG	390 bp
EYFP	GGAGCGGGAGAAATGGATATG (wt) AAGACCGCGAAGAGTTTGTC (tg)	AAAGTCGCTCTGAGTTGTTAT	600 bp (wt) 320 bp (tg)
Hbbt1	CCAATCTGCTCACACAGGATAGA GAGGGCAGG	CCTTGAGGCTGTCCAAGTGATTC AGGCCATCG	500 bp
rtTA	CCATGTCTAGACTGGACAAGA	CTCCAGGCCACATATGATTAG	600 bp

Table 3. Primers for quantitative Real-Time PCR				
Target	Forward Primer (5'-3')	Reverse Primer (5'-3')	UPL#	Sequence Reference
Acta2	GCATCCACGAAACCACCTAT	AGGTAGACAGCGAAGCCAAG		X13297
Actb	TGGAATCCTGTGGCATCCATGAAA	TAAAACGCAGCTCAGTAACAGTCCG		NM_007393
Adam10	GGGAAGAAATGCAAGCTGAA	CTGTACAGCAGGGTCCTTGAC	38	NM_007399
Col1a1	GAGCGGAGAGTACTGGATCG	TACTCGAACGGGAATCCATC		NM_007742
Cxcr4	TGGAACCGATCAGTGTGAGT	GGGCAGGAAGATCCTATTGA	38	NM_009911
Cxcr7	AGAAGATGGTACGCCGTGTT	ATCAGGCAGGGACACAAAGA		BC015254.1
Id1	GCGAGATCAGTGCCTTGG	CTCCTGAAGGGCTGGAGTC		NM_010495.2
Mmp2	CAGCAAGTAGATGCTGCC	CAGCAGCCAGCCAGTC		NM_008610
Mmp13	TTTGAGAACACGGGGAAGAC	TGGGCCCATTGAAAAAGTAG		NM_008607
Spp1	CTCTGATCAGGACAACAAC	CCTCAGAAGATGAACTCTC		AF515708
Tgfb1	TGGAGCAACATGTGGAACTC	GTCAGCAGCCGGTTACCA	72	NM_011577
Tgfb2	CCTTCGCCCTCTTTACATTG	TTCGATCTTGGGCGTATTTC		NM_009367
Timp1	GCAAAGAGCTTTCTCAAAGACC	AGGGATAGATAAACAGGGAAACACT		NM_001044384.1/NM_011593.2/NM_001294280.2
Tnfrsf12a	ATTCGGCTTGGTGTTGATG	CCATGCACTTGTCGAGGTC		NM_013749.2
Tnfsf12	CAGGATGGAGCACAAGCAG	GGCTGGAGCTGTTGATTTTG		NM_011614.3
Tuba1a1	CTGGAACCCACGGTCATC	GTGGCCACGAGCATAGTTATT	88	NM_011653

2.1.3 Antibodies

Table 4. Primary antibodies			
Target	Host species	Dilution (application)	Distributed by (Product#)
beta-actin	mouse	1:10 000 (Immunoblot)	Sigma-Aldrich (clone AC-15, A1978)
beta-actin	rabbit	1:1 000 (Immunoblot)	Sigma-Aldrich (A2066)
ADAM10	rabbit	1:1 000 (Immunoblot)	Genetex (GTX63486)
GFP	rabbit	1:1 000 (Immunoblot)	Roche (11814460001)
TGFβRI	rabbit	1:1 000 (Immunoblot)	Santa Cruz (sc398)
TGFβRII	mouse	1:1 000 (Immunoblot)	Santa Cruz (sc17792)
SMAD2	rabbit	1:1 000 (Immunoblot)	Cell signaling (5339)
pSMAD2	rabbit	1:1 000 (Immunoblot)	Cell signaling (3108)
c-Met	mouse	1:1 000 (Immunoblot)	Cell signaling (3127)
p-Met	rabbit	1:1 000 (Immunoblot)	Cell signaling (3077)
ERK1/2	mouse	1:1 000 (Immunoblot)	Cell signaling (4696)

Table 4. Primary antibodies (cont.)			
Target	Host species	Dilution (application)	Distributed by (Product#)
p-ERK1/2	rabbit	1:1 000 (Immunoblot)	Cell signaling (9101)
IkB	mouse	1:1 000 (Immunoblot)	Cell signaling (4814)
CK19	mouse	1:500 (Immunohistochemistry)	DSHB (TromaIII)
Radixin	goat	1:200 (Immunohistochemistry)	Santa Cruz (sc6408)
Mrp2	mouse	1:200 (Immunohistochemistry)	Biozol (BLD-SIG-38785-500)
Ly6G	rat	1:400 (Immunohistochemistry)	eBioscience (14-5931)
CD3	rabbit	1:100 (Immunohistochemistry)	Dako (A0452)
Ki67	rabbit	1:200 (Immunohistochemistry) 1:400 (Immunohistochemistry)	Pierce Thermo Scientific (MA5-14520) Cell Signaling (12202)
F4/80	rat	1:150 (Immunohistochemistry)	gift from Ruth Ganss (University of Western Australia, Perth, Australia)
CD44	rat	1:150 (Immunohistochemistry)	eBioscience
panCK	rabbit	1:200 (Immunohistochemistry)	Dako
panCK	mouse	1:100 (Immunohistochemistry)	Dako
SMA	mouse	1:400 (Immunohistochemistry)	Dako
GFP	rabbit	1:1 000 (Immunohistochemistry)	abcam

Table 5. Secondary antibodies			
Target	Tag	Dilution	Distributed by
rabbit	Alexa Flour® 488	1:200	Life Technologies (A-11034)
rat	Alexa Flour® 594	1:200	Life Technologies (A-11007)
mouse	Alexa Flour® 594	1:200	Life Technologies (A-11005)
mouse	Horseradish peroxidase	1:5 000	ThermoScientific (31432)
rabbit	Horseradish peroxidase	1:10 000	Dianova (111-035-144)
rat	Horseradish peroxidase	1:15 000	Dianova (112-0,35-143)
mouse	Biotin	1:200	Dako (E0433)
rabbit	Biotin	1:600	Dako (E0432)
rat	Biotin	1:200	Dako (E0468)
goat	Biotin	1:200	Dako (E0466)

2.1.4 Cell lines

Table 6. Cell lines and respective culture media				
Cell line	Source of cells	Culture medium	Source	Remarks
BMOL	Murine liver	Williams' E +2-5% FCS + 2mM Glutamine + 15 ng/ml IGF-II + 10 ng/ml EGF + 5 µg/ml Insulin	Nina Tirnitz-Parker (Curtin University, Perth, Australia)	bipotential [109]

2.1.5 Mice

Table 7. Mice

Mouse line	Source	Reference
129P2-Adam10^{tm2Psa}/Ph	Paul Saftig (University Kiel, Germany)	[108]
B6.Tg(Alb1-cre)7Gsc/Cnrm	Thomas Wunderlich (University Cologne, Germany)	[110]
B6.129X1-*Gt(ROSA)26Sor*$^{tm1(EYFP)Cos}$/J	Radislav Sedlacek (Institute of molecular genetics, Academy of Science of the Czech Republic, Prague, Czech Republic)	[111]

2.2 Methods

2.2.1 Animal experimentation

2.2.1.1 Housing of mice

All mice were housed in a specified pathogen free environment. Room temperature was stable at 22°C. Light conditions were according to a 12-hour day-night cycle. Mice were fed a standard laboratory chow (10 mm pellets; V1534-000, Ssniff, Soest, Germany) ad libitum. Animals were treated humanely according to the criteria outlined by the German government. Experiments with CCl_4 were approved by the according authority with the reference number V242-7224.121-3 (36-4/14).

2.2.1.2 Breeding of mice

Mice were at least 10 week old when used for breeding. For the duration of the breeding they received special breeding food (10 mm pellets; V1124-000, Ssniff, Soest, Germany) ad libitum. Pups were weened 3 weeks after birth. Until then, they received the same food as the parents. Breeding schematics for the different strains are depicted below:

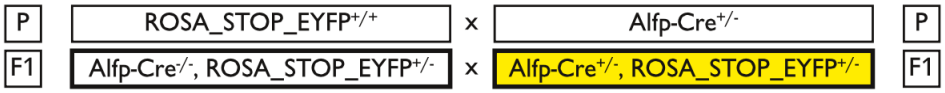

Figure 2.1: Breeding schematic for Cre-activity reporter mice

Genotypes used in experiments are marked by a thick black frame. Mice expressing EYFP are highlighted in yellow.

P: parental generation; F1: first generation (progeny of P)

Figure 2.2: Breeding schematic for conditional ADAM10 knockout in hepatocytes, cholangiocytes and liver progenitor cells

Genotypes used in experiments are marked by a thick black frame. Color schemes are equivalent to the ones used in bar charts for the respective genotype.

P: parental generation; F1: first generation (progeny of P); F2: second generation (progeny of F1)

2.2.1.3 Tail biopsy and genotyping

A 3-5 mm long biopsy was taken from the tail of 3-4 week old mice. To avoid cross-contamination or inflammation of the tail we used a hot-bead sterilizer in between animals. Tails were digested over night at 55°C and 1 000 rpm in 0.5 ml DNA-digestion buffer[1]. Insoluble materials were pelleted at maximum speed for 5 min and supernatant (SN) was transferred to a fresh tube. 170 µl of saturated NaCl were added and the sample was vigorously shaken. Samples were centrifuged at maximum speed for 20 min to pellet proteins and SN was transferred to a new tube. DNA was precipitated by the addition of 1 ml EtOH and was pelleted at maximum speed for 5 min. Pelleted DNA was washed with 70% EtOH and dried at room temperature. It was then resuspended in 100µl TE-Buffer and incubated at 50°C for 5-20 min to ensure complete dissolution. DNA was then ready-to-use for genotyping PCRs.

For detailed information on genotyping primers please refer to Table 2.

Standard PCR mix:

2 µl	DNA
3 µl	10x DreamTaq™ Buffer
3 µl	dNTPs (2 mM)
1.5 µl	5' Primer (10 µM)
1.5 µl	3' Primer (10 µM)
0.2 µl	DreamTaq™ Polymerase
	adjust to 30 µl with ddH_2O

Cycle conditions:

Table 8. ADAM10-flox PCR conditions

Step	Temperature	Time	Cycles
Initial Denaturation	95°C	2'	1
Denaturation	95°C	30"	30
Annealing	55°C	30"	
Elongation	72°C	30"	
Final Elongation	72°C	10'	1
Storage	4°C	∞	1

1 DNA-digestion buffer: 100 mM Tris-HCl pH 8.5, 5 mM EDTA, 200 mM NaCl, 0,2 % SDS, 0,3 mg/ml proteinase K (added fresh)

Table 9. Cre PCR conditions			
Step	Temperature	Time	Cycles
Initial Denaturation	95°C	2'	1
Denaturation	95°C	30''	30
Annealing	56°C	30''	
Elongation	72°C	30''	
Final Elongation	72°C	10'	1
Storage	4°C	∞	1

Table 10. ROSA_STOP_EYFP PCR conditions			
Step	Temperature	Time	Cycles
Initial Denaturation	95°C	2'	1
Denaturation	95°C	30''	35
Annealing	57°C	30''	
Elongation	72°C	30''	
Final Elongation	72°C	5'	1
Storage	4°C	∞	1

2.2.1.4 Treatment with CCl_4

8 to 10 week old mice received a total of 4 intraperitoneal injections of CCl_4 in three day intervals. CCl_4 was diluted 1:4 in sunflower oil and mice received 793 µg CCl_4 per g body weight. Mice were sacrificed 2 days, 15 days, or 30 days after the last injection.

2.2.1.5 Organ harvesting

Mice were killed by cervical dislocation. We took blood as described in 2.2.1.7. Following perfusion with ice-cold PBS[2] liver, spleen, and kidney were harvested, weighed, and processed according to the requirements of the destined use.

2 PBS: 136 mM NaCl, 2.68 mM KCl, 10 mM Na_2HPO_4, 1.76 mM KH_2PO_4, adjust to pH 7.4

2.2.1.6 Bile duct plastination

Bile ducts were plastinated as described previously [7]. In brief, the common bile duct was isolated and flushed with PBS[2]. Liquid Mercox II resin was mixed with catalyst (10% w/v, Ladd Industries, Burlington (VT, USA). The mixture was injected into the common bile duct which was then ligated. Livers were allowed to sit for approximately 10 min for resin to polymerize and were then resected from the abdominal cavity. Liver tissue surrounding the cast was digested with DNA-digestion buffer. Isolated casts were rinsed with H_2O, dried, and imaged with a AZ100 microscope with a DS-Fi2 camera (Nikon, Düsseldorf, Germany).

2.2.1.7 Blood sampling and serological analysis

Blood was taken from the heart and transferred to microtubes with Lithium-Heparin (25 I.U. Heparin/ ml blood). Tubes were inverted to release the Heparin into the blood sample. Samples were centrifuged at 2 000g for 10 min at RT. Plasma was transferred to fresh tubes and stored at -20°C or -80°C until further usage. Alanine transaminase and alkaline phosphatase serum levels were measured with Reflotron® teststripes on a Reflotron® Plus System (Roche, Penzberg, Germany)

2.2.1.8 Hydroxyproline assay

Approximately 100 mg of liver tissue was homogenized with beads in a power homogenizer (Precellys, with an additional Cryolys cooling unit; distributed by Peqlab, Erlangen, Germany) in 900 µl ice cold H_2O for 2 min at 6 000 rpm. Blended contents were transferred to a fresh tube and mixed with 50% Trichloracetic Acid to precipitate total protein. The mixture was vortexed and incubated for 20 min on ice. Afterwards the samples were centrifuged at 6 000 rpm for 10 min at 4°C. SN was discarded and the pellet was washed twice with ice-cold 100% EtOH. The pellets were then dried at RT, dissolved in 800 µl 6M HCl, and incubated ON at 100°C. Samples were centrifuged at 13 000 rpm and supernatant was withdrawn from the tubes using a syringe with a needle. Total volume within the syringe was documented for later calculations. The SN was filtered through a 0.22 µm filter. 40 µl of the filtered liquid were mixed with 10 µl 10M NaOH and then 450 µl of a freshly prepared Chloramine-T solution[3] was added. Samples were incubated 25-30 min at RT. Afterwards 500 µl of Ehrlich's Reagent[4] were added and samples incubated 20

3 Chloramine-T solution: 56 mM Chloramine-T, 10% n-Propanol, 704 mM Sodium Acetate Tri-hydrate, 192 mM Citric Acid, 160 mM Acetic Acid, 680 mM NaOH, pH 6.5

4 Ehrlich's Reagent: 1M 4-(Dimethylamino)benz-aldehyd in 67% n-Propanol and 33% Perchloric Acid

min at 65°C. Once samples had room temperature they were measured in triplicates using a Tecan microplate reader (Tecan, Männedorf, Switzerland) at 544 nm against a known standard.

Hydroxyproline content was calculated as follows:

$$\mu g/ml[\text{measured}] \times \frac{\frac{SN\ \mu l}{40}}{\text{mg liversample}} = \frac{\mu g\ HYP}{\text{mg liver}}$$

2.2.1.9 Immunohistochemistry

Tissue was fixed ON at 4°C in 4% buffered Formaldehyde and subsequently stored in 1% Formaldehyde. Tissue samples were washed several times in ddH_2O and then incubated ON in 50% EtOH. The next day samples were treated as follows:

60 min	70% EtOH
30 min	96% EtOH
60 min	96% EtOH
90 min	100% EtOH
120 min	100% EtOH
90 min	Xylol
90 min	Xylol
30 min	Paraffin
ON	Paraffin
30 min	Paraffin

Tissue samples were then stored in paraffin blocks and when needed cut into 4 µm thick sections for immunohistochemistry. Sections were deparaffinized, rehydrated, and subjected to heat-induced antigen retrieval in either citrate buffer[5] or EDTA buffer[6].

Sections were stained with hematoxylin-eosin, Sirius Red or Periodic-acid-Schiff using standard protocols.

Further sections were stained with primary antibodies (Table 4). Primary antibodies were either detected by biotyinlated secondary antibodies (Table 5), stained using a peroxidase DAB kit (Dako, Hamburg, Germany), and counterstained with Hematoxylin or detected by secondary flourescence-coupled antibodies (Table 5) and counterstained with Hoechst 33342.

5 Citrate buffer: 10 mM citric acid, 0.05% Tween20, adjust to pH 6
6 EDTA-Buffer: 1 mM EDTA, 0.05% Tween20, adjust to pH 8

Sirius Red$^+$ and Ki67$^+$ areas were quantified by morphometric evaluation with ImageJ software (IJ 1.46r, NIH, USA). 10 non-overlapping fields (20x magnification) per section were analysed for each mouse.

2.2.1.10 Transmission electron microscopy

Tissue was fixed in 6% glutaraldehyde in 0.1 M phosphate buffer pH 7.2, postfixed with 2% osmiums tetroxide and embedded in araldite. Sections were cut and stained with lead citrate and uranyl acetate. Images were taken on an EM900 Zeiss electron microscope (Zeiss, Oberkochen, Germany).

2.2.1.11 Cytokine Array on tissue samples

The cytokine array (Mouse Cytokine Array, Panel A #ARY006, R&D Systems, Wiesbaden-Nordenstadt, Germany) was performed on murine liver tissue according to the manufacturer's instructions.

2.2.1.12 ELISA

ELISAs detecting TNFα (#DY410, R&D Systems, Wiesbaden-Nordenstadt, Germany), IL-1RA (#DY480, R&D Systems, Wiesbaden-Nordenstadt, Germany), and CCL2 (#88-7931-88, affymetrix eBioscience, Frankfurt a.M., Germany) were performed with murine liver tissue samples according to the manufacturer's instructions.

Multiplex assay analysis of sMet, HGF and amphiregulin levels in serum was executed with a Bio-Plex mouse array (Bio-Rad Laboratories, Prague, Czech Republic) using the Bio-Plex 200 System (Bio-Rad Laboratories, Prague, Czech Republic). Multiplex beads were produced by amine coupling reaction with primary antibodies from R&D (Minneapolis, USA) and validated in accordance with validation procedures and recommendations from Luminex.

2.2.1.13 Genomic DNA extraction from organs

Genomic DNA from organs was extracted as described in 2.2.1.3 for genomic DNA from tails. Approximately 10-20 mg organ was used per extraction.

2.2.1.14 Deletion PCR

Standard PCR mix was prepared as described in 2.2.1.3 with the primers listed in Table 2 for Δ*Adam10* and *Hbbt1*. Cycle conditions were as stated below:

Table 11. ADAM10 deletion PCR conditions			
Step	Temperature	Time	Cycles
Initial Denaturation	95°C	5'	1
Denaturation	95°C	1'	30
Annealing	61°C	1'	
Elongation	72°C	3'	
Final Elongation	72°C	10'	1
Storage	4°C	∞	1

Table 12. Beta-globin PCR conditions			
Step	Temperature	Time	Cycles
Initial Denaturation	95°C	5'	1
Denaturation	95°C	30''	30
Annealing	55°C	30''	
Elongation	72°C	30''	
Final Elongation	72°C	10'	1
Storage	4°C	∞	1

2.2.1.15 mRNA Isolation

Total RNA was isolated from whole liver tissue using TRIzol (LifeTechnologies, Darmstadt, Germany) according to the manufacturer's instructions. RNA was always precipitated ON at -20°C.

2.2.1.16 cDNA generation through reverse transcription

mRNA was transcribed to cDNA with RevertAid™ Reverse Transcriptase (ThermoScientific, Darmstadt, Germany). In short, equal amounts (≈ 1 µg) of mRNA were mixed with Oligo(dT)$_{18}$ primer, reaction buffer, RiboLock™ RNase Inhibitor, dNTPs (10 mM), and RevertAid™ Reverse Transcriptase. Volume was adjusted with ddH_2O to 20 µl. The mixture was incubated for 60 min at 42°C and the reaction was terminated by heating to 70°C for 10 min. Reaction product was directly used for quantitative Real-Time PCR.

2.2.1.17 Quantitative Real-Time PCR

Samples for qRT-PCR were either analysed on a CFX Real-Timesystem (BIO-RAD, München, Germany) or a roche light cycler 480 II (Roche, Penzberg, Germany). Primers are listed in Table 3.

2.2.2 Cell culture

2.2.2.1 Cell culture conditions

All cells were cultured in incubators at 37°C under a constant atmosphere of 5% CO_2 and a relative humidity (RH) of 95%. The culture media were prepared and used as indicated in Table 6. All work was performed under aseptic conditions and all used materials were autoclaved or sterilized before-hand.

2.2.2.2 Passaging

Cells were expanded and upon confluency passaged 1:5 – 1:10, depending on the cell line. Since all cell lines were adherent, they were detached using trypsin/EDTA. After the cells were visibly detached, they were resuspended in medium and spun down by centrifugation. The supernatant was then removed and the cells resuspended in fresh medium and distributed to new cell culture flasks.

2.2.2.3 Freezing and thawing of cells

Cells in presence of DMSO can be stored for a longer time period at -80°C or -150 °C. The steps for freezing cells were the same as for passaging them, but instead of resuspending them in fresh medium they were resuspended in freezing medium (50% FCS, 40% cell type specific medium, 10% DMSO). They were slowly cooled down in a freezing container until they reached -80°C. Storage was continued at -80°C or frozen stocks were transferred to -150°C.

For thawing the cells, they were rapidly thawed at 37°C, then resuspended in their respective medium. Cells were spun down by centrifugation, supernatant was removed and cells were seeded in fresh medium.

2.2.2.4 Determination of cell count

To determine the concentration of cells in a solution, a small amount of the cells was counted in an improved neubauer hemocytometer. Number of cells in a volume of 100 nl was counted and multiplied by 10^4, to determine the amount of cells per ml.

2.2.2.5 TGFβ2, HGF, and Tnfsf12 (TWEAK) stimulation

BMOL cells were seeded in 5 ml regular medium at a density of $1x10^5$ cells/ml in 6-cm dishes. After cells were adherent they were starved (0.5% FCS, 1mM Glutamine, 7.5 ng/ml IGF-II, 5 ng/ml EGF, 2.5 µg/ml Insulin) overnight. Following pretreatment with

3µM GI254023X or DMSO for 1 h cells were stimulated with 1 ng/ml rhTGFβ2, 20 ng/ml rmHGF, 50 ng/ml Tnfsf12 (TWEAK), or solvent for 15 min at 37°C.

2.2.2.6 Proliferation assay

BMOL cells were starved over several passages to 0.5% FCS and half the growth factors used in the growth medium (see Table 6). Cells were seeded in a 96-well plate with $2x10^4$ cells per well in 200 µl medium. At the time of the seeding cells were treated with the ADAM10 inhibitor GI254023X (3µM) or DMSO. Cells were incubated for 48h under normal cell culture conditions. Afterwards, medium was changed to 3-(4,5-dimethylthiazol-2-yl)-2,5-diphenyltetrazolium bromide (MTT)-containing medium (0.5 mg/ml) and cells were incubated for another 4 hours. Medium was removed and formazan crystals were dissolved in equal amounts of isopropanol. Adsorption was measured at 595 nm.

2.2.2.7 Tube formation assay

A 24-well plate was coated with 300 µl slowly thawed Matrigel per well. Matrigel had a protein concentration of > 10 mg/ml and was left for at least 3h at 37°C, 5% CO_2, and 95% RH to solidify. 300 µl of a $2x10^5$ cells/ml cell suspension plus the respective inhibitors were seeded on top of the Matrigel in each pre-coated well. Cells were incubated for approximately 24 h to form tubes. Pictures of formed tubes were taken with a AZ100 microscope with a DS-Fi2 camera (Nikon, Düsseldorf, Germany) and tube length and branching was evaluated with the ImageJ plugin 2D Skeleton.

2.2.3 Proteinbiochemistry

2.2.3.1 Protein lysate

Murine tissue samples were disrupted with beads in RIPA Buffer[7] in a power homogenizer (Precellys, with an additional Cryolys cooling unit; distributed by Peqlab, Erlangen, Germany) for 2 min at 6 000 rpm. Cultured cells were taken up directly in RIPA-Buffer. Lysates were incubated for 15 min on ice. Afterwards cell debris was spun down and supernatant was used for down-stream applications.

2.2.3.2 Determination of protein concentration

Protein concentration of lysates was determined via the Bradford test in technical duplicates. Briefly, 1 µl sample was added to 200 µl of Bradford solution (AppliChem, Darm-

7 RIPA-Buffer: 50 mM HEPES pH7.4, 150 mM NaCl, 1mM EDTA, 2 mM EGTA, 0,5% NP-40 , 50 mM NaF
add fresh: 1 mM PMSF, 1 mM NaV, 1.46 µM Pepstatin A, 1.54 µM Aprotinin, 2.1 µM Leupeptin

stadt, Germany) and carefully mixed. Absorption was measured at 595 nm. For quantification purposes calibration solutions, composed of known BSA concentrations in water (0.2 – 1 µg/µl), were measured in parallel.

2.2.3.3 Separation of proteins via SDS-PAGE

Proteins were separated according to their molecular weight by sodium dodecyl sulfate polyacrylamide gel electrophoresis (SDS-PAGE) under reducing conditions. A 10% separating gel[8] was prepared between two glass plates and after polymerization covered with a stacking gel[9] in which a comb was inserted. After complete polymerization the gel was put in an electrophoresis chamber, immersed in electrophoresis buffer[10], and the comb was removed. Protein samples were mixed with 5x loading buffer[11] and then heated for 5 min at 95°C. The samples were then put for a short time on ice to cool them down. Prestained protein marker (PageRuler™ Prestained Protein Ladder, ThermoScientific, Darmstadt, Germany) and the samples were loaded in the prepared pockets. The gel was then run until the tracking dye reached the anodic end of the gel.

2.2.3.4 Immunoblot analysis of proteins

The electrophoretically separated proteins were transferred to a polyvinylidene flouride membrane or a nitrocellulose membrane via so-called electroblotting. The blotting apparatus was assembled as follows (from anode to cathode): sponge, 2 layers of 3MM Whatman paper, membrane, gel, 2 layers of 3MM Whatman paper, sponge. The assembly of the apparatus took place in transfer buffer[12]. It is important to put the composition together without air bubbles, because otherwise the transfer does not work properly. The blotting apparatus was then positioned in a blotting chamber, which was filled with transfer buffer. The transfer was either for 90 min at RT (100 V) or over night at 4°C (30 V). After a successful transfer, the membrane was incubated for at least 1h in 5% BSA in PBS-T[13] to block unspecific binding sites. Thereafter, the membrane was incubated with the primary anti-body[14] also at least for one hour but preferably over night at 4°C. Following 3 wash steps with PBS-T, each 10 min, the membrane was treated for minimum 1 hour with the secondary HRP-coupled antibody[15]. Finally the membrane was washed 3 more times in

8 Separating gel (10%): 10 % Acrylamide, 350 mM bis-Tris pH6.5, 0.1% SDS, 0.1% APS, 0.06% TEMED
9 Stacking gel: 4% Acrylamide, 350 mM bis-Tris pH6.5, 0.1% SDS, 0.1 % APS, 0.1% TEMED
10 Running buffer: 250 mM MOPS, 250 mM Tris, 5 mM EDTA, 0.5% SDS, 5 mM Sodium bisulfite
11 5x Laemmli buffer: 250 mM Tris-HCl pH 6.8, 10% SDS, 50% Glycerine, 5% β-Mercaptoethanol 0.5% Bromophenol blue
12 Transfer buffer: 25 mM Tris, 200 mM Glycine, 20% Methanol
13 PBS-T: 136 mM NaCl, 2.68 mM KCl, 10 mM Na_2HPO_4, 1.76 mM KH_2PO_4, adjust to pH 7.4 and add 0.05% Tween-20
14 primary antibody diluted in 5% BSA, 0.1 % Sodium azide in PBS-T, specific dilution given in Table 4
15 secondary antibody diluted in PBS-T, specific dilutions given in Table 5

PBS-T and once in water. For developing, one volume reagent 1 was mixed with one volume reagent 2 from a chemoluminescence kit (ThermoScientific, Darmstadt, Germany). The mixture was incubated for 1 min, then put on the membrane and incubated for 5 min. After the removal of superfluous liquid, blots were developed in an intelligent dark box (Fujifilm, Düsseldorf, Germany) with a LAS-1000 camera (Fujifilm, Düsseldorf, Germany). The particular exposure times were determined individually.

2.2.3.5 Stripping of membranes

Membranes were covered with mild stripping buffer[16] and incubated at RT for 5-10 min. This step was repeated with fresh buffer. Membranes were washed twice in PBS for at least 10 min and afterwards washed twice in PBS-T for at least 5 min. Membranes were then ready for the blocking stage.

2.2.4 Statistics

Data are shown as mean ± standard error of mean if not stated otherwise. Comparisons between two groups were performed by applying the student's t-test. If data did not have equal variances or were not normally distributed, the Mann-Whitney-U test was employed instead. All analyses were conducted using SigmaPlot 12.0 Software (Systat Software, Erkrath, Germany). A p-value <0.05 was considered statistically significant.

16 Mild stripping buffer: 200 mM Glycine, 3,47 mM SDS, 1% Tween-20, adjust pH to 2.2

3 Results

ADAM 10 was shown to play a vital role in both organ development and tissue integrity in several organs. Yet, there are little data concerning ADAM10 in physiological and pathological situations of the liver. To assess the function of ADAM10 in the liver we conceived the following study.

3.1 Alfp-Cre is active in hepatoblasts, cholangiocytes, and hepatocytes

A complete knockout of ADAM10 is embryonic lethal. Therefore we used previously generated ADAM10$^{fl/fl}$ mice. ADAM10$^{fl/fl}$ mice have loxP sites flanking exon 2 [108] (see Figure 1.10). Excision of exon 2 using a Cre-recombinase leads to a frame shift and consequently to an immediate premature stop-codon, leading ultimately to an abrogation of ADAM10 expression. We crossed ADAM10$^{fl/fl}$ mice with mice carrying a Cre-recombinase under an albumin promoter with an additional α-fetoprotein enhancer [110]. Activity of the Cre-recombinase starts at embryonic day of gestation 10.5 and is limited to hepatoblasts, adult liver progenitor cells, cholangiocytes and hepatocytes [110].To confirm the location of Cre-induced recombination events we cross-bred Alfp-Cre^{+} mice with a reporter strain for Cre activity. These reporter mice are transgenic for a loxP-flanked STOP cassette followed by a sequence coding for enhanced yellow fluorescent protein (EYFP) which are inserted in the ROSA26 locus. ROSA26 is a locus known for constitutive, ubiquitious expression in mice. When Cre-recombinase is present in these mice the STOP sequence is excised and enhanced yellow fluorescent protein is expressed in the Cre-positive tissues. These ROSA_STOP_EYFP mice can be used to monitor Cre-expression and for lineage-tracing (Figure 3.1 A).

We detected EYFP expression in ROSA_STOP_EYFP reporter mice that are heterozygous for Alfp-Cre by anti-GFP immunohistochemistry. Staining was observed in both 4 week and 15 week old animals. Distribution of EYFP was in both age groups clearly limited to hepatocytes and cholangiocytes. Endothelial cells lining blood vessel are not stained (Figure 3.1 B, magnified area shows a bile duct surrounded by hepatic parenchyma and endothelial cells). Next to immunohistochemistry we also investigated EYFP expression by immunoblot analysis. In the livers of mice lacking Cre-recombinase no GFP signal was detectable whereas in the livers of mice with Cre-recombinase activity a signal was detect-

able (Figure 3.1 C). Other tissues tested, like kidney and spleen, did neither show signals in immunohistochemistry nor in immunoblot analysis even if animals were Alfp-Cre^{+} (data not shown).

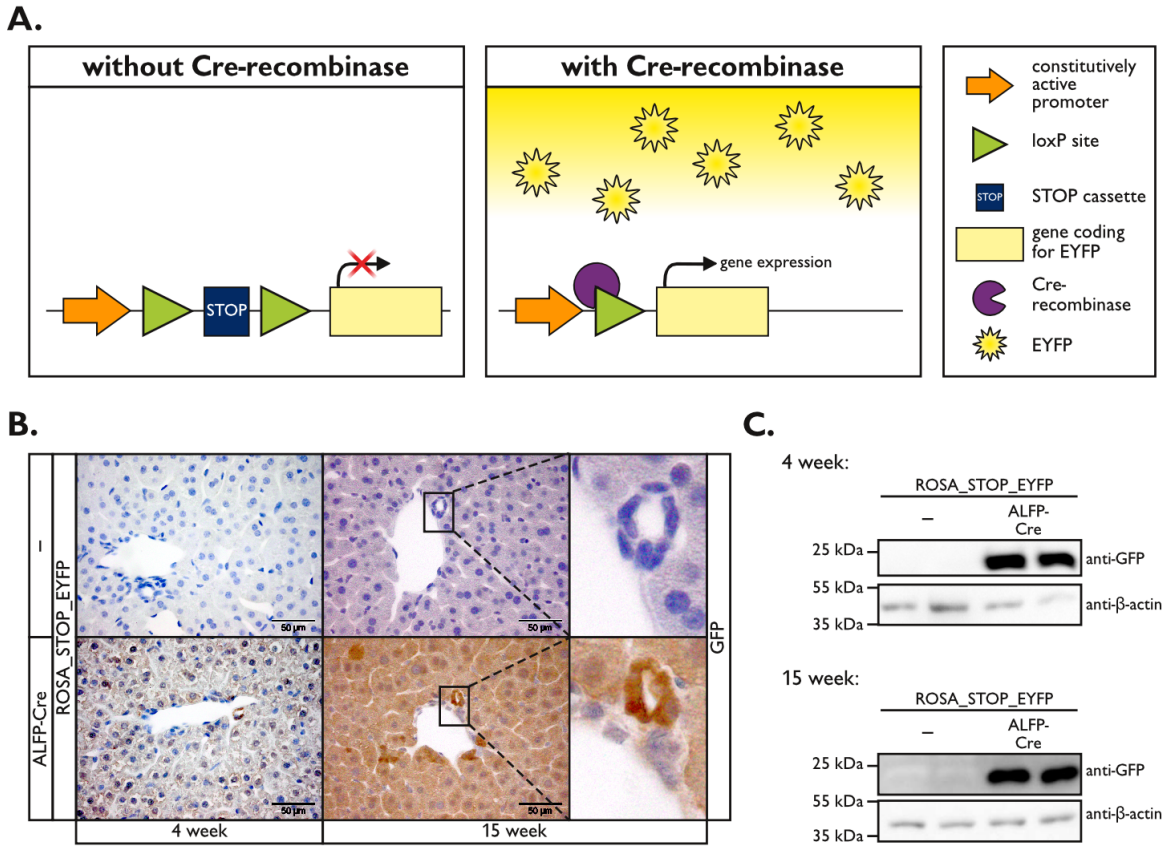

Figure 3.1: Alfp-Cre targets liver progenitor cells, cholangiocytes, and hepatocytes

A: Schematic of the ROSA_STOP_EYFP Cre reporter system. A floxed stop cassette followed by a sequence coding for EYFP is inserted in the constitutively active ROSA26 locus. Cre-recombinase leads to deletion of the stop cassette and accordingly to expression of EYFP. **B:** Alfp-Cre targets hepatocytes and cholangiocytes as demonstrated by cross-breeding with ROSA_STOP_EYFP mice and subsequent anti-GFP (also detecting EYFP) immunohistochemistry of liver tissue sections. Scale bars indicate 50 µm. **C:** Immunoblotting of total liver extracts of ROSA_STOP_EYFP mice with or without Alfp-Cre using anti-GFP antibodies. β-actin serves as loading control. (Immunoblot courtesy of S. Wetzel.)

3.2 ADAM10$^{\Delta hep\Delta ch}$ mice show efficient recombination and deletion of ADAM10 in the liver

We bred mice that are homozygous for floxed ADAM10. 50% carry the Alfp-Cre transgene heterozygously, the other 50% are Cre-negative (see Figure 2.2). They are of a mixed 129/C57BL6 background. Mice without Alfp-Cre will be from now on termed ADAM10$^{fl/fl}$ and serve as littermate control. Mice that are tested positive for Alfp-Cre will be referred to as ADAM10$^{\Delta hep/\Delta ch}$.

All further analysis was based on the premise that the bulk mass of the liver consists of the targeted hepatocytes and cholangiocytes. All tests were therefore performed on whole liver tissue unless stated otherwise.

ADAM10$^{\Delta hep/\Delta ch}$ mice show an efficient recombination of the floxed exon 2 of *adam10* as proven by analysis of liver-derived genomic DNA (Figure 3.2 A). They furthermore display a significant reduction of ADAM10 on the transcriptional level at the age of 4 week. At the age of 15 week ADAM10 mRNA is still reduced compared to controls. However, the reduction is not statistically significant anymore at this age (Data shown in doctoral thesis of S. Wetzel). A reason for this can be the increased presence of cell types other than liver progenitor cells, hepatocytes, and cholangiocytes in the liver due to the later described occurring phenotype.

On the protein level we observed a reduction of both the pro-form and the mature form of ADAM10 in the KO-mice. The residual ADAM10 stems probably from non-targeted cells in the liver, like hepatic stellate cells (Figure 3.2 B).

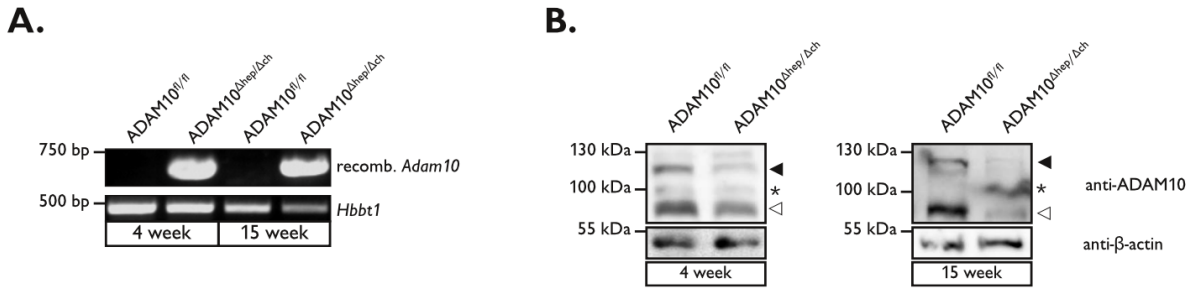

Figure 3.2: Alfp-Cre expressing mice show an efficient recombination and deletion of ADAM10

A: Successful recombination of exon 2 of *adam10* in ADAM10$^{fl/fl}$ mice expressing Cre under the Alb promoter and Afp enhancer elements. **B:** ADAM10 protein expression is decreased in total liver extracts of ADAM10$^{fl/fl}$ mice expressing Cre under the Alb promoter and Afp enhancer elements as shown by immunoblot. Asterisk marks unspecific band. Filled arrowhead marks pro-form of ADAM10. Blank arrowhead marks mature form of ADAM10. (Immunoblot courtesy of S. Wetzel.)

Data represent the mean ± standard error of the mean. (** - P<0.01)

ADAM10$^{\Delta hep/\Delta ch}$ mice varied in the penetrance of the resulting phenotype. However, mice with a liver-specific deletion of ADAM10 on a pure (100%) C57BL/6 background developed a similar phenotype but with a slower kinetic (personal communication with K. Chalupsky/ R. Sedlacek, Institute of molecular genetics, Academy of Science of the Czech Republic, Prague, Czech Republic). We concluded therefore, that the observed phenotype can be specifically traced back to a lack of ADAM10 in liver progenitor cells, hepatocytes, and cholangiocytes.

For our analysis we focused on 129/C57BL6 mice that showed strong necrosis and/or fibrosis. This was the case for approximately 30-50% of the ADAM10$^{fl/fl}$ offspring that were also Alfp-Cre^{+}.

3.3 Hepatic deficiency of ADAM10 leads to postnatal necrosis

Mice with a hepatic deficiency of ADAM10 showed macroscopic signs of liver damage at the age of 4 week. At the age of 15 week the white spots were no longer macroscopically visible. All ADAM10$^{\Delta hep/\Delta ch}$ animals had elevated serum levels of alanine transaminases and alkaline phosphatases (data shown in the doctoral thesis of S. Wetzel). Both serve as markers for liver damage. We then analyzed hematoxylin and eosin (H&E) stained histological liver sections. In 4 week old mice we detected numerous foci of a pale pink staining that were located mainly in zone 2 of the liver between the portal triad and the central vein. The areas had a distinct sharp border and show most likely necrotic areas due to hepatocyte death. In 15 week old ADAM10$^{\Delta hep/\Delta ch}$ mice the necrotic regions are drastically reduced (Figure 3.3 A).

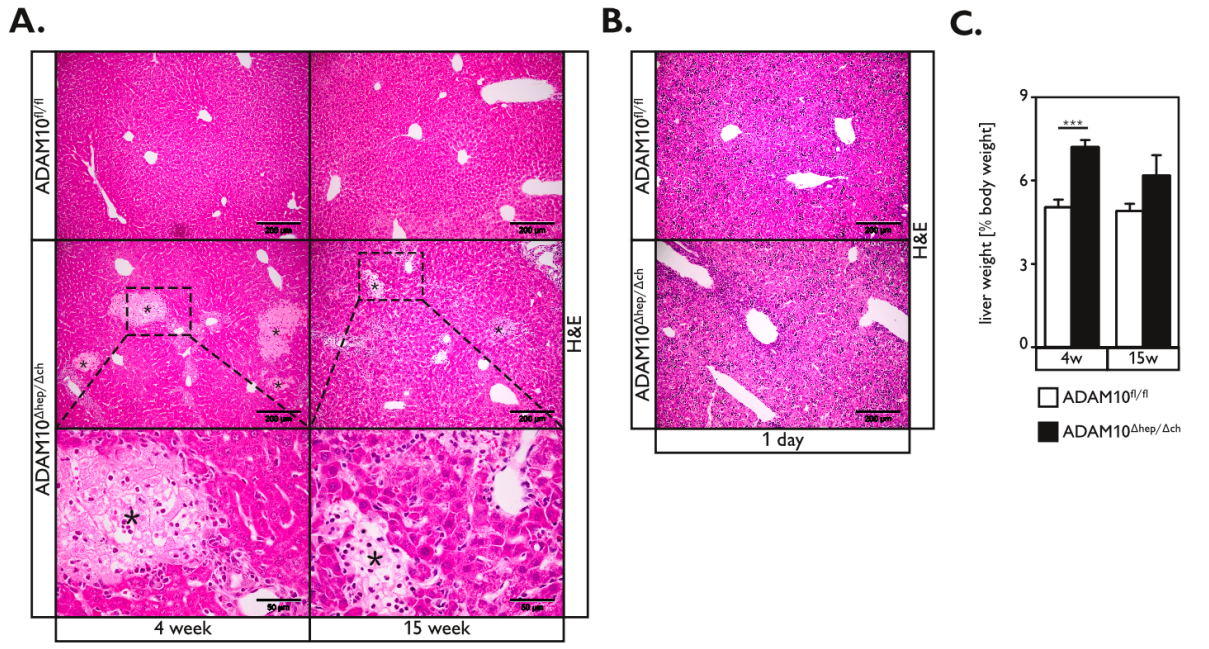

Figure 3.3: Mice deficient for ADAM10 in the liver develop spontaneous hepatocyte necrosis

A: Hematoxylin and Eosin (H&E) staining of histological sections reveals necrotic areas in zone 2 in the livers of ADAM10$^{\Delta hep/\Delta ch}$ mice. The amount of necrotic areas is reduced in older mice. Necrotic areas are marked by asterisk. Scale bars indicate 200 µm and in magnified areas 50 µm **B:** Livers of newborn ADAM10$^{\Delta hep/\Delta ch}$ mice show no abnormalities compared to control mice. Scale bars represent 200 µm. **C:** ADAM10$^{\Delta hep/\Delta ch}$ mice develop hepatomegaly. (n=4-16)

Data represent the mean ± standard error of the mean. (*** - P<0.001)

We wanted to examine if the necrotic spots were due to an embryonic developmental defect. To that end we sacrificed newborn mice and evaluated their livers in H&E stained histological sections for appearance of necrotic areas. Interestingly, the livers of newborn ADAM10$^{\Delta hep/\Delta ch}$ mice showed no signs of necrosis or other alterations (Figure 3.3 B). We hence deduced that hepatocyte death is triggered by an event in postnatal liver development.

Furthermore, we noticed that the liver weight (normalized to the body weight) of 4 week old ADAM10-deficient mice was significantly increased compared to control mice. In older mice liver weight, though still elevated, approximates that of WT animals (Figure 3.3 C). It is probable that the increased liver weight is caused by a compensatory liver growth to adjust for the necrotic foci.

3.4 Bile duct function but not formation is impaired in ADAM10$^{\Delta hep\Delta ch}$ mice

We hypothesized that, while not being caused by a prenatal developmental defect, hepatocyte death could be caused by impaired bile duct formation after birth. This seemed a likely explanation considering reports linking the ADAM10 substrate Notch2 to biliary development [6, 7, 112].

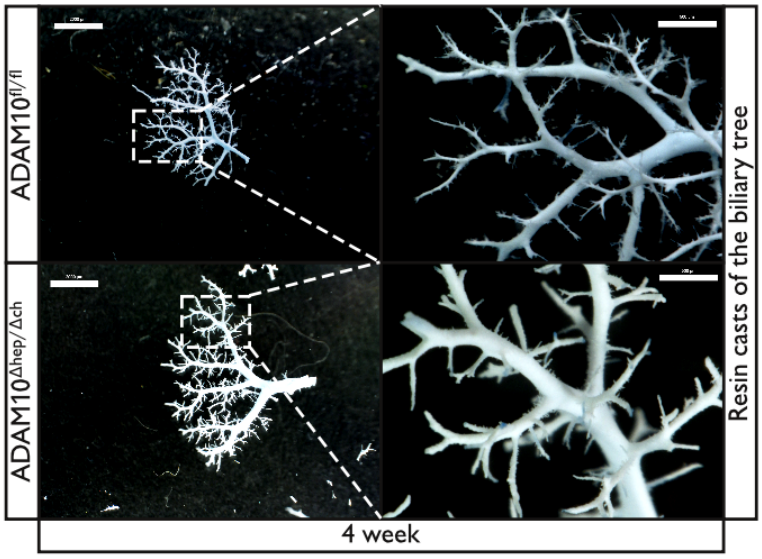

Figure 3.4: ADAM10$^{\Delta hep/\Delta ch}$ mice show normal development of the biliary tree

Resin casts of the biliary tree show no distinct differences between WT and KO animals. Scale bars indicate 2000 µm and in magnified areas 500 µm

In order to analyze the gross morphology of ADAM10$^{\Delta hep/\Delta ch}$ mice we generated resin casts of the biliary tree of 4 week old mice. Resin casts of KO and WT animals look identical (Figure 3.4 A).

To investigate a possible effect of ADAM10 on biliary tube formation we set up an *in vitro* experiment with the bipotential BMOL progenitor cell line. BMOL cells are described to form luminal tubular structures, similar to bile ducts, when plated on Matrigel [113]. We used inhibitors to block the activity of ADAM10 (GI254023X), ADAM10 and -17 (GW208264X), and γ-secretases (DAPT) in BMOL cells.

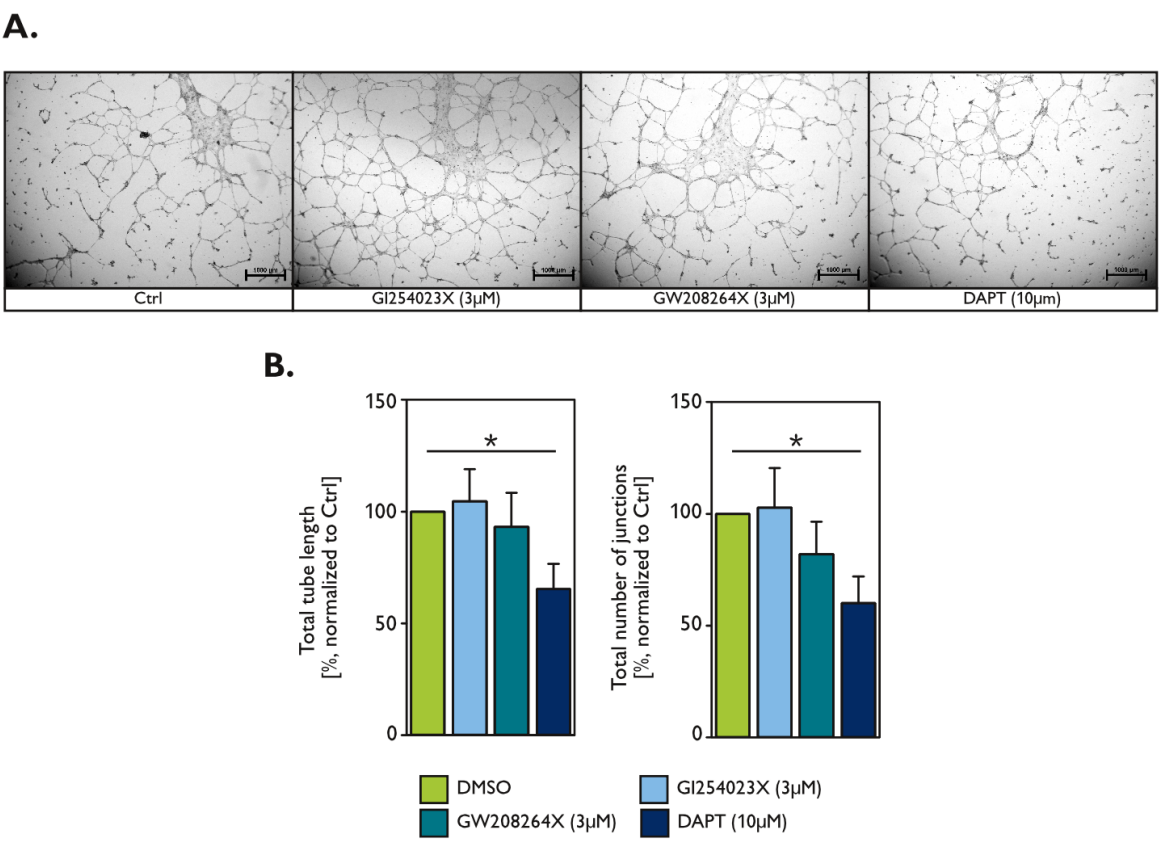

Figure 3.5: ADAM10 does not impair Notch-dependent tube formation

A: Tube formation of BMOL cells on a matrigel layer is not diminished in the presence of the ADAM-Inhibitors GI251023X and GW208264X but by the γ-Secretase-Inhibitor DAPT. Scale bar represents 1000 µm **B:** Quantification of A. All branches with at least one junction were counted and data were normalized to the control to account for variations between experiments. (n=5)

Data represent the mean ± standard error of the mean. (* - P<0.05)

We observed no differences in tube formation in cells when ADAM10 is blocked by GI254023X. We see a slight but not significant reduction of both, total tube length and number of junctions, in cells treated with GW208264X. However, we can reproduce the

findings by Fiorotto et al [113] that inhibition of γ-secretase mediated cleavage by DAPT leads to shorter overall tube length and also to less junctions. Fiorotto et al correlated the reduction in tube length and junctions to Notch activation. Interestingly, we do not see an effect on tube-formation by blocking ADAM10 activity (Figure 3.5 A+B). This suggests that ADAM 10 is, in this model, not the α-sheddase responsible for Notch cleavage.

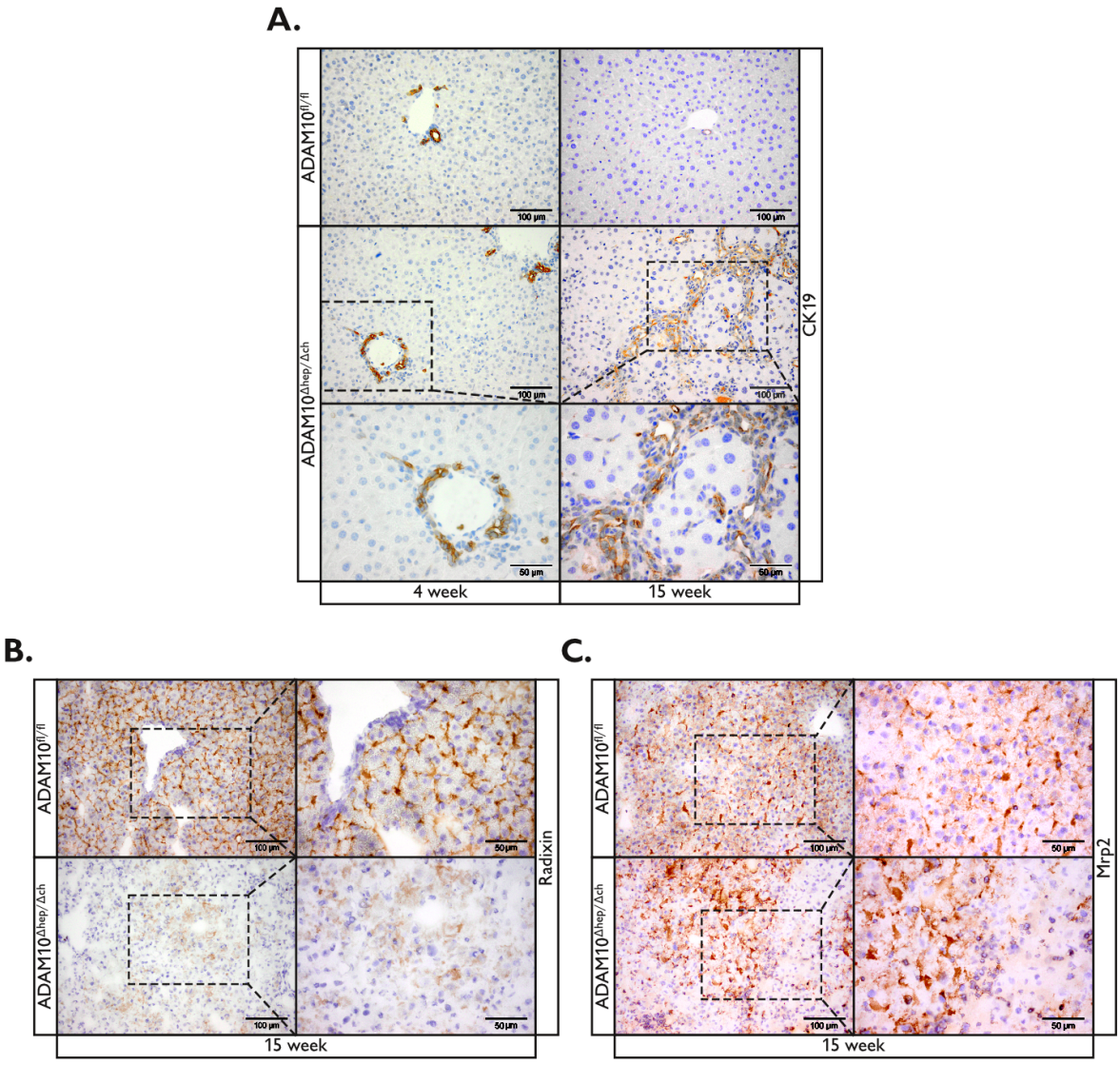

Figure 3.6: ADAM10$^{\Delta hep/\Delta ch}$ mice have more ductular biliary structures but less functional bile canaliculi

A: Immunohistological staining of cytokeratin (CK) 19^{+} liver progenitor and biliary cells demonstrates a ductular reaction in the livers of ADAM10-deficient animals that increases over time. Scale bars indicate 100 µm and in magnified areas 50 µm. **B+C:** Immunohistological staining of Radixin and multidrug resistance-associated protein 2 (Mrp2) in liver tissue sections reveals reduced number of bile canaliculi in ADAM10-deficient livers. Scale bars indicate 100 µm and in magnified areas 50 µm.

We wanted to examine biliary functionality in more detail in case of alterations on a cellular level. We stained histological liver sections for Cytokeratin (CK)-19^{+} cells. Cytokerat-

in19 is a known marker for cells of the hepatobiliary tract. Although Cytokeratin19 staining did not differ in livers of newborn mice (data are shown in the doctoral thesis of S. Wetzel), we detected slightly more Cytokeratin19^{+} structures in 4 week old ADAM10-deficient mice. The accumulation of Cytokeratin19^{+} cells was further amplified in 15 week old ADAM10$^{\Delta hep/\Delta ch}$ mice (Figure 3.6 A). This frustrane proliferation of biliary structures is termed ductular reaction. The underlying cause is proliferation of liver progenitor cells that, driven by Notch signaling, adopt a biliary fate. We examined the transcription levels of Notch receptors as well as those of downstream targets of the Notch pathway (data are shown in the doctoral thesis of S. Wetzel). Albeit we detected a slight decrease in Notch signaling we do not consider this critical for the observed phenotype.

Radixin is an ezrin-radixin-moesin protein in hepatocytes that is located to the bile canalicular membrane [114]. It is known to control the transport of apical bile transporters like the multidrug resistance-associated protein 2 (Mrp2) [115]. In the immunohistochemical stainings for Radixin we noted a striking difference between WT and KO in 15 week old mice. Whilst Radixin is evenly distributed in the livers of ADAM10$^{fl/fl}$ animals, it is almost extinct in ADAM10$^{\Delta hep/\Delta ch}$ mice (Figure 3.6 B). Mrp2 staining was as well reduced in 15 week old ADAM10$^{\Delta hep/\Delta ch}$ mice (Figure 3.6 C).

These results suggest that while the general architecture and formation of the biliary tree is unaffected by a liver-specific KO of ADAM10 the bile acid transport is impaired.

3.5 Liver inflammation is not strongly upregulated despite massive hepatic parenchymal damage

Damage in liver tissue leads to a strong inflammatory response. Levels of pro-inflammatory cytokines are increased and macrophages and granulocytes infiltrate the liver [17, 116]. Notwithstanding massive hepatic parenchymal damage, presence of F4/80^{+} macrophage was not increased in ADAM10-deficient mice. However F4/80^{+} macrophage clustered around the arising biliary structures in 4 week old ADAM10$^{\Delta hep/\Delta ch}$ mice. This is not completely surprising since macrophages secrete growth factors for liver progenitor cells [26]. This distribution of macrophages was also found in 15 week old ADAM10$^{\Delta hep/\Delta ch}$ mice (Figure 3.13 A).

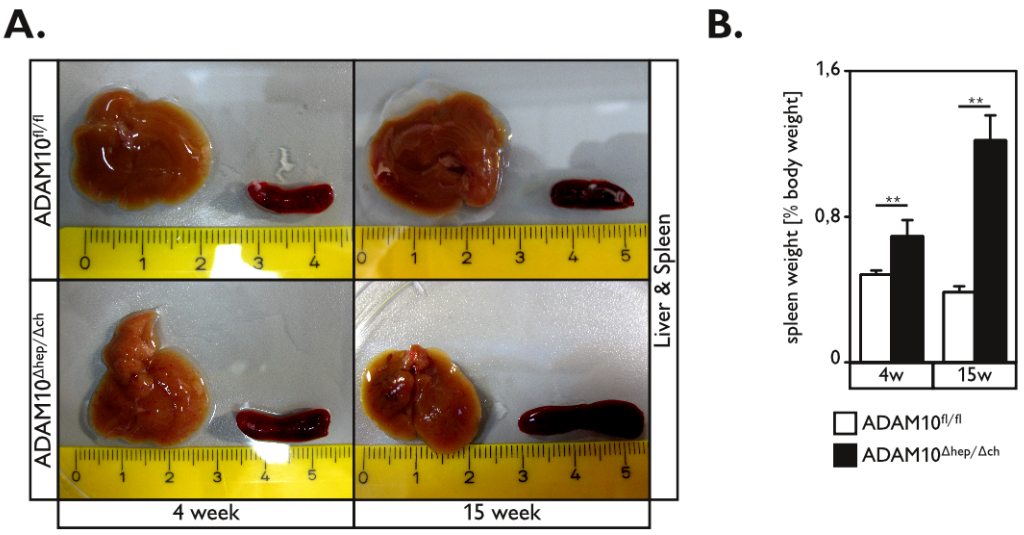

Figure 3.7: ADAM10$^{\Delta hep/\Delta ch}$ mice show enlarged spleen.

A: Macroscopic pictures of the liver and spleen. The spleens in animals with a hepatic deficiency of ADAM10 are increased. Linear dimension of the ruler is cm. **B:** Quantification of the spleen weight compared to the body weight. (n=4-16)

Data represent the mean ± standard error of the mean. (** - P<0.01)

We observed mild infiltration of Ly6G^{+} neutrophil granulocytes to the necrotic foci of both age groups of ADAM10-deficient animals (Figure 3.8 A). The infiltrated neutrophilic granulocytes removed necrotic tissue as demonstrated by ultrastructural analysis (Figure 3.8 B). ADAM10$^{\Delta hep/\Delta ch}$ mice had an increase in CD3^{+} T-lymphocytes that was mainly restricted to the immediate vicinity of the portal triad. We noticed almost no CD3^{+} cells in or around the necrotic areas (Figure 3.8 C).

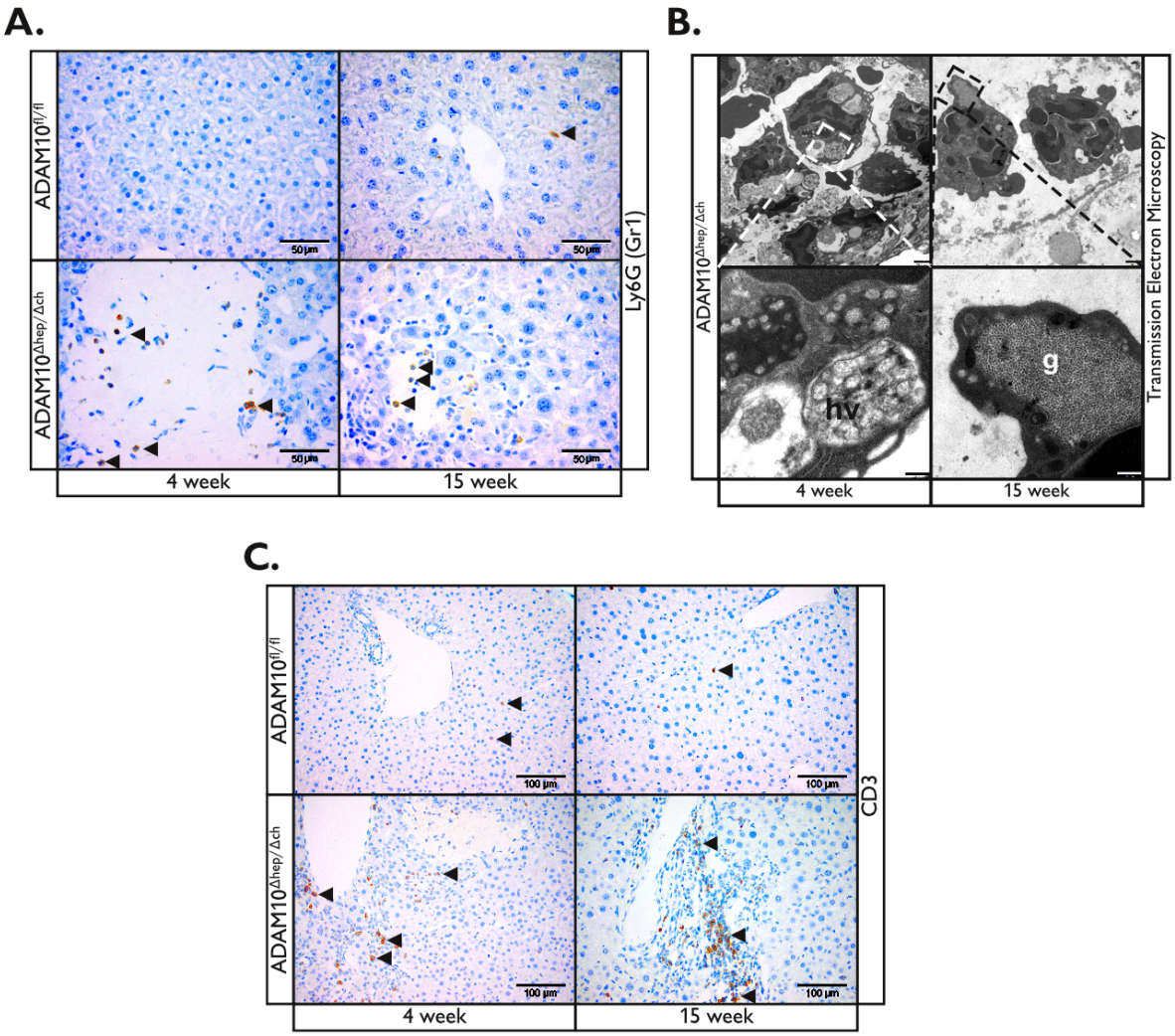

Figure 3.8: The inflammatory response to the hepatic damage in ADAM10$^{\Delta hep/\Delta ch}$ is limited

A: Immunohistochemical staining of Ly6G in liver tissue discloses infiltration of neutrophils (marked by arrowheads) to the necrotic areas. Scale bars indicate 50 µm **B:** Transmission electron micrographs of neutrophils removing necrotic liver tissue. Scale bars indicate 1000nm and in magnified areas 250 nm. hv: engulfed hepatocyte vacuole, g: engulfed glycogen-filled vacuole. (courtesy of R. Lüllmann-Rauch) **C:** Liver tissue sections of ADAM10$^{\Delta hep/\Delta ch}$ mice show an increase of CD3^{+} cells in the vicinity of biliary structures and few in the hepatic parenchyma. Arrowheads point to CD3^{+} cells. Scale bars represent 100 µm.

Despite a comparatively moderate immune response, ADAM10$^{\Delta hep/\Delta ch}$ animals showed spleenomegaly already at 4 week of age which was further increased at 15 week of age (Figure 3.7 A+B).

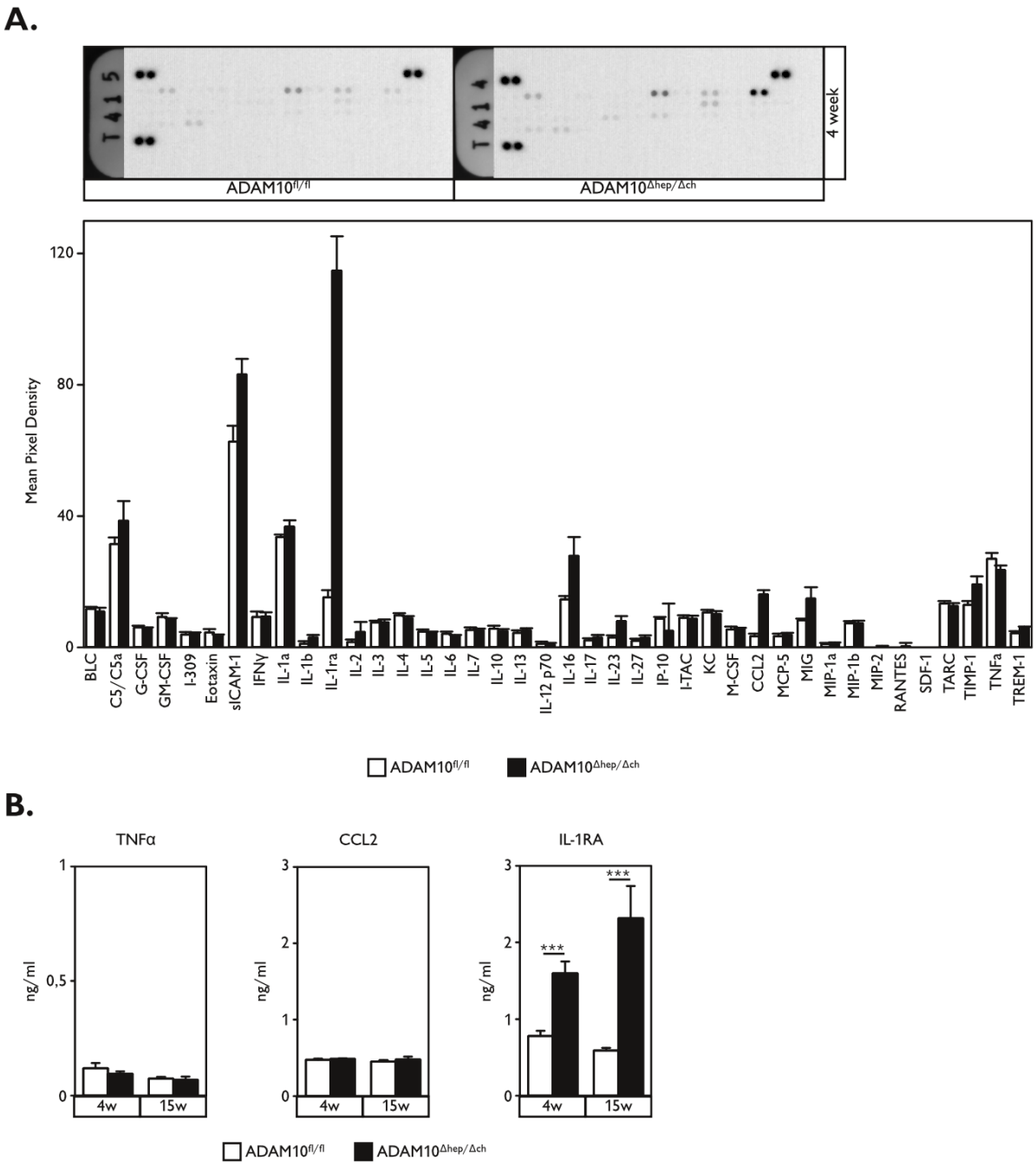

Figure 3.9: Anti-inflammatory cytokines are upregulated in mice with liver-specific deficiency of ADAM10

A: A cytokine array was performed on the total liver extracts of 4 week old animals. A representative image for both control and ADAM10 lacking animals is shown. All arrays are quantified in the bar chart. (n=2) **B:** Quantification of ELISAs for tumor necrosis factor α (TNFa), chemokine C-C motif ligand 2 (CCL2), and Interleukin-1 receptor antagonist (IL-1RA) from total liver extract. (n=3-5)

Data represent the mean ± standard error of the mean. (*** - P<0.001)

We performed a cytokine array on tissue samples of 4 week old mice to test for alterations in cytokine and chemokine levels of KO mice compared to WT mice.

Surprisingly, only few proteins showed an alteration compared to the control samples (Figure 3.9 A). We decided to examine the proteins with the most distinct differences between WT and KO animals by ELISA. Despite an upregulation in the cytokine array, Chemokine C-C motif ligand 2 (CCL2) was not found to be upregulated in the ELISA. Neither was the pro-inflammatory cytokine Tumor necrosis factor α (TNFα). But we confirmed a striking upregulation of interleukin-1 receptor antagonist (IL-1RA) (Figure 3.9 B). IL-1RA blocks interleukin-1 signaling and thus acts anti-inflammatory [117]. IL-1RA is also known to oppose senescence, possibly interfering with deactivation of hepatic stellate cells [118]. We reasoned that, whilst levels of pro-inflammatory proteins stay constant, upregulation of anti-inflammatory proteins lead to the observed mild inflammatory response, independent of the damage.

3.6 Hepatic regeneration processes are efficient in the repair of the lesions

When we stained for glycogen content with Periodic acid-Schiff we noticed that necrotic spots are surrounded by hepatocytes that have a lower glyogen content than hepatocytes in non-damaged areas (Figure 3.10 A).

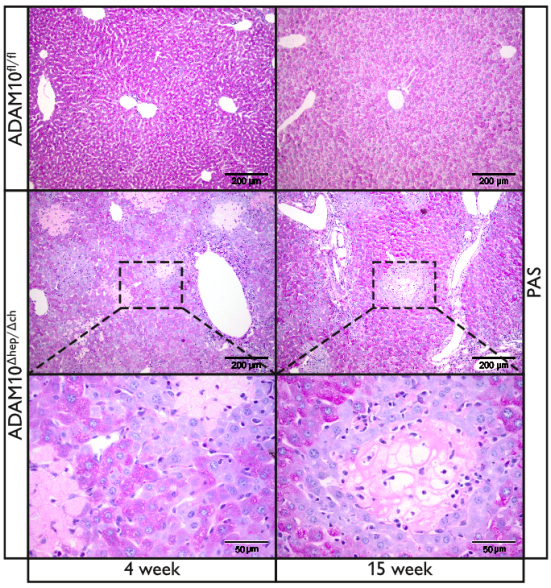

Figure 3.10: Glycogen content of hepatocytes in the livers of ADAM10$^{\Delta hep/\Delta ch}$ animals is reduced around necrotic areas.

New healthy hepatocytes arise around the necrotic areas. Due to their low glycogen content they appear lighter than the surrounding older hepatocytes. Scale bars indicate 200µm and in the magnified areas 50 µm.

Since the latter hepatocytes are stained strongly for glycogen and since animals were not starved, we concluded that those are newly formed hepatocytes indicating regeneration.

The observation that the lighter stained cells appear only around older necrotic areas (partially dissolved cells, 15 week panel) and not around fresher necrotic areas (cells still have hepatocytic morphology, 4 week panel) suggests that the lighter stained cells are not newly necrotic cells.

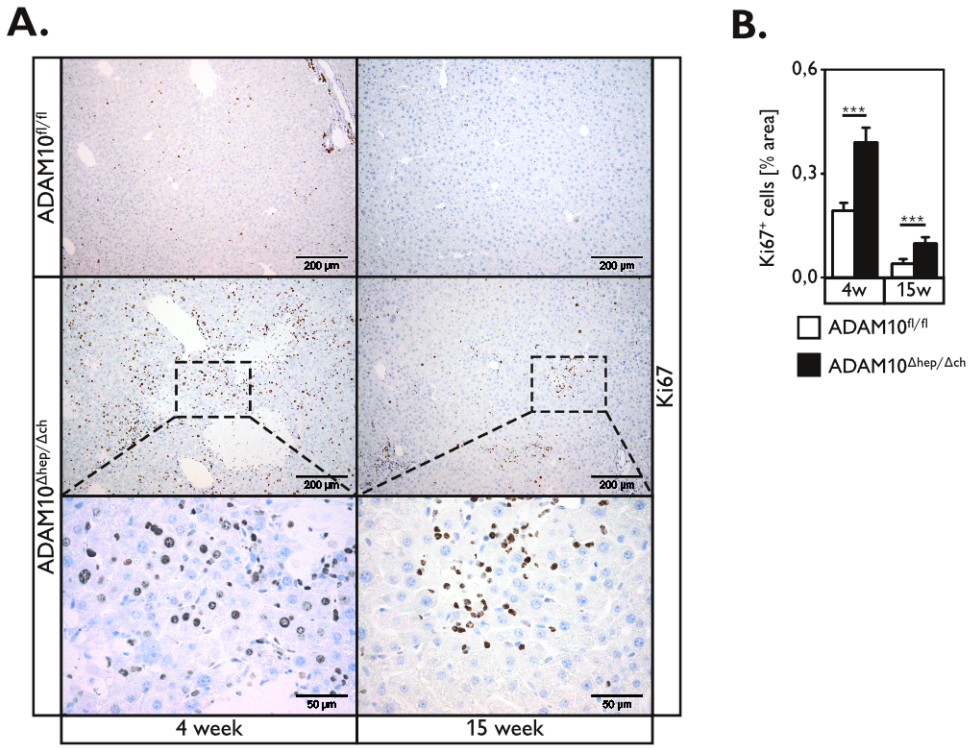

Figure 3.11: Increased proliferation in ADAM10$^{\Delta hep/\Delta ch}$ animals

A: Proliferative areas in the liver as assessed by Ki67 staining. Scale bars represent 200 µm and in the magnified areas 50µm. **B:** Quantification of B attests the increase of proliferation in the livers of ADAM10$^{\Delta hep/\Delta ch}$ animals. (n=3-15)

Data represent the mean ± standard error of the mean. (*** - P<0.001)

Due to the earlier observation that necrotic lesions are reduced in 15 week old KO mice compared to 4 week old KO mice we investigated hepatic regeneration processes. We thus stained liver sections with Ki67 antibody to assess proliferative activity. In 4 week old ADAM10$^{\Delta hep/\Delta ch}$ mice the amount of proliferating cells was almost doubled compared to controls. The same is the case for 15 week old animals, although total area covered by Ki67^{+} cells was lower. We reasoned that total numbers are reduced in older animals because less proliferation is needed to repair the few remaining necrotic lesions (Figure 3.11 A+B).

3.7 Loss of ADAM10 leads to activation and proliferation of the liver progenitor cell compartment

Interestingly, we found not only hepatocytes that were positive for Ki67 but also small cells with little cytoplasm. Their morphology led us to hypothesize that they are liver progenitor cells. To investigate this, we stained liver tissue sections for pan-cytokeratin (panCK), a marker found in both biliary epithelial cells and liver progenitor cells, and Ki67 (Figure 3.12).

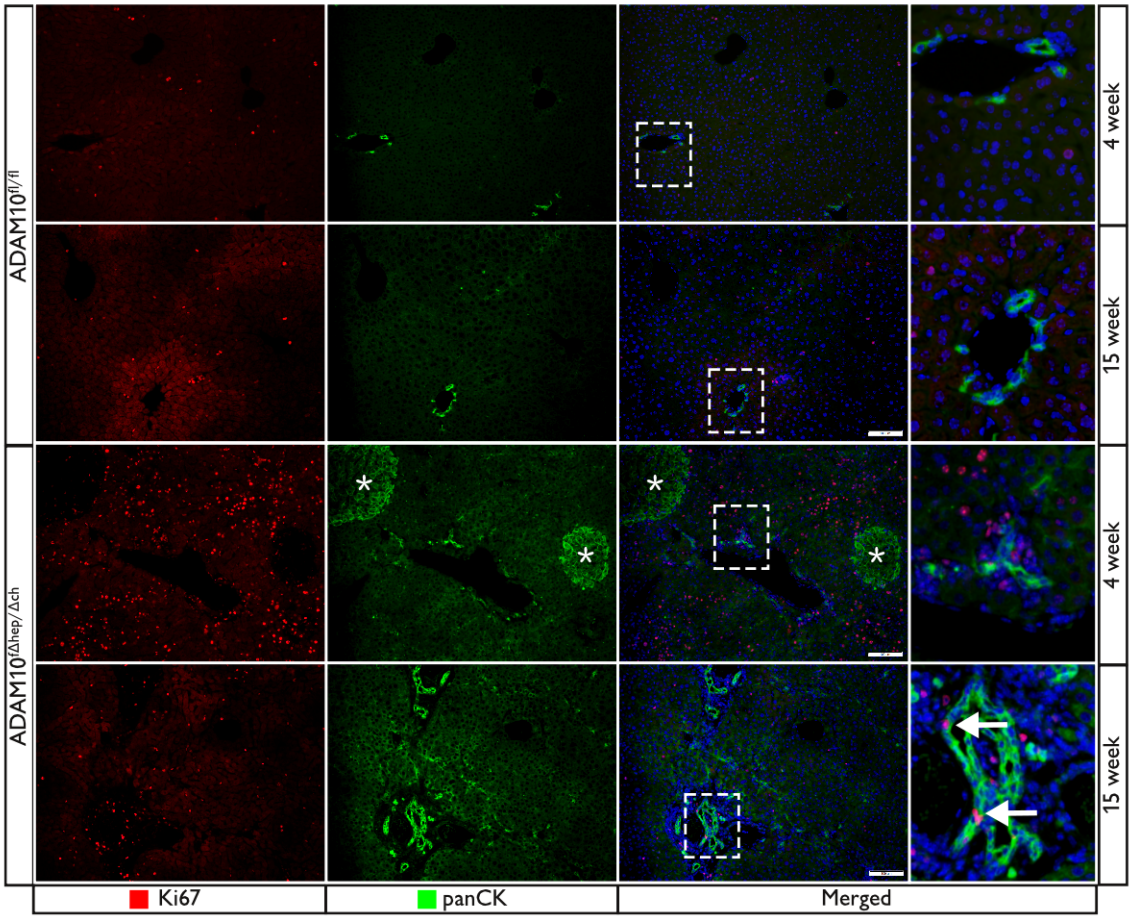

Figure 3.12: Detection of proliferating liver progenitor cells in 15 week ADAM10$^{\Delta hep/\Delta ch}$ mice.

Immunofluorescent co-staining of pan-cytokeratin (panCK) and the proliferation marker Ki67 in liver tissue. Asterisk mark unspecific panCK staining of necrotic hepatocytes. Arrows indicate panCK$^+$ Ki67$^+$ liver progenitor cells. Scale bars indicate 100 µm. Magnified areas are marked by dashed squares.

In ADAM10$^{fl/fl}$ mice we detected only pan-cytokeratin$^+$ biliary epithelial cells in the portal triad. Whereas in animals deficient for ADAM10 in the liver we saw the earlier described ductular reaction (see page 38) as well as single pan-cytokeratin$^+$ liver progenitor cells in the parenchyma. And indeed, we observed pan-cytokeratin$^+$ Ki67$^+$ liver progenitor cells in

15 week old animals supporting our earlier notion of proliferating liver progenitor cells in the older animals.

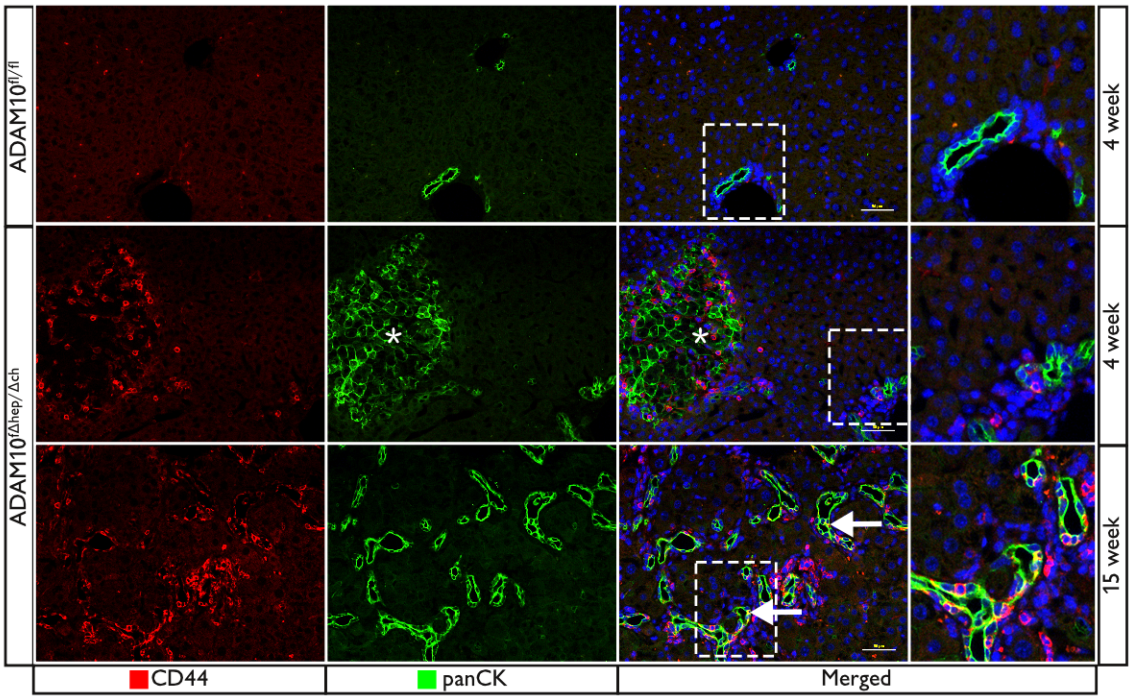

Figure 3.13: Liver progenitor cells in the vicinity of ductular reactions

Ductular reaction and accumulation of liver progenitor cells as marked by pan-cytokeratin (panCK) and CD44 staining of liver tissue sections of ADAM10$^{\Delta hep/\Delta ch}$ mice. Images from 4-week old wild type animals are representative for both age groups. Asterisk mark unspecific panCK staining of necrotic hepatocytes. Arrows indicate potentially tumorigenic panCK^{+} CD44^{+} liver progenitor cells. Scale bars indicate 50 µm. Magnified areas are marked by dashed squares.(courtesy of J. Köhn)

To examine the pan-cytokeratin^{+} cells more thoroughly, we additionally investigated CD44 expression. CD44 is a receptor for hyaluronic acid but can also bind other ligands, such as osteopontin. CD44 is proposed to regulate cell-cell and cell-matrix interactions and thereby influences cell adhesion and migration [119]. CD44 signaling can be regulated through ADAM10-mediated ectodomain shedding [58]. Due to its role in migration and tumor progression, CD44 has been discussed as a liver cancer stem cell marker [29]. In the thioacetamide model of chronic liver injury CD44 is initially mainly found on macrophages but as injury progresses CD44 expression is also found in panCK^{+} progenitor cells (personal communication with J. Köhn/ N. Tirnitz-Parker, School of Biomedical Sciences, Curtin University, Perth, Australia). We observe in our model a similar distribution of CD44. In younger animals CD44 staining is restricted to immunocytes in necrotic areas or surrounding ductular areas, whereas in 15 week old mice CD44 co-localized with panCK (Figure 3.13).

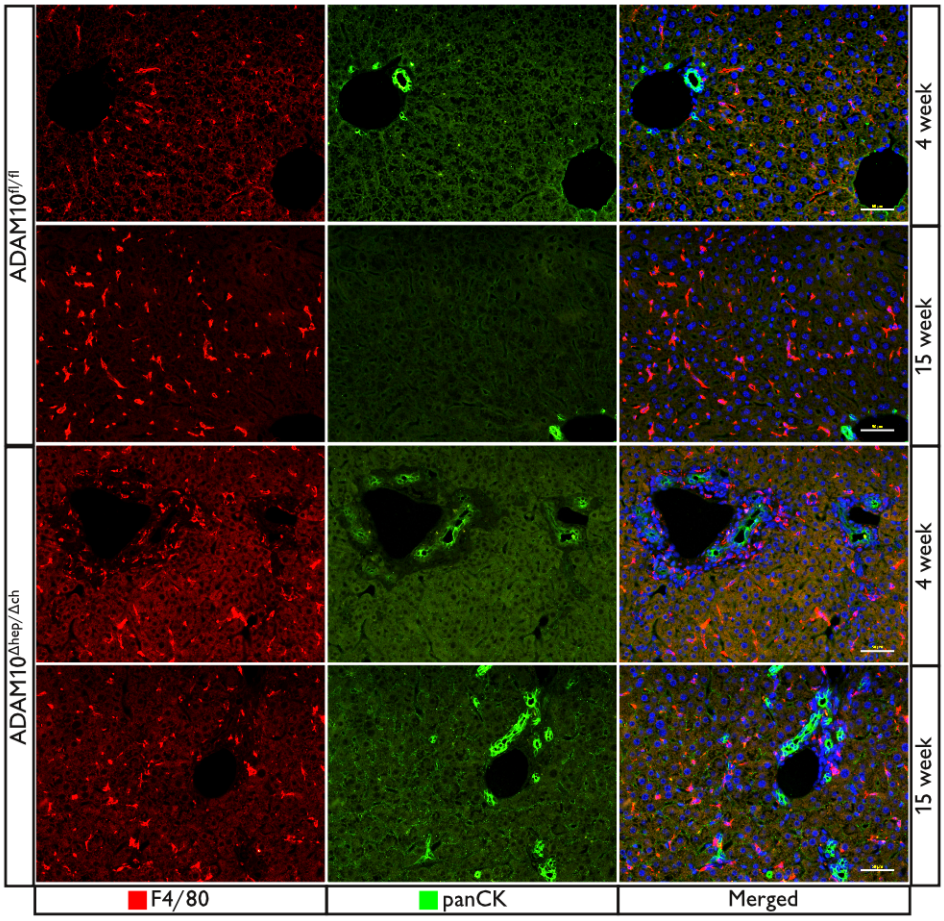

Figure 3.14: Ductular reaction and proliferation of liver progenitor cells

Ductular reaction and accumulation of liver progenitor cells in ADAM10$^{\Delta hep/\Delta ch}$ mice as marked by pan-cytokeratin and F4/80 macrophage staining of liver tissue sections Scale bars represent 50 µm. (courtesy of J. Köhn)

In co-stainings for pan-cytokeratin and F4/80 we noted a clustering of macrophages in ADAM10$^{\Delta hep/\Delta ch}$ mice compared to controls, where macrophages were distributed more equally. The clustered macrophages were mainly in close proximity to pan-cytokeratin^{+} cells (Figure 3.14). At present we can not state whether the F4/80 cells consist of Kupffer cell or also of infiltrated macrophages. Macrophages are described to be the source of the liver progenitor cell mitogen tumor necrosis factor-like weak inducer of apoptosis (Tnfsf12, also known as TWEAK) that binds to its receptor Tnfrsf12a (also known as Fn14) expressed by liver progenitor cells and thereby driving progenitor cell proliferation [26].

Thus we measured mRNA levels of Tnfsf12 and Tnfrsf12a in whole liver extracts. While we did not observe an upregulation of Tnfsf12, we discovered significantly increased levels of Tnfrsf12a in ADAM10$^{\Delta hep/\Delta ch}$ animals (Figure 3.15 A). This increase can be due to an

upregulation of expression, to an increase in numbers of cells expressing Tnfrsf12a, or to a combination of both.

These observations are in accordance with previous findings showing that release, but not expression, of Tnfsf12 is altered whereas Tnfrsf12a expression on liver progenitor cells is upregulated [26]. This supports the notion that these mice show an increased proliferation of liver progenitor cells.

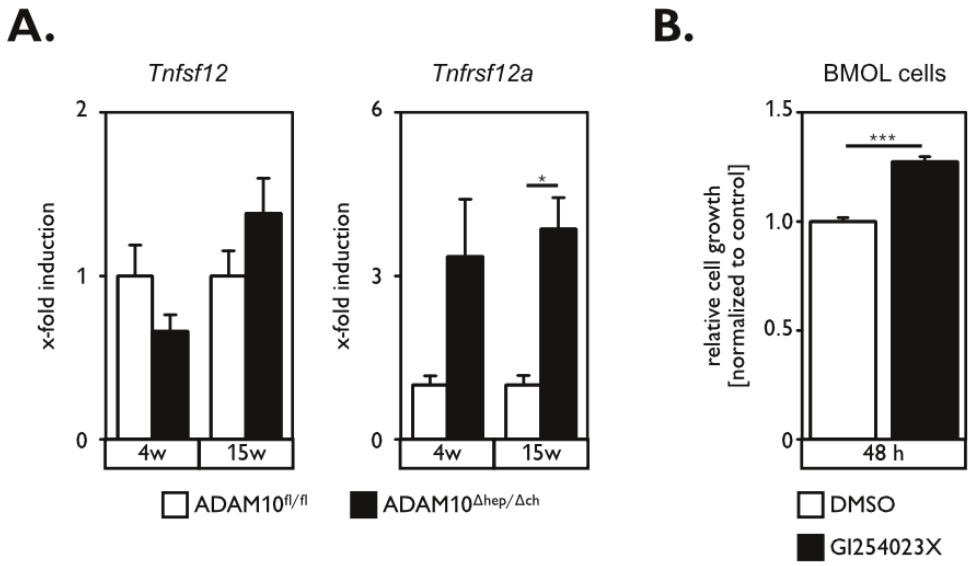

Figure 3.15: Proliferation of Liver progenitor cells is elevated in the absence of ADAM10 activity

A: Expression levels for *Tnfsf12* and *Tnfrsf12a* show an increased expression of the receptor *Tnfrsf12a* in ADAM10$^{\Delta hep/\Delta ch}$ mice. (n=4-5) **B:** BMOL cells with inhibited ADAM10 activity show a stronger proliferation after 48h (n=3)

Data represent the mean ± standard error of the mean. (* - P<0.05; *** - P<0.001)

In line with these findings we detected increased proliferation of the progenitor cell line BMOL when ADAM10 activity is blocked by the inhibitor GI254023X (Figure 3.15 B).

3.8 ADAM10 regulated signaling in liver progenitor cells

We decided to explore signaling pathways that contribute to liver progenitor cell activation and proliferation and that might be regulated by ADAM10. As described above, we found Tnfrsf12a upregulated, indicating increased signaling in the Tnfsf12-Tnfrf12a pathway. Additionally, we found increased levels of hepatocyte growth factor in the sera of ADAM10$^{\Delta hep/\Delta ch}$ mice whereas levels of its receptor c-Met were not altered (Figure 3.16 A). We also detected upregulation of amphiregulin in the serum of ADAM10$^{\Delta hep\Delta ch}$ mice that was, however, not significant. We thus stimulated the liver progenitor cell line BMOL

with recombinant Tnfsf12 and hepatocyte growth factor while downregulating ADAM10 activity either by adding the inhibitor GI254023X or by downregulating ADAM10 expression through siRNA. We then analyzed phosphorylation of the hepatocyte growth factor receptor c-Met and the downstream target extracellular-signal-regulated kinase (ERK) by immunobloting. We additionally examined IκB by immunoblot, since stimulation with Tnfsf12 leads to phosphorylation and consequently degradation of IκB, releasing NF-κB to the nucleus [120]. We detected phosphorylation of c-Met after stimulation with hepatocyte growth factor and that this was increased after downregulation of ADAM10 activity either by GI254023X-mediated inhibition or siRNA. Accordingly, we noted phosphorylation of extracellular-signal-regulated kinase that was also increased after downregulation of ADAM10 activity (Figure 3.16 B, siRNA experiments shown in doctoral thesis of S. Wetzel). We observed no alteration in post-stimulatory IκB levels independent of ADAM10 activity (Figure 3.16 B, siRNA experiments shown in doctoral thesis of S. Wetzel).

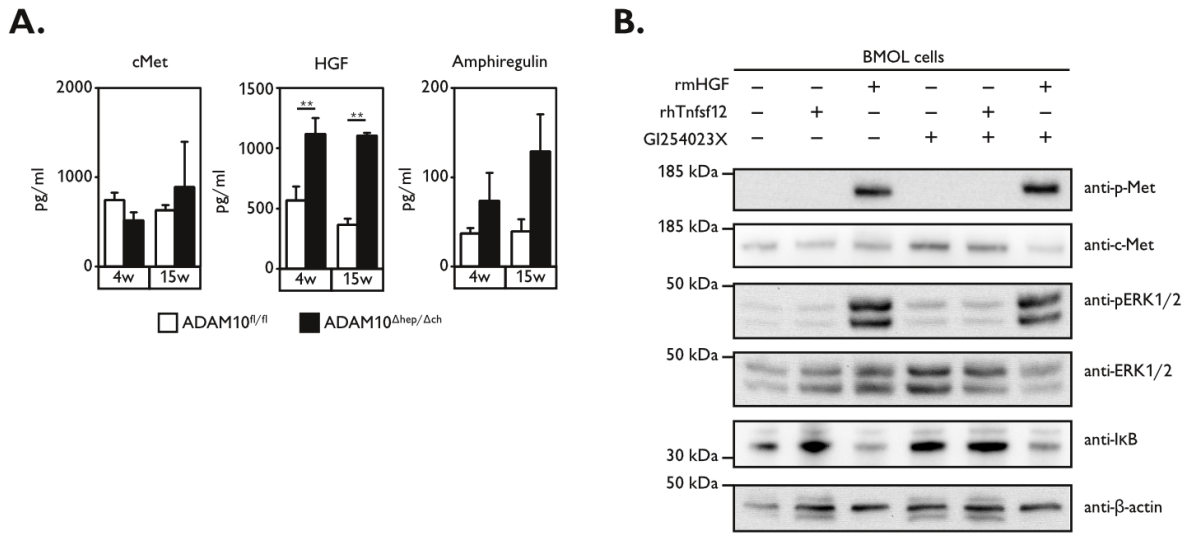

Figure 3.16: Enhanced c-Met signaling in liver progenitor cells in the absence of ADAM10 activity

A: Multiplex ELISA shows increased levels of the liver progenitor cell mitogens amphiregulin and hepatocyte growth factor (HGF) in the serum of ADAM10$^{\Delta hep/\Delta ch}$ animals. (n=3-15, courtesy of K. Chalupsky). **B:** HGF-induced c-Met signaling but not TWEAK-induced Fn14 signaling is increased in the presence of the ADAM10 inhibitor GI254023X. Shown is one out of three independent experiments. (Blot courtesy of B. Wöhner)

Data represent the mean ± standard error of the mean. (** - P<0.01)

TGFβ ligands are known to be upregulated in chronic liver injuries and to contribute to a preference of liver progenitor cell-driven regeneration over hepatocyte-driven regeneration [121]. We thus investigated expression levels of *Tgfb1* and *Tgfb2*. Whilst *Tgfb1* was

only mildly upregulated in livers of 15 week old KO mice, we found *Tgfb2* to be strongly elevated in these animals (Figure 3.17 A). We analyzed additionally TGFβ2 signaling in liver progenitor cells in an *in vitro* setting. Our experiments show that phosphorylation of Smad2, downstream of TGFβ2, is enhanced in BMOL cells in the presence of the ADAM10 inhibitor GI254023X while total levels of TGFβ receptors I and II are not changed (Figure 3.17 B). Future analyses will show whether the increased phosphorylation of SMAD2 also results in altered expression levels of genes downstream of TGFβ signaling.

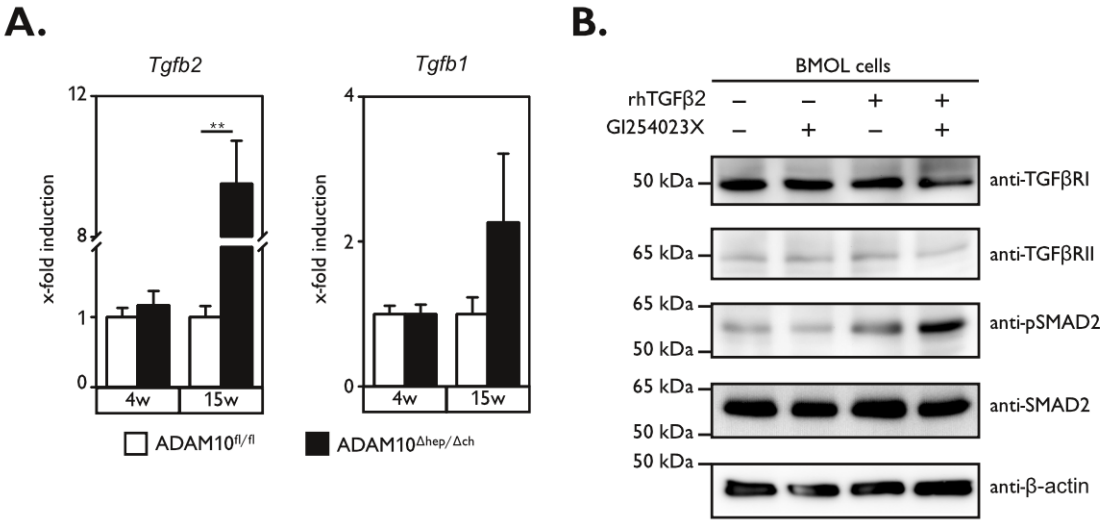

Figure 3.17: Increased TGFβ2 signaling in the absence of ADAM10 activity

A: Elevated expression levels of *Tgfb1* and *Tgfb2* in mice lacking ADAM10 in the liver. (n=4-5). **B:** Inhibition of ADAM10 activity increases TGFβ2 signaling in liver progenitor cells. BMOL cells were stimulated with 1 ng/ml rhTGFβ2 for 15 min at 37°C, subsequently lysed and analysed by immunoblotting using the indicated antibodies. Shown is one representative out of three independent experiments.

Data represent the mean ± standard error of the mean. (** - P<0.01)

3.9 Animals with hepatic deletion of ADAM10 show progressing liver fibrosis

Liver progenitor cell activation and proliferation after chronic liver injury has been demonstrated to activate hepatic stellate cells and lead to the development of liver fibrosis [122].

Both age groups of ADAM10$^{\Delta hep/\Delta ch}$ mice show strong activation of hepatic stellate cells as detected by immunohistological staining of α smooth muscle actin (αSMA). In control animals only αSMA expressing myofibroblasts were detected (Figure 3.18 A). This finding can be further substantiated by analysis of expression levels of αSMA that show a significant increase in 15 week old ADAM10$^{\Delta hep/\Delta ch}$ animals compared to controls (Figure 3.18 B).

In electronmicrographs of 15 week old ADAM10$^{fl/fl}$ animals we found quiescent hepatic stellate cells that feature huge intracellular lipid droplets. We found, in accordance with our previous findings, activated hepatic stellate cells in 15 week old ADAM10$^{\Delta hep/\Delta ch}$ animals that have hardly any lipid vacuoles and are surrounded by deposited collagen fibers (Figure 3.18 C).

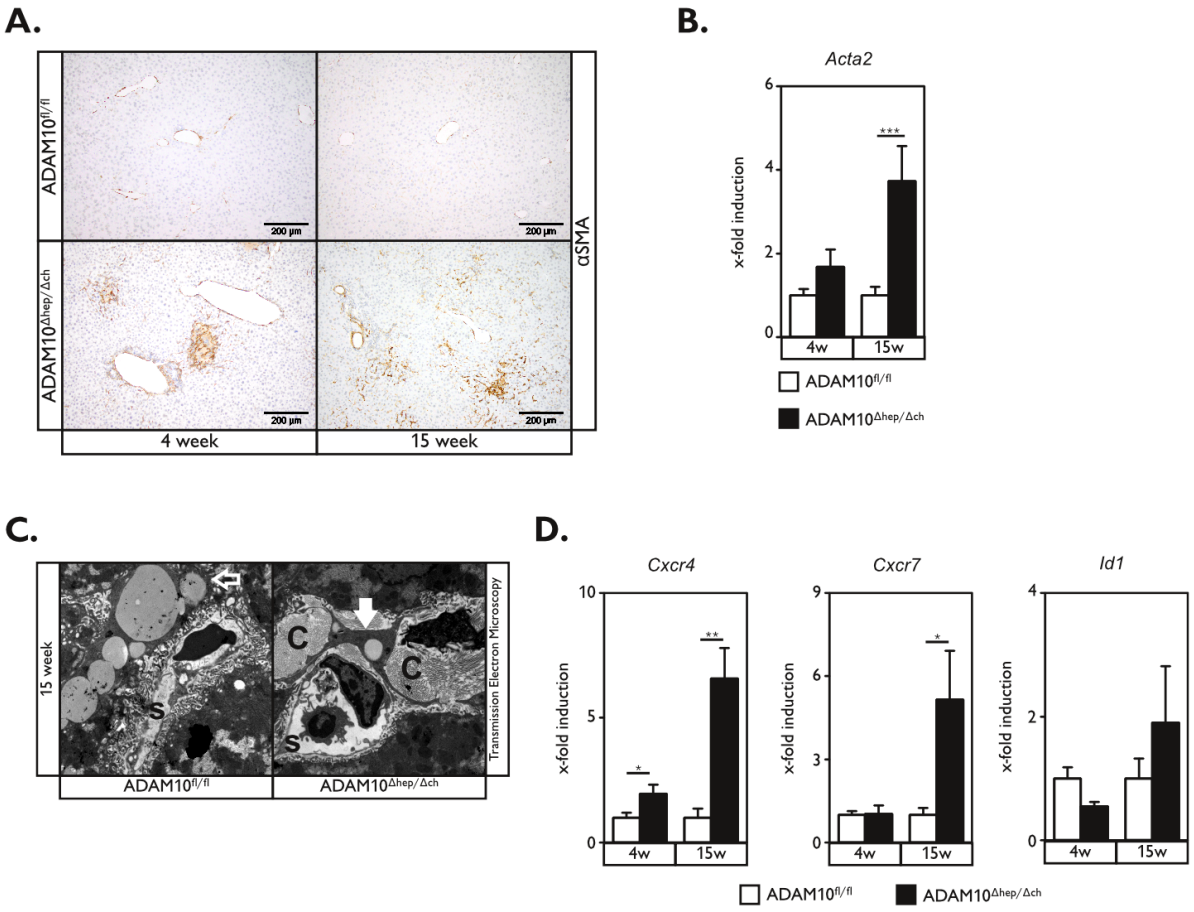

Figure 3.18: Activation of hepatic stellate cells in ADAM10$^{\Delta hep/\Delta ch}$ mice

A: Histological staining of α smooth muscle actin in liver sections demonstrates activation of hepatic stellate cells. Scale bars represent 200 µm. **B:** Expression levels of the α smooth muscle actin gene (*Acta2*) is increased in animals that are deficient for ADAM10 in the liver. (n=4-9) **C:** Electronmicrograph of hepatic stellate cells in control animals and animals lacking ADAM10 in the liver. Open arrow indicates quiescent hepatic stellate cell with many intracellular lipid vesicles. Filled arrow points to activated hepatic stellate cell. S: sinusoid. C: collagen fibers. (courtesy of R. Lüllmann-Rauch) **D:** Expression levels of the fibrosis-associated genes for the chemokine-receptors *Cxcr4* and *Cxcr7* and the downstream transcription factor *Id1*. (n=4-5).

Data represent the mean ± standard error of the mean. (* - P<0.05; ** - P<0.01; *** - P<0.001)

It has recently been described, that liver sinusoidal endothelial cell in the hepatic vascular niche deploy angiocrine factors in response to liver injury to stimulate regeneration. Depending on the differential recruitment of angiocrine factors this supports either regeneration or fibrosis. In the vascular niche the CXCR7-Id1 pathway stimulates a pro-

regenerative response, whereas the FGFR1-CXCR4 pathway promotes fibrosis [123]. We therefore analyzed expression levels of both chemokine receptors as well as that of the downstream transcription factor Id1 in whole liver tissue. We discovered that on the one hand expression levels of *Cxcr4* are upregulated in both 4 week and 15 week KO mice. *Cxcr7* expression levels on the other hand are only elevated in 15 week old mice. Expression of *Id1* is not elevated compared to healthy controls (Figure 3.18 D) suggesting a pro-fibrotic response, which we observed in our animals.

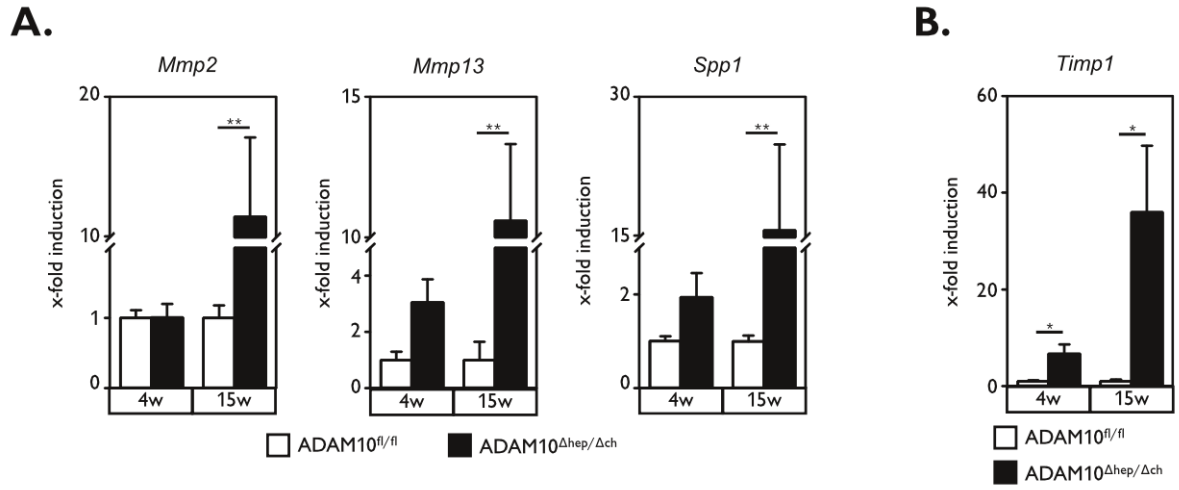

Figure 3.19: Mice deficient for ADAM10 in the liver show upregulation of fibrosis-associated genes.

A: Expression of fibrosis-related matrix metalloproteases 2 (*Mmp2*) and 13 (*Mmp13*) as well as secreted phosphoprotein 1 (*Spp1*) assessed by qRT-PCR. (n=4-9). **B:** Upregulated expression level of tissue inhibitor of metalloprotease (*Timp1*) in livers of ADAM10$^{\Delta hep/\Delta ch}$ mice. (n=4-5).

Data represent the mean ± standard error of the mean. (* P<0.05; ** P<0.01)

In an extended study of other fibrosis-associated genes we identified also *secreted phosphoprotein 1* (*spp1*, also known as osteopontin), *matrix metalloprotease 2* (*Mmp2*) and *13* (*Mmp13*), and *tissue inhibitor of metalloprotease 1* (*Timp1*) to be upregulated in 15 week old ADAM10$^{\Delta hep/\Delta ch}$ mice. *Timp1* was already significantly elevated in 4 week old ADAM10$^{\Delta hep/\Delta ch}$ mice (Figure 3.19 A+B). This was of special interest to us since TIMP1 does not only inhibit MMP activity but has also been described to inhibit ADAM10 [124].

Strikingly though, we already observed mild but significant increased amounts of collagen compared to control mice in 4 week old mice. As can be clearly seen in the tissue stainings, collagen deposits were mainly limited to the vicinity of vessels in this age group. However in 15 week old ADAM10$^{\Delta hep/\Delta ch}$ mice collagen staining by sirius red increased greatly in comparison to both 15 week old ADAM10$^{fl/fl}$ mice. Collagen staining was also

elevated in 15 week old ADAM10$^{\Delta hep/\Delta ch}$ mice compared to 4 week old ADAM10$^{\Delta hep/\Delta ch}$ mice (Figure 3.20 A+B). Observed fibrotic patterns can be classified as a mixture between portal fibrosis and pericellular fibrosis (compare Figure 1.4) Analyses of hydroxyproline content and expression levels of *Collagen1A1* consistently support the previous findings of massive fibrosis in 15 week old ADAM10$^{\Delta hep/\Delta ch}$ mice (Figure 3.20 C).

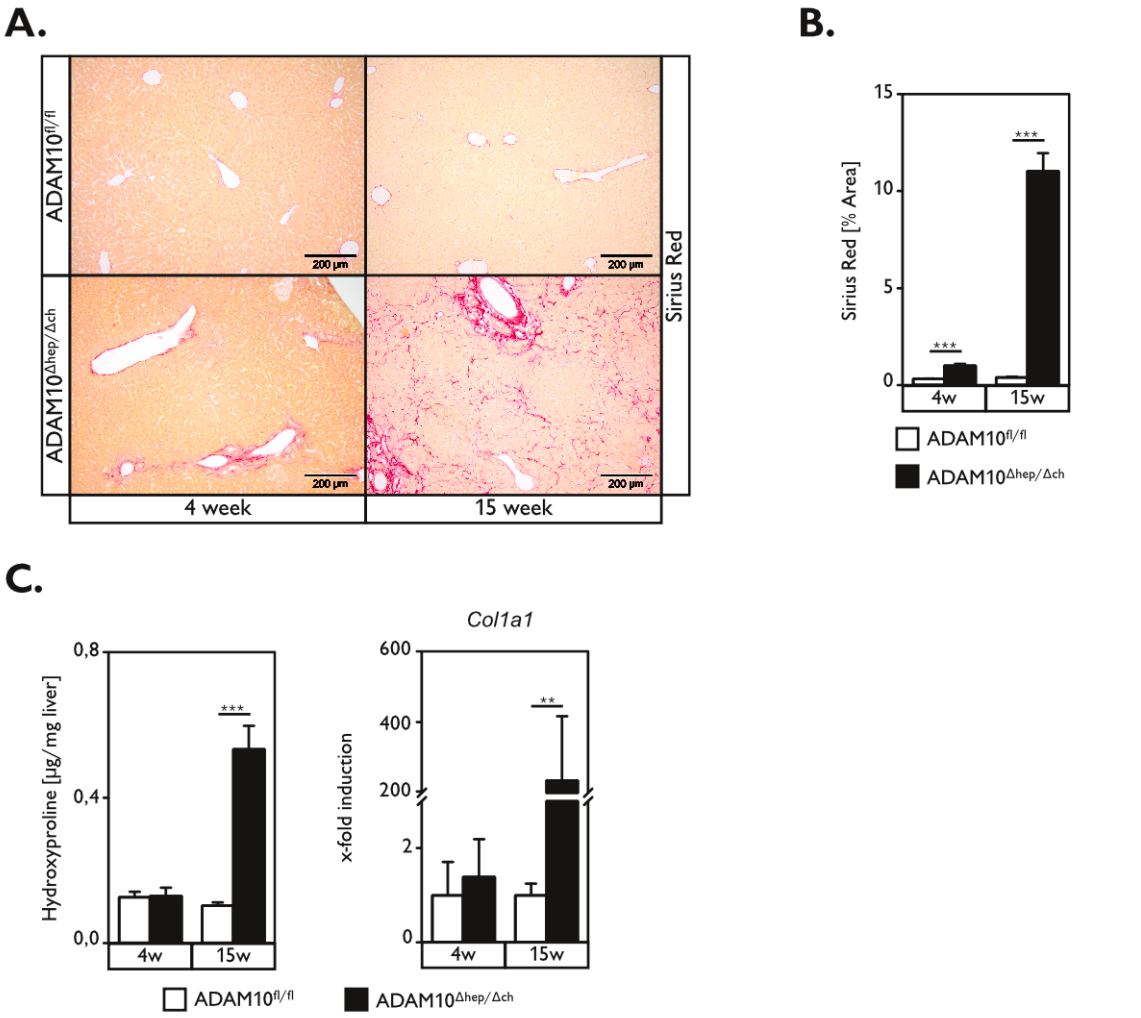

Figure 3.20: Mice deficient for ADAM10 in the liver present progressing liver fibrosis.

A: Histological liver sections stained for collagen deposition with Sirius Red. Scale bars represent 200 µm. **B:** Quantification of Sirius Red–positive areas proves significant collagen deposition in the livers of ADAM10$^{\Delta hep/\Delta ch}$ animals. (n=4-16) **C:** Quantification of hydroxyproline content (n=3-9) and analysis of *Collagen1a1* expression (n=4-9) from total liver extracts. Both confirming elevated levels of collagen in mice lacking ADAM10 in the liver.

Data represent the mean ± standard error of the mean. (** P<0.01; *** P<0.001)

3.10 Induced liver damage via CCl_4 does not lead to sustained liver fibrosis in ADAM10$^{\Delta hep\Delta ch}$ animals

We observed that ADAM10 apparently plays a role in liver progenitor cell-driven regeneration. However, we wanted to investigate if ADAM10 is involved in hepatocyte-driven regeneration as well. We thus employed a CCl_4-induced damage model known to provoke repair through hepatocyte proliferation [125]. The experimental setup is depicted in Figure 3.21 A.

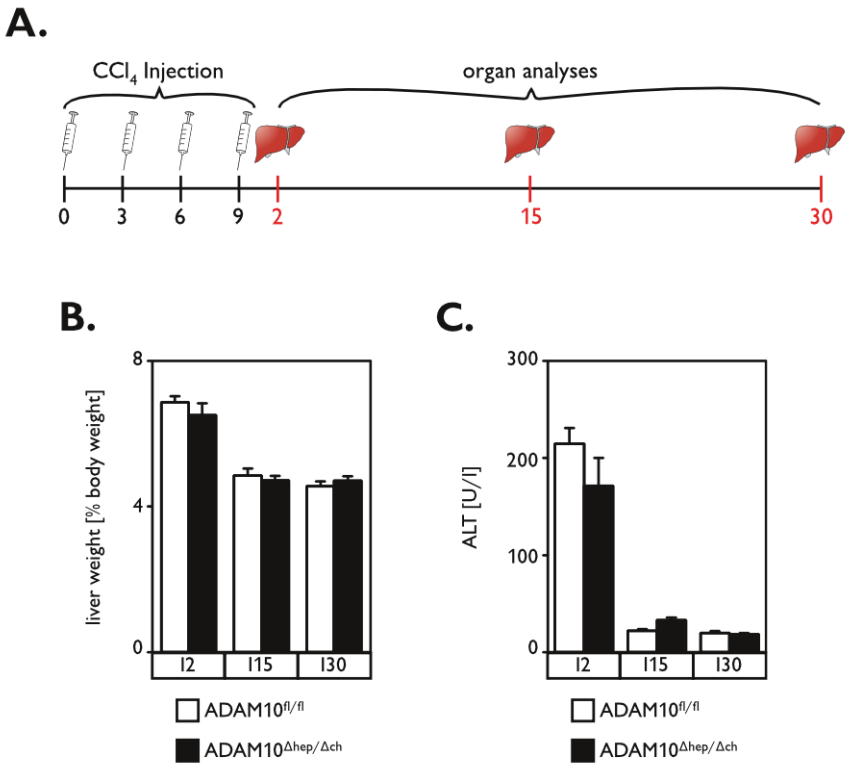

Figure 3.21: Recovery from CCl_4-induced damage is not altered in ADAM10$^{\Delta hep\Delta ch}$ mice

A: Schematic of CCl_4 treatment and subsequent liver analyses. Animals were injected 4 times with CCl_4 in three day intervals. 2, 15, and 30 days after the last injection animals were sacrificed and their livers examined **B:** Liver weight, compared to body weight, is elevated 2 days (I2) after the last CCl_4-injection but returns to normal if more time passed between the injection and analysis (I15, I30). (n=5-11) **C:** Alanine transaminase (ALT) levels are elevated 2 days (I2) after the last CCl_4-injection but return to normal if more time passed between the injection and analysis (I15, I30). (n=6-11)

Data represent the mean ± standard error of the mean.

We detected an increase in alanine transaminase levels and relative liver weight two days after the last injection, indicating liver damage. Yet, the injury seems to be resolved between 2 days after the last injection and 15 days after the last injection, since values for both alanine transaminases and relative liver weight return to normal during that time span. We did not observe differences between control animals and ADAM10$^{\Delta hep/\Delta ch}$ animals

at any time point of investigation. Neither amount of damage nor time needed for resolution differs between the two groups (Figure 3.21 B+C). We hence concluded, that ADAM10 does not play a role in hepatocyte-driven regeneration in this model, but further analysis is needed to corroborate this hypothesis.

4 Discussion

The liver is a very resilient organ and can regenerate from severe acute injuries, including loss of over 70% of its mass. However, chronic injuries through virus infections, alcoholic liver disease or non-alcoholic fatty liver disease cause the liver to become fibrotic and, if injury continues, cirrhotic (see chapter 1.1.4). Although regeneration from fibrosis is possible, the only available therapy that helps patients suffering from cirrhosis in the long-term is organ transplantation. But organ donors are sparse and transplantation, as a surgical intervention, always carries a risk. Therefore, it is crucial to get a better understanding of the molecular mechanisms orchestrating regeneration, fibrosis and liver homeostasis. ADAM10 was reported to be an essential regulator of homeostasis in the skin, intestine, and in B cells [92-94]. We were thus interested if ADAM10 is also involved in liver tissue homeostasis.

4.1 ADAM10 in bile duct development and hepatocyte necrosis

One of the most prominent targets of ADAM10 is Notch which, after ligand binding, undergoes ADAM10-mediated shedding and leads to altered gene expression. Processing of Notch by ADAM10 has not only been implicated in tissue homeostasis but also in embryonic development [93, 108]. Notch receptors, amongst them foremost Notch2, have been shown to be fundamental for biliary development and correct formation of the three-dimensional architecture of the biliary tree, as well as for biliary specification of adult progenitor cells [6, 7]. Very interestingly though, mice deficient for ADAM10 in hepatoblast after e9.5 and consequently in hepatocytes and cholangiocytes did not show a developmental defect in their biliary structure. Adult ADAM10$^{\Delta hep/\Delta ch}$ mice also exhibit functional cholangiocyte differentiation after injury. These findings suggest, that either ADAM10 is not processing Notch during biliary-development or that loss of ADAM10 is compensated for by another protease (see Figure 4.1). Although the closely related ADAM17 shares many substrates with ADAM10, it was shown recently, that ADAM17 does not play a role in shedding of Notch2 [56]. We additionally tested in cell-culture based experiments whether tube formation of the liver progenitor cell line BMOL on matrigel is abrogated in the presence of ADAM- and γ-secretase inhibitors. In accordance with our *in vivo* data inhibition of ADAM10 activity by GI254023X did not lead to an

altered tube formation. Inhibition with GW208264X, reported to block ADAM10 and 17 activity, did lead to a slight but not significant decrease in either tube formation or branching. However, inhibiting γ-secretase cleavage by DAPT caused a significant reduction in tube length and junctions. These results indicate, that another protease is responsible for Notch2 processing in the context of biliary development. Membrane-tethered matrix metalloproteinase (MT1-MMP) was shown to cleave Notch in melanoma cells and can reconstitute Notch processing in ADAM10/17 double knock-out murine embryonal fibroblasts [126].

These results should be confirmed with studies using siRNA or shRNA. It might also be interesting to use broad-spectrum metalloprotease inhibitors like marimastat to see if blocking all metalloproteases leads to a similar decrease in branching and tube length as γ-secretase inhibition.

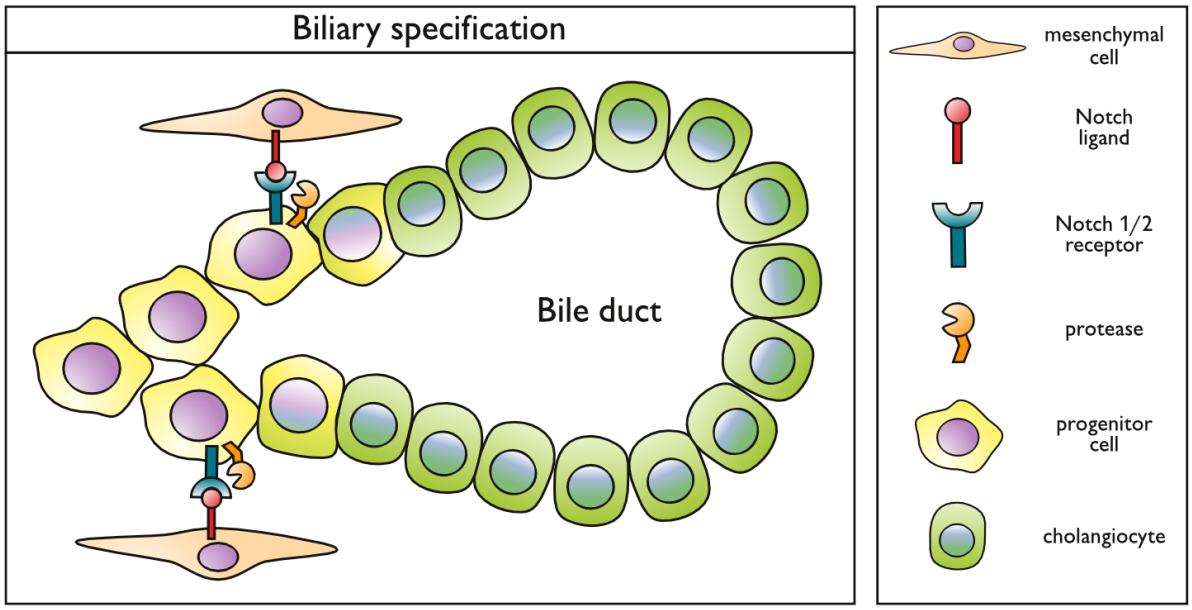

Figure 4.1: Biliary specification of progenitor cells depends on Notch-signaling

Schematic of the Notch-dependent differentiation process of hepatoblasts during development or liver progenitor cells after chronic damage. After binding to Jagged-1 of surrounding mesenchymal cells Notch undergoes shedding and regulated intramembrane proteolysis and the intracellular domain translocates to the nucleus. There the intracellular domain initiates gene transcription inducing differentiation towards cholangiocytes. We show in our study that ADAM10 is not the protease responsible for the α-secretase cleavage of Notch during biliary differentiation.

Bile acids are produced in hepatocytes and then exported via bile acid transporters to the bile canaliculi. We observed a loss of radixin in ADAM10$^{\Delta hep/\Delta ch}$ mice. Radixin is responsible for directing the bile acid transporter multidrug resistence-associated protein 2 (also ATP-binding cassette sub-family C member 2, Abcc2) to the bile canalicular membrane.

As a consequence multidrug resistance-associated protein2 staining on the cell surface was also reduced in these mice. Additionally we observed a downregulation on mRNA level for both *rdx* and *abcc2* (data shown in doctoral thesis of S. Wetzel). There are no reports linking ADAM10 or Notch to bile transporters. It has been reported that impaired bile export from hepatocytes leads to hepatocyte necrosis mediated via reactive oxygen formation of attracted neutrophils [127]. Areas of hepatocyte necrosis caused by biliary accumulation are referred to as bile infarcts. In accordance with these observations we also detect neutrophils in the necrotic areas of ADAM10$^{\Delta hep/\Delta ch}$ mice. We will therefore measure reactive oxygen species in tissue of these mice to investigate if this is the cause of the observed cell death. Considering though, that Radixin-deficient mice only show a mild phenotype it is possible that other bile acid transporters are impaired as well [114]. Another reason for the observed bile infarcts might be an altered bile metabolism. To investigate this further, we will not only analyze expression of several bile acid transporters but also examine total bile acid composition in ADAM10$^{\Delta hep/\Delta ch}$ mice.

Further experiments are also needed to confirm experimentally that the detected cell death is indeed necrotic and not apoptotic.

Despite the massive necrosis, infiltration of immune cells and inflammation is rather low in the ADAM10-KO mice. We see a few neutrophil granulocytes in the bile infarcts and CD3$^+$ T-cells in the vicinity of the portal triad. F4/80$^+$ macrophage presence was not increased in ADAM10$^{\Delta hep/\Delta ch}$ mice but they were localized in clusters compared to an uniform distribution in control animals (see Figure 3.14). These observations correspond to the cytokine profile that shows no increase for pro-inflammatory cytokines or chemokines. Instead the anti-inflammatory interleukin-1 receptor antagonist is highly upregulated. Interleukin-1 receptor antagonist is known for balancing IL-1 signaling and exerting an anti-inflammatory function [117]. Interleukin-1 receptor antagonist has been shown to reduce inflammation and accelerate liver regeneration through acceleration of hepatocyte proliferation after partial hepatectomy [128]. It is possible that interleukin-1 receptor antagonist also exerts this role in favor of regeneration after a different type of liver injury. Interleukin-1 receptor antagonist can also act anti-senescent, possibly interfering with deactivation of hepatic stellate cells or even with deactivation of liver progenitor cells [118].

Additionally, absence of ADAM10 can contribute to a less inflammatory profile. Substrates of ADAM10 including pro-inflammatory cytokines like tumor necrosis factor α and interleukin-12 might not be released by ectodomain shedding. No elevation of tumor necrosis factor α levels was detectable in the respective ELISA for ADAM10$^{\Delta hep\Delta ch}$ animals despite the obvious injury. It has recently been shown that deletion of ADAM10 in myeloid cells results in a less inflammatory and more fibrotic phenotype in artherosclerosis [129].

4.2 Proliferation of liver progenitor cells

After liver injury two modes of regeneration are known that depend on the type of damage. Proliferation of hepatocytes usually occurs after acute damage whereas if damage persists liver progenitor cells get activated, proliferate, and differentiate (see chapter 1.1.2).

Several observations in the ADAM10$^{\Delta hep/\Delta ch}$ mice lead us to hypothesize that regeneration in these mice is liver progenitor cell-driven. First, though necrosis is strongly decreased in 15 week old animals it is still present, arguing for a rather chronic damage. Second, we see in Ki67 stainings that mostly cells with an oval nucleus and little cytoplasm are proliferating instead of the bigger hepatocytes. Third, we detect a ductular reaction in cytokeratin 19 stainings that is known to accompany liver progenitor cell-driven regeneration. Last, we observe cells that are double-positive for the progenitor marker pan-cytokeratin and the proliferation marker Ki67. We therefore investigated macrophage localization and expression of *Tnfsf12* (coding for TWEAK) and *Tnfrsf12a* (coding for Fn14) known to drive liver progenitor cell proliferation [26]. While we see a clustering of macrophages especially around pan-cytokeratin^{+} cells, expression of *Tnfsf12* is not increased. This is in accordance with previous reports showing constitutive *Tnfsf12* expression [26]. But we found *Tnsfrsf12a* to be increased which can either indicate increased expression on the same amount of cells or more cells expressing the receptor.

Liver progenitor cell proliferation increased although damage decreased over time. We hypothesize hence that ADAM10 is involved in termination of liver progenitor cell proliferation in mice with a liver-specific deficiency of ADAM10. It could be that ADAM10 is needed for shedding of Tnfrsf12a to abrogate signaling. Although Tnfrsf12a is not described as a substrate for proteolysis other members of the tumor necrosis factor receptor superfamily are known to undergo ADAM-mediated shedding [130].

Yet, also other substrates of ADAM10 could be responsible for driving liver progenitor cell proliferation. Hepatocyte growth factor and its receptor c-met are important in hepatoblast proliferation, and this also holds true for adult progenitor cells [25, 131]. C-met is a substrate of ADAM10 and loss of ADAM10 may cause prolonged and intensified c-met signaling [124]. We detected increased levels of hepatocyte growth factor in serum of mice with a liver-deficiency of ADAM10 arguing for an activation of the hepatocyte growth factor signaling pathway. In *in vitro* experiments we showed that c-Met signaling is increased in a liver progenitor cell line in the absence of ADAM10 activity. However, the consequences of the increased activation of this pathway need to be clarified in future experiments. ADAM10-mediated regulation of the hepatocyte growth factor signaling pathway is also interesting under the assumption, that deregulation of liver progenitor cell differentiation and proliferation leads to a malignant transformation.

The group of Achim Krüger showed that inhibition of ADAM10 by its natural inhibitor tissue inhibitor of metalloproteinase-1 leads to increased metastasis to the liver due to increase hepatocyte growth factor signaling indicating that ADAM10 may also play a role in the metastatic niche in the liver [124, 132]. It might be interesting to further evaluate the role of ADAM10 in the hepatocyte growth factor signaling pathway in liver tumor and metastases.

Another interesting substrate of ADAM10 is CD44. CD44 is a receptor for osteopontin, that was recently shown to drive progenitor cell proliferation and fibrosis [133, 134] We noticed that staining for CD44 in ADAM10$^{\Delta hep/\Delta ch}$ mice is more prominent than in control animals. *In vitro* studies will give more insight if CD44 signaling is responsible for liver progenitor cell proliferation.

TGFβ signaling is increased in fibrotic liver disease. We could show that ADAM10$^{\Delta hep/\Delta ch}$ mice also have elevated levels of TGFβ ligands. To investigate if the increase of TGFβ2 also effects liver progenitor cells, e.g. transition to a more mesenchymal phenotype, we stimulated BMOL cells with rhTGFβ2 in the presence and absence of an ADAM10 inhibitor. Phosphorylation of Smad2 is increased after stimulation and even further increased if ADAM10 is inhibited. We will perform qRT-PCR tests to examine downstream targets of ADAM10-regulated TGFβ2 signaling in liver progenitor cells.

4.3 ADAM10 in two liver damage models inducing different repair mechanisms

We showed that ADAM10 is involved in liver progenitor cell-mediated liver regeneration. To analyze whether ADAM10 also plays a role in liver regeneration by hepatocyte proliferation we made use of a carbon tetrachloride (CCl_4) induced damage model. In first results we see that control and ADAM10-deficient animals respond to CCl_4 administration and show elevated alanine transaminase levels immediately after treatment. Contrary to what we observe in the strong phenotypes of ADAM10$^{\Delta hep/\Delta ch}$ mice, alanine transaminase levels returned to normal in 2 weeks after the last dose of CCl_4 independent of ADAM10 expression. A more detailed evaluation is needed, but the, so far, acquired data point towards a negligible role of ADAM10 in hepatocytic proliferation dependent liver regeneration.

Additionally, we plan to feed the mice with a choline-deficient, ethionine-supplemented (CDE) diet leading to chronic liver injury with a subsequent liver progenitor cell-dependent regeneration [135]. ADAM10$^{\Delta hep/\Delta ch}$ mice, as discussed in chapter 3.2, showed the observed phenotype only in 30-50% of the offspring. By feeding mice with the CDE-diet we will subject all mice, KO and WT, to the same injury and induce activation of liver progenitor cells in all animals. This allows for direct comparison in liver progenitor cell-driven regeneration in animals with or without ADAM10. We expect that proliferation in the liver progenitor cell-response in ADAM10$^{\Delta hep/\Delta ch}$ mice is increased compared to controls.

Original necrotic damage and fibrosis might still be interfering with induced damage. Thus, we bred inducible conditional KO-mice. Unfortunately, the first chosen mouse strains with tetracycline-inducible ADAM-10 deletion in hepatocytes did not deliver the desired penetrance (see Supplementary Figure 2 for the basic principle of tetracycline-inducible deletion and Supplementary Figure 3). We will therefore replace the doxycyline-inducible Cre-recombinase with a tamoxifen-inducible Cre-recombinase under an albumin promoter (for a basic principle of tamoxifen-induced recombination see Figure 4.2) [136]. But, as *alb* is not expressed in progenitor cells, these experiments result only in information about involvement of hepatocytic ADAM10 in liver progenitor cell-driven liver regeneration. In a recent report it was described that hepatocytes can dedifferentiate after injury to progenitor cells and later, after the chronic injury subsided, differentiate

back to functional liver cells [137]. We can investigate in the conditional KO-mice whether the process of hepatocytic dedifferentiation to progenitor cells in chronic liver damage relies on ADAM10.

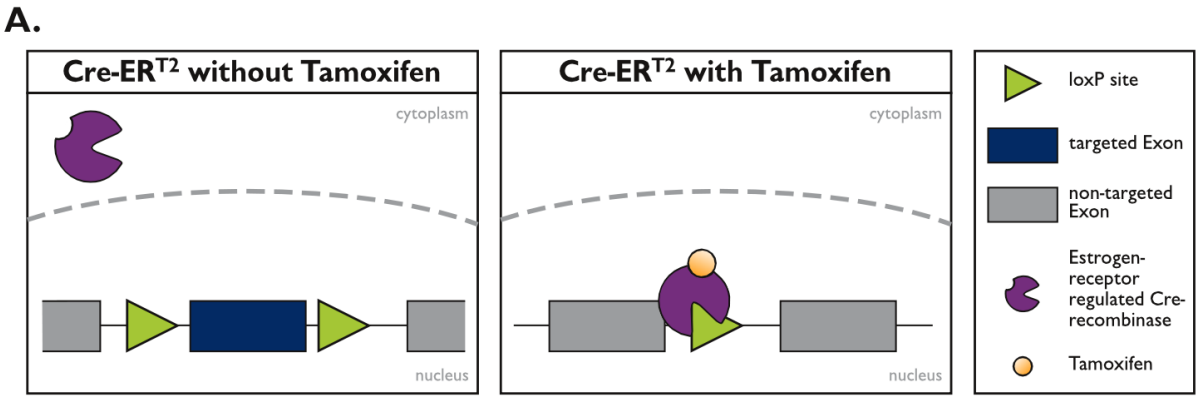

Figure 4.2: Tamoxifen-inducible Cre-recombinase

A: Schematic of the tamoxifen-inducible Cre-ER^{T2} system. Under unstimulated conditions the Cre-recombinase is located in the cytoplasm. Once tamoxifen binds to the estrogen-receptor fused to the Cre-recombinase the complex translocates to the nucleus and mediates site specific recombination

Another option to follow up on our findings on ADAM10 in liver progenitor cells is to knock-out ADAM10 specifically in adult hepatic progenitors. A suitable Cre-recombinase for these experiments is Foxl1-Cre which was shown to be active in adult progenitor cells but not in fetal hepatoblasts [138]. We can then examine in an CDE-diet model if loss of ADAM10 on liver progenitor cells is sufficient to get prolonged liver progenitor cell proliferation after chronic damage. As a proof of principle, treatment with adenoviral administered ADAM10 should rescue the phenotype.

It has been proposed that fibrotic and cirrhotic livers are often leading to development of hepatocellular carcinomas [31]. Lack of ADAM10 leads in our model to an increased fibrosis in an liver progenitor cell-dependent damage repair, and inhibition of ADAM10 leads to increased liver metastases but it is also found upregulated in hepatocellular carcinomas [63, 132]. These findings seem to exclude each other, but one should consider that hepatocellular carcinoma can also form without preceding cirrhosis. Nonetheless, it will be telling if, how and what kind of tumors develop in ADAM10$^{\Delta hep/\Delta ch}$ mice.

4.4 Regulation of ADAMs through substrate selectivity

This study and others show that ADAMs can regulate many different and even opposing signals. It is therefore essential to understand mechanisms that target ADAMs to specific substrates. Proteins with multi-transmembrane domains are discussed to be facilitators of this process, for example inactive members of the rhomboid family [139].

Another family of multi-pass transmembrane proteins are tetraspanins [140]. Recent studies showed interactions between members of the ADAM family and members of the tetraspanin family [79, 141]. We thus want to examine the potential of select tetraspanins to influence ADAMs in their substrate selection. Our hypothesis is that tetraspanins gather proteases and substrates in membrane regions like tetraspanin-enriched microdomains. In preliminary experiments we see an interaction between the investigated tetraspanins and ADAMs and a trend that expression of different tetraspanins leads to ADAMs favoring different substrates (Supplementary Figure 4, Supplementary Figure 5, Supplementary Figure 6). These findings are an excellent start for a more detailed future research on the mechanism by which tetraspanins bring together ADAMs and their substrates.

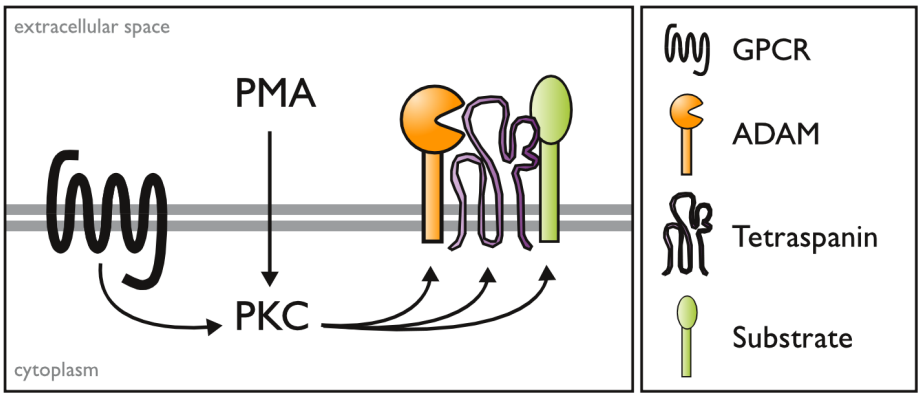

Figure 4.3: Tetraspanins might influence target selectivity of ADAM17 in PKC dependent shedding

PKC activation through either G-protein-coupled receptor (GPCR) signaling or PMA leads to shedding of ADAM17 substrates. We hypothesize that substrate-selectivity will be influenced by members of the tetraspanin family. Besides activating ADAM17, PKC is also known to interact with tetraspanins and ADAM17 substrates [0, 140].

In future investigations we will, with the help of markers for membrane regions like cholera toxin B-FITC, examine membrane localization in more detail.

We would finally also like to investigate tetraspanin-mediated substrate-selectivity in regard to physiological processes, especially in the liver. It has been shown that co-expression of CD9 leads to an increase of pro-heparin binding-epidermal growth factor and pro-

amphiregulin, both epidermal growth factor receptor (EGFR) ligands, and thereby enhanced juxtacrine signaling [142]. EGFR signaling is crucial in the liver with functions from hepatoprotection to hepatocarcinogenesis and ADAMs are known sheddases of EGFR ligands [143]. Tspan8 is upregulated in heaptocellular carcinoma and especially in intrahepatic metastases [144]. Future analysis will have to show if Tspan8 is connected to increased amounts of shed ADAM substrates found in hepatocellular carcinoma such as amphiregulin.

We therefore think that by following up on the tetraspanin-ADAM connection we will gain crucial insights into the intricate regulatory network that balances ADAM-activity.

4.5 Conclusion

Our experiments describe for the first time a potentially essential function of ADAM10 in regulating proliferation in adult liver progenitor cells and hence hepatic stellate cell activation and the progression of liver fibrosis in chronic liver injury. We define ADAM10 as a novel major key player in murine liver tissue homeostasis (Figure 4.4).

We are confident, that our findings will aid greatly in developing new treatments for fibrosis and cirrhosis. Upregulation of ADAM10 on a transcriptional level by retinoic acids has been shown to result in an increased ADAM10 activity [145]. A recent clinical phase II study demonstrated that these observation can be also confirmed in human patients suffering from Alzheimer's disease. After oral treatment with acitretin cleavage of amyloid precursor protein at the ADAM10 cleavage site was increased [146]. If the therapy would be transferable to liver disease, chronic proliferation of liver progenitor cells could become treatable. On the other hand, transient inhibition of ADAM10 could be used to enhance liver regeneration.

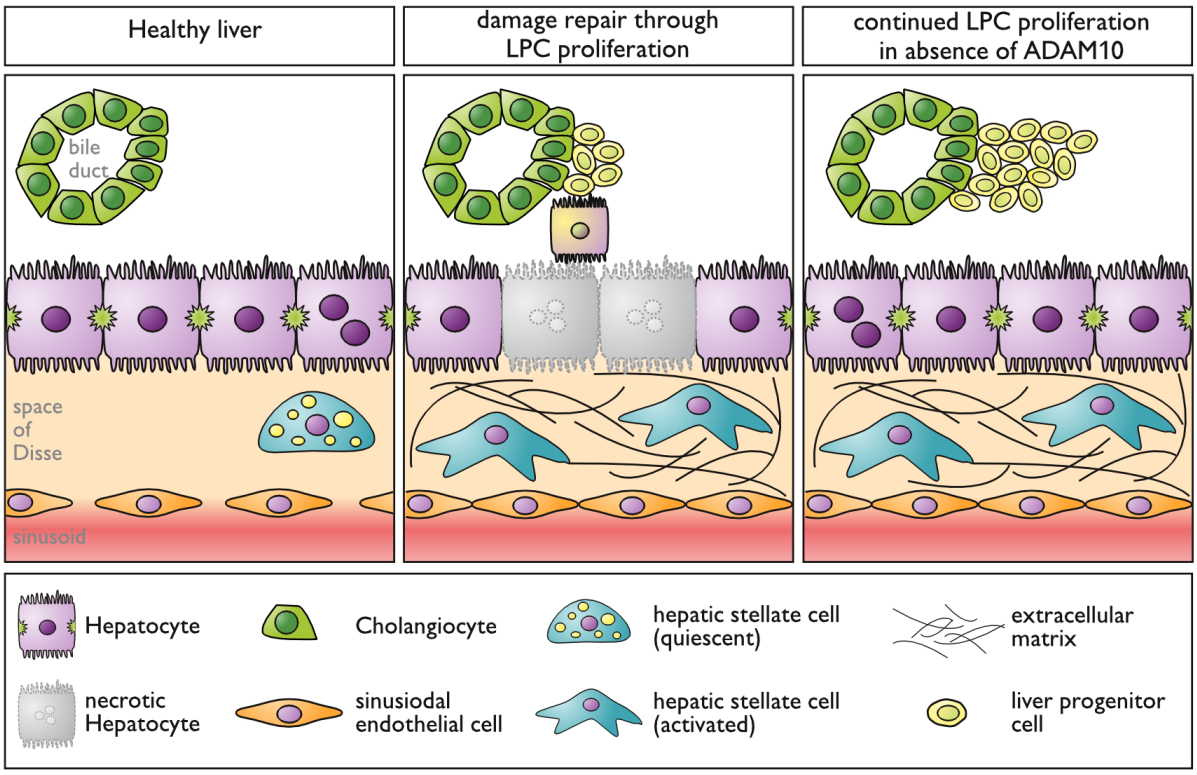

Figure 4.4: Loss of ADAM10 leads to continued LPC proliferation in chronic liver injury

Schematic of the findings described in this study. Hepatocyte necrosis in chronic liver injury leads to activation and proliferation of the liver progenitor cell (LPC) compartment. LPCs then activate hepatic stellate cells (HSC) resulting in deposition of extracellular matrix. Although the damage is repaired by differentiation of LPCs to mature hepatocytes, LPC proliferation continues, HSC stay activated, and continued deposition of ECM causes fibrosis.

5 References

1. **Power, C. & Rasko, J.E.J.** Whither prometheus' liver? Greek myth and the science of regeneration. Ann. Intern. Med. 149, 421-6 (2008).
2. **Michalopoulos, G.K.** Liver regeneration. J. Cell. Physiol. 213, 286-300 (2007).
3. **Zorn, A.M.** Liver development. StemBook ed. The Stem Cell Research Community, http://www.stembook.org (2008).
4. **Tremblay, K.D. & Zaret, K.S.** Distinct populations of endoderm cells converge to generate the embryonic liver bud and ventral foregut tissues. Dev. Biol. 280, 87-99 (2005).
5. **Lemaigre, F.P.** Development of the biliary tract. Mech. Dev. 120, 81-7 (2003).
6. **Geisler, F., Nagl, F., Mazur, P.K., Lee, M., Zimber-Strobl, U., Strobl, L.J., Radtke, F., Schmid, R.M. & Siveke, J.T.** Liver-specific inactivation of Notch2, but not Notch1, compromises intrahepatic bile duct development in mice. Hepatology 48, 607-16 (2008).
7. **Sparks, E.E., Huppert, K.A., Brown, M.A., Washington, M.K. & Huppert, S.S.** Notch signaling regulates formation of the three-dimensional architecture of intrahepatic bile ducts in mice. Hepatology 51, 1391-400 (2010).
8. **Zender, S., Nickeleit, I., Wuestefeld, T., Sörensen, I., Dauch, D., Bozko, P., El-Khatib, M., Geffers, R., Bektas, H., Manns, M.P., Gossler, A., Wilkens, L., Plentz, R., Zender, L. & Malek, N.P.** A critical role for notch signaling in the formation of cholangiocellular carcinomas. Cancer Cell 23, 784-95 (2013).
9. **Oda, T., Elkahloun, A.G., Pike, B.L., Okajima, K., Krantz, I.D., Genin, A., Piccoli, D.A., Meltzer, P.S., Spinner, N.B., Collins, F.S. & Chandrasekharappa, S.C.** Mutations in the human Jagged1 gene are responsible for Alagille syndrome. Nat. Genet. 16, 235-42 (1997).
10. **Frevert, U., Engelmann, S., Zougbédé, S., Stange, J., Ng, B., Matuschewski, K., Liebes, L. & Yee, H.** Intravital observation of Plasmodium berghei sporozoite infection of the liver. PLoS Biol. 3, e192 (2005).
11. **Benedetti, A., Jézéquel, A.M. & Orlandi, F.** Preferential distribution of apoptotic bodies in acinar zone 3 of normal human and rat liver. J. Hepatol. 7, 319-24 (1988).
12. **Danial, N.N. & Korsmeyer, S.J.** Cell death: critical control points. Cell 116, 205-19 (2004).
13. **Masubuchi, Y., Suda, C. & Horie, T.** Involvement of mitochondrial permeability transition in acetaminophen-induced liver injury in mice. J. Hepatol. 42, 110-6 (2005).
14. **Nanji, A.A. & Hiller-Sturmhöfel, S.** Apoptosis and necrosis: two types of cell death in alcoholic liver disease. Alcohol Health Res World 21, 325-30 (1997).
15. **Kew, M.C.** Serum aminotransferase concentration as evidence of hepatocellular damage. Lancet 355, 591-2 (2000).
16. **Reichling, J.J. & Kaplan, M.M.** Clinical use of serum enzymes in liver disease. Dig. Dis. Sci. 33, 1601-14 (1988).
17. **Forbes, S.J. & Rosenthal, N.** Preparing the ground for tissue regeneration: from mechanism to therapy. Nat. Med. 20, 857-69 (2014).
18. **Pellicoro, A., Ramachandran, P., Iredale, J.P. & Fallowfield, J.A.** Liver fibrosis and repair: immune regulation of wound healing in a solid organ. Nat. Rev. Immunol. 14, 181-94 (2014).
19. **Fausto, N., Campbell, J.S. & Riehle, K.J.** Liver regeneration. Hepatology 43, S45-53 (2006).
20. **Viebahn, C.S. & Yeoh, G.C.T.** What fires prometheus? The link between inflammation and regeneration following chronic liver injury. Int. J. Biochem. Cell Biol. 40, 855-73 (2008).
21. **Oertel, M. & Shafritz, D.A.** Stem cells, cell transplantation and liver repopulation. Biochim. Biophys. Acta 1782, 61-74 (2008).
22. **Huch, M., Dorrell, C., Boj, S.F., van Es, J.H., Li, V.S.W., van de Wetering, M., Sato, T., Hamer, K.,**

Sasaki, N., Finegold, M.J., Haft, A., Vries, R.G., Grompe, M. & Clevers, H. In vitro expansion of single Lgr5+ liver stem cells induced by Wnt-driven regeneration. Nature 494, 247-50 (2013).

23. **Boulter, L., Govaere, O., Bird, T.G., Radulescu, S., Ramachandran, P., Pellicoro, A., Ridgway, R.A., Seo, S.S., Spee, B., Van Rooijen, N., Sansom, O.J., Iredale, J.P., Lowell, S., Roskams, T. & Forbes, S.J.** Macrophage-derived Wnt opposes Notch signaling to specify hepatic progenitor cell fate in chronic liver disease. Nat. Med. 18, 572-9 (2012).

24. **Nakamura, T., Sakai, K., Nakamura, T. & Matsumoto, K.** Hepatocyte growth factor twenty years on: Much more than a growth factor. J. Gastroenterol. Hepatol. 26 Suppl 1, 188-202 (2011).

25. **Ishikawa, T., Factor, V.M., Marquardt, J.U., Raggi, C., Seo, D., Kitade, M., Conner, E.A. & Thorgeirsson, S.S.** Hepatocyte growth factor/c-met signaling is required for stem-cell-mediated liver regeneration in mice. Hepatology 55, 1215-26 (2012).

26. **Tirnitz-Parker, J.E.E., Viebahn, C.S., Jakubowski, A., Klopcic, B.R.S., Olynyk, J.K., Yeoh, G.C.T. & Knight, B.** Tumor necrosis factor-like weak inducer of apoptosis is a mitogen for liver progenitor cells. Hepatology 52, 291-302 (2010).

27. **Dwyer, B.J., Olynyk, J.K., Ramm, G.A. & Tirnitz-Parker, J.E.E.** TWEAK and LTβ Signaling during Chronic Liver Disease. Front Immunol 5, 39 (2014).

28. **Lee, T.K.W., Castilho, A., Ma, S. & Ng, I.O.L.** Liver cancer stem cells: implications for a new therapeutic target. Liver Int. 29, 955-65 (2009).

29. **He, G., Dhar, D., Nakagawa, H., Font-Burgada, J., Ogata, H., Jiang, Y., Shalapour, S., Seki, E., Yost, S.E., Jepsen, K., Frazer, K.A., Harismendy, O., Hatziapostolou, M., Iliopoulos, D., Suetsugu, A., Hoffman, R.M., Tateishi, R., Koike, K. & Karin, M.** Identification of liver cancer progenitors whose malignant progression depends on autocrine IL-6 signaling. Cell 155, 384-96 (2013).

30. **Hernandez-Gea, V. & Friedman, S.L.** Pathogenesis of liver fibrosis. Annu Rev Pathol 6, 425-56 (2011).

31. **El-Serag, H.B. & Rudolph, K.L.** Hepatocellular carcinoma: epidemiology and molecular carcinogenesis. Gastroenterology 132, 2557-76 (2007).

32. **Rippe, R.A. & Brenner, D.A.** From quiescence to activation: Gene regulation in hepatic stellate cells. Gastroenterology 127, 1260-2 (2004).

33. **Win, K.M., Charlotte, F., Mallat, A., Cherqui, D., Martin, N., Mavier, P., Preaux, A.M., Dhumeaux, D. & Rosenbaum, J.** Mitogenic effect of transforming growth factor-beta 1 on human Ito cells in culture: evidence for mediation by endogenous platelet-derived growth factor. Hepatology 18, 137-45 (1993).

34. **Mullhaupt, B., Feren, A., Fodor, E. & Jones, A.** Liver expression of epidermal growth factor RNA. Rapid increases in immediate-early phase of liver regeneration. J. Biol. Chem. 269, 19667-70 (1994).

35. **Stöcker, W. & Bode, W.** Structural features of a superfamily of zinc-endopeptidases: the metzincins. Curr. Opin. Struct. Biol. 5, 383-90 (1995).

36. **Rawlings, N.D., Waller, M., Barrett, A.J. & Bateman, A.** MEROPS: the database of proteolytic enzymes, their substrates and inhibitors. Nucleic Acids Res. 42, D503-9 (2014).

37. **Huxley-Jones, J., Clarke, T., Beck, C., Toubaris, G., Robertson, D.L. & Boot-Handford, R.P.** The evolution of the vertebrate metzincins; insights from Ciona intestinalis and Danio rerio. BMC Evol. Biol. 7, 63 (2007).

38. **Escrevente, C., Morais, V.A., Keller, S., Soares, C.M., Altevogt, P. & Costa, J.** Functional role of N-glycosylation from ADAM10 in processing, localization and activity of the enzyme. Biochim. Biophys. Acta 1780, 905-13 (2008).

39. **Roghani, M., Becherer, J.D., Moss, M.L., Atherton, R.E., Erdjument-Bromage, H., Arribas, J., Blackburn, R.K., Weskamp, G., Tempst, P. & Blobel, C.P.** Metalloprotease-disintegrin MDC9: intracellular maturation and catalytic activity. J. Biol. Chem. 274, 3531-40 (1999).

40. **Leonard, J.D., Lin, F. & Milla, M.E.** Chaperone-like properties of the prodomain of TNFalpha-converting enzyme (TACE) and the functional role of its cysteine switch. Biochem. J. 387, 797-805 (2005).

41. **Endres, K., Anders, A., Kojro, E., Gilbert, S., Fahrenholz, F. & Postina, R.** Tumor necrosis factor-alpha converting enzyme is processed by proprotein-convertases to its mature form which is degraded upon

phorbol ester stimulation. Eur. J. Biochem. 270, 2386-93 (2003).

42. **Hwang, E.M., Kim, S., Sohn, J., Lee, J.Y., Kim, Y., Kim, Y.S. & Mook-Jung, I.** Furin is an endogenous regulator of alpha-secretase associated APP processing. Biochem. Biophys. Res. Commun. 349, 654-9 (2006).

43. **Gonzales, P.E., Solomon, A., Miller, A.B., Leesnitzer, M.A., Sagi, I. & Milla, M.E.** Inhibition of the tumor necrosis factor-alpha-converting enzyme by its pro domain. J. Biol. Chem. 279, 31638-45 (2004).

44. **Moss, M.L., Bomar, M., Liu, Q., Sage, H., Dempsey, P., Lenhart, P.M., Gillispie, P.A., Stoeck, A., Wildeboer, D., Bartsch, J.W., Palmisano, R. & Zhou, P.** The ADAM10 prodomain is a specific inhibitor of ADAM10 proteolytic activity and inhibits cellular shedding events. J. Biol. Chem. 282, 35712-21 (2007).

45. **White, J.M.** ADAMs: modulators of cell-cell and cell-matrix interactions. Curr. Opin. Cell Biol. 15, 598-606 (2003).

46. **Janes, P.W., Saha, N., Barton, W.A., Kolev, M.V., Wimmer-Kleikamp, S.H., Nievergall, E., Blobel, C.P., Himanen, J., Lackmann, M. & Nikolov, D.B.** Adam meets Eph: an ADAM substrate recognition module acts as a molecular switch for ephrin cleavage in trans. Cell 123, 291-304 (2005).

47. **Takeda, S., Igarashi, T., Mori, H. & Araki, S.** Crystal structures of VAP1 reveal ADAMs' MDC domain architecture and its unique C-shaped scaffold. EMBO J. 25, 2388-96 (2006).

48. **Seals, D.F. & Courtneidge, S.A.** The ADAMs family of metalloproteases: multidomain proteins with multiple functions. Genes Dev. 17, 7-30 (2003).

49. **Bode, W., Gomis-Rüth, F.X. & Stöckler, W.** Astacins, serralysins, snake venom and matrix metalloproteinases exhibit identical zinc-binding environments (HEXXHXXGXXH and Met-turn) and topologies and should be grouped into a common family, the 'metzincins'. FEBS Lett. 331, 134-40 (1993).

50. **Edwards, D.R., Handsley, M.M. & Pennington, C.J.** The ADAM metalloproteinases. Mol. Aspects Med. 29, 258-89 (2008).

51. **Sahin, U., Weskamp, G., Kelly, K., Zhou, H., Higashiyama, S., Peschon, J., Hartmann, D., Saftig, P. & Blobel, C.P.** Distinct roles for ADAM10 and ADAM17 in ectodomain shedding of six EGFR ligands. J. Cell Biol. 164, 769-79 (2004).

52. **Iwamoto, R. & Mekada, E.** Heparin-binding EGF-like growth factor: a juxtacrine growth factor. Cytokine Growth Factor Rev. 11, 335-44 (2000).

53. **Uchikawa, S., Yoda, M., Tohmonda, T., Kanaji, A., Matsumoto, M., Toyama, Y. & Horiuchi, K.** ADAM17 regulates IL-1 signaling by selectively releasing IL-1 receptor type 2 from the cell surface. Cytokine 71, 238-45 (2015).

54. **Rose-John, S.** IL-6 trans-signaling via the soluble IL-6 receptor: importance for the pro-inflammatory activities of IL-6. Int. J. Biol. Sci. 8, 1237-47 (2012).

55. **Wolfe, M.S. & Kopan, R.** Intramembrane proteolysis: theme and variations. Science 305, 1119-23 (2004).

56. **Groot, A.J., Habets, R., Yahyanejad, S., Hodin, C.M., Reiss, K., Saftig, P., Theys, J. & Vooijs, M.** Regulated proteolysis of NOTCH2 and NOTCH3 receptors by ADAM10 and presenilins. Mol. Cell. Biol. 34, 2822-32 (2014).

57. **Murphy, G., Murthy, A. & Khokha, R.** Clipping, shedding and RIPping keep immunity on cue. Trends Immunol. 29, 75-82 (2008).

58. **Nagano, O. & Saya, H.** Mechanism and biological significance of CD44 cleavage. Cancer Sci. 95, 930-5 (2004).

59. **Chantry, A., Gregson, N.A. & Glynn, P.** A novel metalloproteinase associated with brain myelin membranes. Isolation and characterization. J. Biol. Chem. 264, 21603-7 (1989).

60. **Yamazaki, K., Mizui, Y. & Tanaka, I.** Radiation hybrid mapping of human ADAM10 gene to chromosome 15. Genomics 45, 457-9 (1997).

61. **Yamazaki, K., Mizui, Y., Sagane, K. & Tanaka, I.** Assignment of a disintegrin and metalloproteinase domain 10 (Adam10) gene to mouse chromosome 9. Genomics 46, 528-9 (1997).

62. **Lammich, S., Buell, D., Zilow, S., Ludwig, A., Nuscher, B., Lichtenthaler, S.F., Prinzen, C., Fahrenholz, F. & Haass, C.** Expression of the anti-amyloidogenic secretase ADAM10 is suppressed by its 5'-untranslated

region. J. Biol. Chem. 285, 15753-60 (2010).

63. **Bai, S., Nasser, M.W., Wang, B., Hsu, S., Datta, J., Kutay, H., Yadav, A., Nuovo, G., Kumar, P. & Ghoshal, K.** MicroRNA-122 inhibits tumorigenic properties of hepatocellular carcinoma cells and sensitizes these cells to sorafenib. J. Biol. Chem. 284, 32015-27 (2009).

64. **Marcello, E., Gardoni, F., Mauceri, D., Romorini, S., Jeromin, A., Epis, R., Borroni, B., Cattabeni, F., Sala, C., Padovani, A. & Di Luca, M.** Synapse-associated protein-97 mediates alpha-secretase ADAM10 trafficking and promotes its activity. J. Neurosci. 27, 1682-91 (2007).

65. **Wild-Bode, C., Fellerer, K., Kugler, J., Haass, C. & Capell, A.** A basolateral sorting signal directs ADAM10 to adherens junctions and is required for its function in cell migration. J. Biol. Chem. 281, 23824-9 (2006).

66. **Marcello, E., Gardoni, F., Di Luca, M. & Pérez-Otaño, I.** An arginine stretch limits ADAM10 exit from the endoplasmic reticulum. J. Biol. Chem. 285, 10376-84 (2010).

67. **Horiuchi, K., Le Gall, S., Schulte, M., Yamaguchi, T., Reiss, K., Murphy, G., Toyama, Y., Hartmann, D., Saftig, P. & Blobel, C.P.** Substrate selectivity of epidermal growth factor-receptor ligand sheddases and their regulation by phorbol esters and calcium influx. Mol. Biol. Cell 18, 176-88 (2007).

68. **Kohutek, Z.A., diPierro, C.G., Redpath, G.T. & Hussaini, I.M.** ADAM-10-mediated N-cadherin cleavage is protein kinase C-alpha dependent and promotes glioblastoma cell migration. J. Neurosci. 29, 4605-15 (2009).

69. **Yan, Y., Shirakabe, K. & Werb, Z.** The metalloprotease Kuzbanian (ADAM10) mediates the transactivation of EGF receptor by G protein-coupled receptors. J. Cell Biol. 158, 221-6 (2002).

70. **Amour, A., Knight, C.G., Webster, A., Slocombe, P.M., Stephens, P.E., Knäuper, V., Docherty, A.J. & Murphy, G.** The in vitro activity of ADAM-10 is inhibited by TIMP-1 and TIMP-3. FEBS Lett. 473, 275-9 (2000).

71. **Jefferson, T., Auf dem Keller, U., Bellac, C., Metz, V.V., Broder, C., Hedrich, J., Ohler, A., Maier, W., Magdolen, V., Sterchi, E., Bond, J.S., Jayakumar, A., Traupe, H., Chalaris, A., Rose-John, S., Pietrzik, C.U., Postina, R., Overall, C.M. & Becker-Pauly, C.** The substrate degradome of meprin metalloproteases reveals an unexpected proteolytic link between meprin β and ADAM10. Cell. Mol. Life Sci. 70, 309-33 (2013).

72. **Tousseyn, T., Thathiah, A., Jorissen, E., Raemaekers, T., Konietzko, U., Reiss, K., Maes, E., Snellinx, A., Serneels, L., Nyabi, O., Annaert, W., Saftig, P., Hartmann, D. & De Strooper, B.** ADAM10, the rate-limiting protease of regulated intramembrane proteolysis of Notch and other proteins, is processed by ADAMS-9, ADAMS-15, and the gamma-secretase. J. Biol. Chem. 284, 11738-47 (2009).

73. **Parkin, E. & Harris, B.** A disintegrin and metalloproteinase (ADAM)-mediated ectodomain shedding of ADAM10. J. Neurochem. 108, 1464-79 (2009).

74. **Kojro, E., Gimpl, G., Lammich, S., Marz, W. & Fahrenholz, F.** Low cholesterol stimulates the nonamyloidogenic pathway by its effect on the alpha -secretase ADAM 10. Proc. Natl. Acad. Sci. U.S.A. 98, 5815-20 (2001).

75. **Harris, B., Pereira, I. & Parkin, E.** Targeting ADAM10 to lipid rafts in neuroblastoma SH-SY5Y cells impairs amyloidogenic processing of the amyloid precursor protein. Brain Res. 1296, 203-15 (2009).

76. **Haag, M.D.M., Hofman, A., Koudstaal, P.J., Stricker, B.H.C. & Breteler, M.M.B.** Statins are associated with a reduced risk of Alzheimer disease regardless of lipophilicity. The Rotterdam Study. J. Neurol. Neurosurg. Psychiatr. 80, 13-7 (2009).

77. **Zandi, P.P., Sparks, D.L., Khachaturian, A.S., Tschanz, J., Norton, M., Steinberg, M., Welsh-Bohmer, K.A., Breitner, J.C.S.** Do statins reduce risk of incident dementia and Alzheimer disease? The Cache County Study. Arch. Gen. Psychiatry 62, 217-24 (2005).

78. **Xu, D., Sharma, C. & Hemler, M.E.** Tetraspanin12 regulates ADAM10-dependent cleavage of amyloid precursor protein. FASEB J. 23, 3674-81 (2009).

79. **Prox, J., Willenbrock, M., Weber, S., Lehmann, T., Schmidt-Arras, D., Schwanbeck, R., Saftig, P. & Schwake, M.** Tetraspanin15 regulates cellular trafficking and activity of the ectodomain sheddase ADAM10. Cell. Mol. Life Sci. 69, 2919-32 (2012).

80. **Arduise, C., Abache, T., Li, L., Billard, M., Chabanon, A., Ludwig, A., Mauduit, P., Boucheix, C., Rubinstein, E. & Le Naour, F.** Tetraspanins regulate ADAM10-mediated cleavage of TNF-alpha and epidermal growth factor. J. Immunol. 181, 7002-13 (2008).

81. **Pruessmeyer, J. & Ludwig, A.** The good, the bad and the ugly substrates for ADAM10 and ADAM17 in brain pathology, inflammation and cancer. Semin. Cell Dev. Biol. 20, 164-74 (2009).

82. **Lammich, S., Kojro, E., Postina, R., Gilbert, S., Pfeiffer, R., Jasionowski, M., Haass, C. & Fahrenholz, F.** Constitutive and regulated alpha-secretase cleavage of Alzheimer's amyloid precursor protein by a disintegrin metalloprotease. Proc. Natl. Acad. Sci. U.S.A. 96, 3922-7 (1999).

83. **Tian, L., Wu, X., Chi, C., Han, M., Xu, T. & Zhuang, Y.** ADAM10 is essential for proteolytic activation of Notch during thymocyte development. Int. Immunol. 20, 1181-7 (2008).

84. **Weskamp, G., Ford, J.W., Sturgill, J., Martin, S., Docherty, A.J.P., Swendeman, S., Broadway, N., Hartmann, D., Saftig, P., Umland, S., Sehara-Fujisawa, A., Black, R.A., Ludwig, A., Becherer, J.D., Conrad, D.H. & Blobel, C.P.** ADAM10 is a principal 'sheddase' of the low-affinity immunoglobulin E receptor CD23. Nat. Immunol. 7, 1293-8 (2006).

85. **Gough, P.J., Garton, K.J., Wille, P.T., Rychlewski, M., Dempsey, P.J. & Raines, E.W.** A disintegrin and metalloproteinase 10-mediated cleavage and shedding regulates the cell surface expression of CXC chemokine ligand 16. J. Immunol. 172, 3678-85 (2004).

86. **Schulte, M., Reiss, K., Lettau, M., Maretzky, T., Ludwig, A., Hartmann, D., de Strooper, B., Janssen, O. & Saftig, P.** ADAM10 regulates FasL cell surface expression and modulates FasL-induced cytotoxicity and activation-induced cell death. Cell Death Differ. 14, 1040-9 (2007).

87. **Schroeder, A., Fahrenholz, F. & Schmitt, U.** Effect of a dominant-negative form of ADAM10 in a mouse model of Alzheimer's disease. J. Alzheimers Dis. 16, 309-14 (2009).

88. **Mumm, J.S. & Kopan, R.** Notch signaling: from the outside in. Dev. Biol. 228, 151-65 (2000).

89. **Kageyama, R., Ohtsuka, T. & Kobayashi, T.** The Hes gene family: repressors and oscillators that orchestrate embryogenesis. Development 134, 1243-51 (2007).

90. **Zhang, C., Tian, L., Chi, C., Wu, X., Yang, X., Han, M., Xu, T., Zhuang, Y. & Deng, K.** Adam10 is essential for early embryonic cardiovascular development. Dev. Dyn. 239, 2594-602 (2010).

91. **Bozkulak, E.C. & Weinmaster, G.** Selective use of ADAM10 and ADAM17 in activation of Notch1 signaling. Mol. Cell. Biol. 29, 5679-95 (2009).

92. **Tsai, Y., VanDussen, K.L., Sawey, E.T., Wade, A.W., Kasper, C., Rakshit, S., Bhatt, R.G., Stoeck, A., Maillard, I., Crawford, H.C., Samuelson, L.C. & Dempsey, P.J.** ADAM10 regulates Notch function in intestinal stem cells of mice. Gastroenterology 147, 822-834.e13 (2014).

93. **Weber, S., Niessen, M.T., Prox, J., Lüllmann-Rauch, R., Schmitz, A., Schwanbeck, R., Blobel, C.P., Jorissen, E., de Strooper, B., Niessen, C.M. & Saftig, P.** The disintegrin/metalloproteinase Adam10 is essential for epidermal integrity and Notch-mediated signaling. Development 138, 495-505 (2011).

94. **Cooper, A.M., Hobson, P.S., Jutton, M.R., Kao, M.W., Drung, B., Schmidt, B., Fear, D.J., Beavil, A.J., McDonnell, J.M., Sutton, B.J. & Gould, H.J.** Soluble CD23 controls IgE synthesis and homeostasis in human B cells. J. Immunol. 188, 3199-207 (2012).

95. **Maretzky, T., Reiss, K., Ludwig, A., Buchholz, J., Scholz, F., Proksch, E., de Strooper, B., Hartmann, D. & Saftig, P.** ADAM10 mediates E-cadherin shedding and regulates epithelial cell-cell adhesion, migration, and beta-catenin translocation. Proc. Natl. Acad. Sci. U.S.A. 102, 9182-7 (2005).

96. **Maretzky, T., Scholz, F., Köten, B., Proksch, E., Saftig, P. & Reiss, K.** ADAM10-mediated E-cadherin release is regulated by proinflammatory cytokines and modulates keratinocyte cohesion in eczematous dermatitis. J. Invest. Dermatol. 128, 1737-46 (2008).

97. **Huh, C., Factor, V.M., Sánchez, A., Uchida, K., Conner, E.A. & Thorgeirsson, S.S.** Hepatocyte growth factor/c-met signaling pathway is required for efficient liver regeneration and repair. Proc. Natl. Acad. Sci. U.S.A. 101, 4477-82 (2004).

98. **Lendeckel, U., Kohl, J., Arndt, M., Carl-McGrath, S., Donat, H. & Röcken, C.** Increased expression of ADAM family members in human breast cancer and breast cancer cell lines. J. Cancer Res. Clin. Oncol. 131, 41-8 (2005).

99. **Gavert, N., Sheffer, M., Raveh, S., Spaderna, S., Shtutman, M., Brabletz, T., Barany, F., Paty, P., Notterman, D., Domany, E. & Ben-Ze'ev, A.** Expression of L1-CAM and ADAM10 in human colon cancer cells induces metastasis. Cancer Res. 67, 7703-12 (2007).

100. **Yoshimura, T., Tomita, T., Dixon, M.F., Axon, A.T.R., Robinson, P.A. & Crabtree, J.E.** ADAMs (a disintegrin and metalloproteinase) messenger RNA expression in Helicobacter pylori-infected, normal, and neoplastic gastric mucosa. J. Infect. Dis. 185, 332-40 (2002).

101. **Wu, E., Croucher, P.I. & McKie, N.** Expression of members of the novel membrane linked metalloproteinase family ADAM in cells derived from a range of haematological malignancies. Biochem. Biophys. Res. Commun. 235, 437-42 (1997).

102. **McCulloch, D.R., Akl, P., Samaratunga, H., Herington, A.C. & Odorico, D.M.** Expression of the disintegrin metalloprotease, ADAM-10, in prostate cancer and its regulation by dihydrotestosterone, insulin-like growth factor I, and epidermal growth factor in the prostate cancer cell model LNCaP. Clin. Cancer Res. 10, 314-23 (2004).

103. **Ko, S., Lin, S., Wong, Y., Liu, C., Chang, K. & Liu, T.** Increase of disintergin metalloprotease 10 (ADAM10) expression in oral squamous cell carcinoma. Cancer Lett. 245, 33-43 (2007).

104. **Fogel, M., Gutwein, P., Mechtersheimer, S., Riedle, S., Stoeck, A., Smirnov, A., Edler, L., Ben-Arie, A., Huszar, M. & Altevogt, P.** L1 expression as a predictor of progression and survival in patients with uterine and ovarian carcinomas. Lancet 362, 869-75 (2003).

105. **Saftig, P. & Reiss, K.** The "A Disintegrin And Metalloproteases" ADAM10 and ADAM17: novel drug targets with therapeutic potential?. Eur. J. Cell Biol. 90, 527-35 (2011).

106. **Hartmann, D., de Strooper, B., Serneels, L., Craessaerts, K., Herreman, A., Annaert, W., Umans, L., Lübke, T., Lena Illert, A., von Figura, K. & Saftig, P.** The disintegrin/metalloprotease ADAM 10 is essential for Notch signalling but not for alpha-secretase activity in fibroblasts. Hum. Mol. Genet. 11, 2615-24 (2002).

107. **Orban, P.C., Chui, D. & Marth, J.D.** Tissue- and site-specific DNA recombination in transgenic mice. Proc. Natl. Acad. Sci. U.S.A. 89, 6861-5 (1992).

108. **Jorissen, E., Prox, J., Bernreuther, C., Weber, S., Schwanbeck, R., Serneels, L., Snellinx, A., Craessaerts, K., Thathiah, A., Tesseur, I., Bartsch, U., Weskamp, G., Blobel, C.P., Glatzel, M., De Strooper, B. & Saftig, P.** The disintegrin/metalloproteinase ADAM10 is essential for the establishment of the brain cortex. J. Neurosci. 30, 4833-44 (2010).

109. **Tirnitz-Parker, J.E.E., Tonkin, J.N., Knight, B., Olynyk, J.K. & Yeoh, G.C.T.** Isolation, culture and immortalisation of hepatic oval cells from adult mice fed a choline-deficient, ethionine-supplemented diet. Int. J. Biochem. Cell Biol. 39, 2226-39 (2007).

110. **Kellendonk, C., Opherk, C., Anlag, K., Schütz, G. & Tronche, F.** Hepatocyte-specific expression of Cre recombinase. Genesis 26, 151-3 (2000).

111. **Srinivas, S., Watanabe, T., Lin, C.S., William, C.M., Tanabe, Y., Jessell, T.M. & Costantini, F.** Cre reporter strains produced by targeted insertion of EYFP and ECFP into the ROSA26 locus. BMC Dev. Biol. 1, 4 (2001).

112. **Tchorz, J.S., Kinter, J., Müller, M., Tornillo, L., Heim, M.H. & Bettler, B.** Notch2 signaling promotes biliary epithelial cell fate specification and tubulogenesis during bile duct development in mice. Hepatology 50, 871-9 (2009).

113. **Fiorotto, R., Raizner, A., Morell, C.M., Torsello, B., Scirpo, R., Fabris, L., Spirli, C. & Strazzabosco, M.** Notch signaling regulates tubular morphogenesis during repair from biliary damage in mice. J. Hepatol. 59, 124-30 (2013).

114. **Kikuchi, S., Hata, M., Fukumoto, K., Yamane, Y., Matsui, T., Tamura, A., Yonemura, S., Yamagishi, H., Keppler, D., Tsukita, S. & Tsukita, S.** Radixin deficiency causes conjugated hyperbilirubinemia with loss of Mrp2 from bile canalicular membranes. Nat. Genet. 31, 320-5 (2002).

115. **Wang, W., Soroka, C.J., Mennone, A., Rahner, C., Harry, K., Pypaert, M. & Boyer, J.L.** Radixin is required to maintain apical canalicular membrane structure and function in rat hepatocytes. Gastroenterology 131, 878-84 (2006).

116. **Jaeschke, H. & Hasegawa, T.** Role of neutrophils in acute inflammatory liver injury. Liver Int. 26, 912-9 (2006).

117. **Arend, W.P. & Guthridge, C.J.** Biological role of interleukin 1 receptor antagonist isoforms. Ann. Rheum. Dis. 59 Suppl 1, i60-4 (2000).

118. **Di Mitri, D., Toso, A., Chen, J.J., Sarti, M., Pinton, S., Jost, T.R., D'Antuono, R., Montani, E., Garcia-Escudero, R., Guccini, I., Da Silva-Alvarez, S., Collado, M., Eisenberger, M., Zhang, Z., Catapano, C., Grassi, F. & Alimonti, A.** Tumour-infiltrating Gr-1+ myeloid cells antagonize senescence in cancer. Nature 515, 134-7 (2014).

119. **Ponta, H., Sherman, L. & Herrlich, P.A.** CD44: from adhesion molecules to signalling regulators. Nat. Rev. Mol. Cell Biol. 4, 33-45 (2003).

120. **Roos, C., Wicovsky, A., Müller, N., Salzmann, S., Rosenthal, T., Kalthoff, H., Trauzold, A., Seher, A., Henkler, F., Kneitz, C. & Wajant, H.** Soluble and transmembrane TNF-like weak inducer of apoptosis differentially activate the classical and noncanonical NF-kappa B pathway. J. Immunol. 185, 1593-605 (2010).

121. **Nguyen, L.N., Furuya, M.H., Wolfraim, L.A., Nguyen, A.P., Holdren, M.S., Campbell, J.S., Knight, B., Yeoh, G.C.T., Fausto, N. & Parks, W.T.** Transforming growth factor-beta differentially regulates oval cell and hepatocyte proliferation. Hepatology 45, 31-41 (2007).

122. **Kuramitsu, K., Sverdlov, D.Y., Liu, S.B., Csizmadia, E., Burkly, L., Schuppan, D., Hanto, D.W., Otterbein, L.E. & Popov, Y.** Failure of fibrotic liver regeneration in mice is linked to a severe fibrogenic response driven by hepatic progenitor cell activation. Am. J. Pathol. 183, 182-94 (2013).

123. **Ding, B., Cao, Z., Lis, R., Nolan, D.J., Guo, P., Simons, M., Penfold, M.E., Shido, K., Rabbany, S.Y. & Rafii, S.** Divergent angiocrine signals from vascular niche balance liver regeneration and fibrosis. Nature 505, 97-102 (2014).

124. **Kopitz, C., Gerg, M., Bandapalli, O.R., Ister, D., Pennington, C.J., Hauser, S., Flechsig, C., Krell, H., Antolovic, D., Brew, K., Nagase, H., Stangl, M., von Weyhern, C.W.H., Brücher, B.L.D.M., Brand, K., Coussens, L.M., Edwards, D.R. & Krüger, A.** Tissue inhibitor of metalloproteinases-1 promotes liver metastasis by induction of hepatocyte growth factor signaling. Cancer Res. 67, 8615-23 (2007).

125. **Fausto, N. & Campbell, J.S.** The role of hepatocytes and oval cells in liver regeneration and repopulation. Mech. Dev. 120, 117-30 (2003).

126. **Ma, J., Tang, X., Wong, P., Jacobs, B., Borden, E.C. & Bedogni, B.** Noncanonical activation of Notch1 protein by membrane type 1 matrix metalloproteinase (MT1-MMP) controls melanoma cell proliferation. J. Biol. Chem. 289, 8442-9 (2014).

127. **Gujral, J.S., Farhood, A., Bajt, M.L. & Jaeschke, H.** Neutrophils aggravate acute liver injury during obstructive cholestasis in bile duct-ligated mice. Hepatology 38, 355-63 (2003).

128. **Sgroi, A., Gonelle-Gispert, C., Morel, P., Baertschiger, R.M., Niclauss, N., Mentha, G., Majno, P., Serre-Beinier, V. & Buhler, L.** Interleukin-1 receptor antagonist modulates the early phase of liver regeneration after partial hepatectomy in mice. PLoS One 6, e25442 (2011).

129. **van der Vorst, E.P.C., Jeurissen, M., Wolfs, I.M.J., Keijbeck, A., Theodorou, K., Wijnands, E., Schurgers, L., Weber, S., Gijbels, M.J., Hamers, A.A.J., Dreymueller, D., Rose-John, S., de Winther, M.P.J., Ludwig, A., Saftig, P., Biessen, E.A.L. & Donners, M.M.P.C.** Myeloid A Disintegrin and Metalloproteinase Domain 10 Deficiency Modulates Atherosclerotic Plaque Composition by Shifting the Balance from Inflammation toward Fibrosis. Am. J. Pathol. , (2015).

130. **Weskamp, G., Schlöndorff, J., Lum, L., Becherer, J.D., Kim, T., Saftig, P., Hartmann, D., Murphy, G. & Blobel, C.P.** Evidence for a critical role of the tumor necrosis factor alpha convertase (TACE) in ectodomain shedding of the p75 neurotrophin receptor (p75NTR). J. Biol. Chem. 279, 4241-9 (2004).

131. **Lemaigre, F.P.** Mechanisms of liver development: concepts for understanding liver disorders and design of novel therapies. Gastroenterology 137, 62-79 (2009).

132. **Schelter, F., Grandl, M., Seubert, B., Schaten, S., Hauser, S., Gerg, M., Boccaccio, C., Comoglio, P. & Krüger, A.** Tumor cell-derived Timp-1 is necessary for maintaining metastasis-promoting Met-signaling via inhibition of Adam-10. Clin. Exp. Metastasis 28, 793-802 (2011).

133. **Coombes, J.D., Swiderska-Syn, M., Dollé, L., Reid, D., Eksteen, B., Claridge, L., Briones-Orta, M.A., Shetty, S., Oo, Y.H., Riva, A., Chokshi, S., Papa, S., Mi, Z., Kuo, P.C., Williams, R., Canbay, A., Adams, D.H., Diehl, A.M., van Grunsven, L.A., Choi, S.S. & Syn, W.K.** Osteopontin neutralisation abrogates the liver progenitor cell response and fibrogenesis in mice. Gut , (2014).

134. **Wang, X., Lopategi, A., Ge, X., Lu, Y., Kitamura, N., Urtasun, R., Leung, T., Fiel, M.I. & Nieto, N.** Osteopontin induces ductular reaction contributing to liver fibrosis. Gut 63, 1805-18 (2014).

135. **Akhurst, B., Croager, E.J., Farley-Roche, C.A., Ong, J.K., Dumble, M.L., Knight, B. & Yeoh, G.C.** A modified choline-deficient, ethionine-supplemented diet protocol effectively induces oval cells in mouse liver. Hepatology 34, 519-22 (2001).

136. **Schuler, M., Dierich, A., Chambon, P. & Metzger, D.** Efficient temporally controlled targeted somatic mutagenesis in hepatocytes of the mouse. Genesis 39, 167-72 (2004).

137. **Tarlow, B.D., Pelz, C., Naugler, W.E., Wakefield, L., Wilson, E.M., Finegold, M.J. & Grompe, M.** Bipotential adult liver progenitors are derived from chronically injured mature hepatocytes. Cell Stem Cell 15, 605-18 (2014).

138. **Sackett, S.D., Li, Z., Hurtt, R., Gao, Y., Wells, R.G., Brondell, K., Kaestner, K.H. & Greenbaum, L.E.** Foxl1 is a marker of bipotential hepatic progenitor cells in mice. Hepatology 49, 920-9 (2009).

139. **Maretzky, T., McIlwain, D.R., Issuree, P.D.A., Li, X., Malapeira, J., Amin, S., Lang, P.A., Mak, T.W. & Blobel, C.P.** iRhom2 controls the substrate selectivity of stimulated ADAM17-dependent ectodomain shedding. Proc. Natl. Acad. Sci. U.S.A. 110, 11433-8 (2013).

140. **Hemler, M.E.** Tetraspanin functions and associated microdomains. Nat. Rev. Mol. Cell Biol. 6, 801-11 (2005).

141. **Imhof, I., Gasper, W.J. & Derynck, R.** Association of tetraspanin CD9 with transmembrane TGF{alpha} confers alterations in cell-surface presentation of TGF{alpha} and cytoskeletal organization. J. Cell. Sci. 121, 2265-74 (2008).

142. **Inui, S., Higashiyama, S., Hashimoto, K., Higashiyama, M., Yoshikawa, K. & Taniguchi, N.** Possible role of coexpression of CD9 with membrane-anchored heparin-binding EGF-like growth factor and amphiregulin in cultured human keratinocyte growth. J. Cell. Physiol. 171, 291-8 (1997).

143. **Berasain, C. & Avila, M.A.** The EGFR signalling system in the liver: from hepatoprotection to hepatocarcinogenesis. J. Gastroenterol. 49, 9-23 (2014).

144. **Kanetaka, K., Sakamoto, M., Yamamoto, Y., Yamasaki, S., Lanza, F., Kanematsu, T. & Hirohashi, S.** Overexpression of tetraspanin CO-029 in hepatocellular carcinoma. J. Hepatol. 35, 637-42 (2001).

145. **Tippmann, F., Hundt, J., Schneider, A., Endres, K. & Fahrenholz, F.** Up-regulation of the alpha-secretase ADAM10 by retinoic acid receptors and acitretin. FASEB J. 23, 1643-54 (2009).

146. **Endres, K., Fahrenholz, F., Lotz, J., Hiemke, C., Teipel, S., Lieb, K., Tüscher, O. & Fellgiebel, A.** Increased CSF APPs-α levels in patients with Alzheimer disease treated with acitretin. Neurology 83, 1930-5 (2014).

147. **Schönig, K., Schwenk, F., Rajewsky, K. & Bujard, H.** Stringent doxycycline dependent control of CRE recombinase in vivo. Nucleic Acids Res. 30, e134 (2002).

148. **Perl, A.T., Wert, S.E., Nagy, A., Lobe, C.G. & Whitsett, J.A.** Early restriction of peripheral and proximal cell lineages during formation of the lung. Proc. Natl. Acad. Sci. U.S.A. 99, 10482-7 (2002).

149. **Cassonnet, P., Rolloy, C., Neveu, G., Vidalain, P., Chantier, T., Pellet, J., Jones, L., Muller, M., Demeret, C., Gaud, G., Vuillier, F., Lotteau, V., Tangy, F., Favre, M. & Jacob, Y.** Benchmarking a luciferase complementation assay for detecting protein complexes. Nat. Methods 8, 990-2 (2011).

150. **Inoue, A., Ishiguro, J., Kitamura, H., Arima, N., Okutani, M., Shuto, A., Higashiyama, S., Ohwada, T., Arai, H., Makide, K. & Aoki, J.** TGFα shedding assay: an accurate and versatile method for detecting GPCR activation. Nat. Methods 9, 1021-9 (2012).

6 Appendix

6.1 Supplementary Information

6.1.1 Supplementary Materials

6.1.1.1 Chemicals

Dulbecco's modified Eagle medium (DMEM)	Sigma-Aldrich, Steinheim, Germany
Polyethylenimine	Polysciences, Eppelheim, Germany
Coelenterazine	Promega, Mannheim, Germany

6.1.1.2 Primers and oligonucleotides

Supplementary Table 1. Primers for DNA inserts

Target	Forward Primer (5'-3')	Reverse Primer (5'-3')	Annealing Temperature
hTspan8 (for pTRIPZ)	GCC**A↓CCGGT**GCCACCATGGCAG GTGTGAGTG	CTT**A↓CGCGT**ACTCACAAGTCCTCTTC AC	54°C/>72°C
hCD9 (for pTRIPZ)	CGCGC**A↓CCGGT**GCCACCATGCC GGTCAAAGGAGGC	CCAGCGAT**A↓CGCGT**CCTGCA↓GGGA CCATCTCGCGGTTCC	56°C/>72°C
hCD9 (for pENTR4)	CGTCGA**GC↓GGCCGC**ATGCCGGT CAAAGG	GACTGCAG**C↓TCGAG**TCGACCATCTCG CGGT	44°C/>72°C
hCD81 (for pTRIPZ)	CGACCGC**A↓CCGGT**GCCACCATG GGAGTGGAGGGCTGCAC	CCAGCGAT**A↓CGCGT**CCTGCA↓GGGTA CACGGAGCTGTTCC	56°C/>72°C
hCD81 (for pENTR4)	CGTCGA**GC↓GGCCGC**ATGGGAGT GGAGGG	GACTGCAG**C↓TCGAG**TCGTACACGGAG CTGTT	44°C/>72°C
hADAM10 (for pENTR4)	ATCATC**G↓TCGAC**ATGGTGTTGCT GAGAGTGTTAATTCTGCTC	ATCATC**GC↓GGCCGC**AAGCGTCTCATG TGTCCC	72°C
hADAM17 (for pENTR4)	CAT**GC↓GGCCGC**CACCATGAGGC AGTCTCTC	CGACGG**G↓TCGAC**CGGCACTCTGTTTC TTT	45°C/>72°C

Supplementary Table 2. Oligonucleotides

	5'-3' Sequence
3x HA insert sense	↓GGATACCCGTATGACGTCCCGGATTACGCTTACCCGTATGACGTCCCGGATTACGC TTACCCGTATGACGTCCCGGATTACGCTTAA**A↓**
3xHA insert antisense	↓**CGCG**TTTAAGCGTAATCCGGGACGTCATACGGGTAAGCGTAATCCGGGACGTCAT ACGGGTAAGCGTAATCCGGGACGTCATACGGGTAT**CCTGCA↓**

6.1.1.3 Primer

Supplementary Table 3. Primers for genotyping and genomic DNA			
Target	Forward Primer (5'-3')	Reverse Primer (5'-3')	Expected bandsize
rtTA	CCATGTCTAGACTGGACAAGA	CTCCAGGCCACATATGATTAG	600 bp

6.1.1.4 Cell lines

Supplementary Table 4. Cell lines and respective culture media				
Cell line	Source of cells	Culture medium	Source	Remarks
HEK293-T	Human embryonic kidney	Dulbecco's modified Eagle Medium (DMEM) + 10% FCS	DSMZ	

6.1.1.5 Mice

Supplementary Table 5. Mice		
Mouse line	Source	Reference
B6.Tg(Cebpb-rtTA2S*S2)1Bjd	EMMA:EM:00404	[147]
B6.Cg-Tg(tetO-cre)1Jaw/J	Paul Saftig (University Kiel, Germany)	[148]

6.1.2 Supplementary Methods

6.1.2.1 Breeding of mice and genotyping PCR conditions

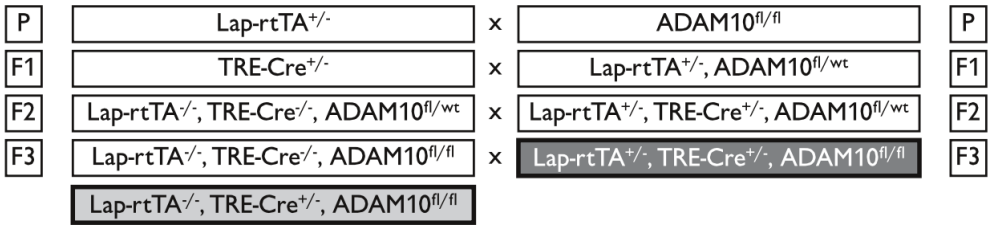

Supplementary Figure 1: Breeding schematic for doxycycline-inducible conditional ADAM10 knockout in hepatocytes.

Genotypes used in experiments are marked by a thick black frame. Color schemes are equivalent to the ones used in bar charts for the respective genotype.

P: parental generation; F1: first generation (progeny of P); F2: second generation (progeny of F1); F3: third generation (progeny of F2)

Supplementary Table 6. rtTA PCR conditions

Step	Temperature	Time	Cycles
Initial Denaturation	95°C	2'	1
Denaturation	95°C	30''	30
Annealing	58°C	30''	
Elongation	72°C	1'	
Final Elongation	72°C	10'	1
Storage	4°C	∞	1

For detailed information on genotyping primers please refer to Supplementary Table 3

6.1.2.2 Doxycycline administration

Doxycycline was added to regular lab chow at a concentration of 1 g/kg (Ssniff, Soest, Germany). Mice were fed ad libitum. Considering that doxycycline is photosensitive, chow was changed two times per week to ensure a constant dosage of doxycycline. Mice were sacrificed after at least 4 week of doxycycline administration.

6.1.2.3 Generation of stable cell lines

HEK293T cells were transfected with plasmids encoding for doxycycline-inducible tetraspanins (Tspan8, CD9, and CD81, see Supplementary Table 6) as well as a puromycine resistance as described in 6.1.2.4. Cells were selected for plasmid uptake by culturing them in the presence of 2 µg/ml puromycine. Cells were tested for tetraspanin expression in the presence and absence of 80 µg/ml doxycycline by immunoblotting of cell lysates.

6.1.2.4 *Luciferase complementation assay*

Luciferase complementation assay was performed as described previously [149]. Briefly, HEK293T cells were seeded at a density of $1x10^5$ cells/ml in 500 µl/well of a 24-well plate. The following day, cells were transfected with plasmid DNA at a ratio of 1:3 to the transfection agent Polyethylenimine. Cells always received a combination of two plasmids, one coding for the C-terminal part of *Gaussia princeps* luciferase and one coding for the N-terminal part of *Gaussia princeps* luciferase, each fused to a protein of interest or as an empty control. On the second day after transfection, cells were washed, lysed in 100 µl passive lysis buffer (#E1941, Promega, Mannheim, Germany) for 15 min at RT, and then transferred, in triplicates of 20 µl each, to a white 96-well bioluminescence plate. Bioluminescence was detected using a Glomax plate injector system (Promega, Mannheim, Germany) by dispensing 50 µl substrate[17] per well and measuring luminescence for ten seconds after a two second premeasurement delay.

Normalized luciferase ratio (NLR) and standard deviation of NLR were calculated as follows:

$$GOI = GOI1\text{-}pSPICA\text{-}C1/GOI2\text{-}pSPICA\text{-}C2$$

$$C1 = GOI1\text{-}pSPICA\text{-}C1/pSPICA\text{-}C2$$

$$C2 = pSPICA\text{-}C1/GOI2\text{-}pSPICA\text{-}C2$$

$$NLR = \frac{GOI}{C1+C2}$$

$$\sigma NLR = \sqrt{\left(\frac{\delta NLR}{\delta GOI}*\sigma GOI\right)^2+\left(\frac{\delta NLR}{\delta C1}*\sigma C1\right)^2+\left(\frac{\delta NLR}{\delta C2}*\sigma C2\right)^2}$$

$$= \sqrt{\left(\frac{1}{C1+C2}*\sigma GOI\right)^2+\left(\frac{GOI}{(C1+C2)^2}*\sigma C1\right)^2+\left(\frac{GOI}{(C1+C2)^2}*\sigma C2\right)^2}$$

$\frac{\delta NLR}{\delta x}$ = partial derivative of the NLR equation with respect to GOI, C1 or C2, respectively

σGOI; σC1; σC2: standard deviation of GOI, C1 or C2, respectively

A NLR above 3.5 was considered a specific interaction.

6.1.2.5 *Alkaline phosphatase-shedding assay*

Shedding of alkaline phosphatase (AP)-tagged substrates was carried out as specified by Inoue et al [150]. In short, the in 6.1.2.3 described cell lines or parental HEK293T cells

17 2.36 µM Coelenterazine (diluted in PBS)

were treated with doxycycline and transiently transfected with plasmids encoding for AP-tagged ADAM17 substrates (TGFα, TNFα, IL-6R, and IL-1R2). Cells were then stimulated with phorbol 12-myristate 13-acetate (PMA) to induce ectodomain shedding. In a variation of the experimental setup histamine-stimulated shedding was investigated. To this end cells were additionally transiently transfected with the histamine H_1 receptor and were stimulated with histamine instead of PMA. AP-activity in the cells and in the supernatant was measured by conversion of colorless *para*-nitrophenolphosphate substrate to yellow *para*-nitrophenol directly after substrate addition and one hour after substrate addition. To determine the relative amount of shed AP-substrate in comparison to the unstimulated controls (AP-release) the following calculations were used:

$$\Delta OD405 = OD405_{1h} - OD405_{0h}$$

$$\text{AP-Substrate in conditioned media (CM) (\%)} = \frac{\Delta OD405\ CM}{\Delta OD405\ CM + \Delta OD405\ Cell}$$

AP-release (%) = AP-Substrate in CM under stimulated conditions - AP-Substrate in CM under vehicle-stimulated conditions

For a schematic of the experimental setting please refer to Supplementary Figure 5 A+B and Supplementary Figure 6 A.

6.1.2.6 Generation of inserts for cloning

cDNAs for the proteins of interest were amplified by PCR from template plasmids or from cellular cDNA using the primers indicated in Supplementary Table 1. PCR mix was prepared as follows:

50 ng	template DNA
10 µl	5x HF or GC Buffer
1 µl	dNTPs (10 mM)
1.5 µl	5' Primer (10 µM)
1.5 µl	3' Primer (10 µM)
0.5 µl	Phusion Hot Start II Polymerase
	adjust to 50 µl with ddH_2O

For amplification by PCR a two step protocol was chosen:

Supplementary Table 7. PCR conditions for cloning			
Step	Temperature	Time	Cycles
Initial Denaturation	98°C	5'	1
Initial Annealing	see Supplementary Table 1	20"	1
Initial Elongation	72°C	25" – 90"	1
Denaturation	98°C	20"	30
Elongation	72°C	25" – 90"	
Final Elongation	72°C	3'	1
Storage	4°C	∞	1

PCR products were purified before being subjected to restriction digestion.

6.1.2.7 Purification of DNA fragments

PCR products were loaded on SafeRed (iNtRON Biotechnologies,distributed by HISS diagnostics, Freiburg, Germany) supplemented agarose gels[18] and separated in an electric field. The according DNA bands were excised with a scalpel under UV light and transferred to a 1.5 ml tube. Per 100 mg gel 400 µl GMII[19] was added and per µg DNA 5 µl GMI[20], but at least 15 µl GMI. Samples were incubated at 50°C under constant agitation until the gel was dissolved. After centrifugating for 1 min at 13 000 rpm, supernatant was discarded, the pellet was washed twice in GMIII[21] , and dried at 37°C for at least 10-15 min. DNA was resuspended in TE-Buffer[22] at 55°C and transferred to a fresh tube.

6.1.2.8 DNA digestion of vector and PCR product

Vector and PCR product were digested with the same restriction enzymes (listed in Supplementary Table 8 and Supplementary Table 9, all enzymes were from ThermoScientific except SbfI (NEB)) at the according temperature for 1 h. The reaction was stopped by incubating the samples for 20 min at 65°C. PCR products were then purified as described in 6.1.2.7. Vectors were directly used for Ligation.

6.1.2.9 Annealing and phosphorylation of oligonucleotides

Oligonucleotides were annealed in NEBuffer 4 by incubation at 95°C for 5 min and then slowly cooling the samples down to 4°C. Afterwards oligonucleotides were phosphorylated for 30 min at 37°C in T4 ligasebuffer using Polynucleotide Kinase (ThermoS-

18 Agarose-gel: 1-2.5% agarose, 40mM Tris, 1,14% acidic acid, 1 mM EDTA; add 0.05% SafeRed
19 GMII: 6 M guanidinium thiocyanate, 0.1 M Tris-HCl, 44 mM EDTA, 2.6% Triton X-100
20 GMI: 5 g diatomaceous earth; adjust volume to 25 ml with ddH_2O and add 25 µl HCl (37%)
21 GMIII: 0.1 NaCl, 10 mM Tris, 2.5 mM EDTA, 50% EtOH
22 TE-Buffer: 5 mM Tris, 0.1 mM EDTA

cientific, Darmstadt, Germany). The reaction was stopped by heating the samples to 70°C for 10 min.

6.1.2.10 Ligation of DNA

Purified, digested PCR products or oligonucleotides were ligated into digested vector DNA with T4 DNA Ligase (ThermoScientific, Darmstadt, Germany) according to the manufacturer's instructions.

Amount of used insert (3-times excess over vector) per 100 ng vector was calculated as follows:

$$\frac{\text{kb Insert}}{\text{kb vector}} * 100\,\text{ng} * 3 \quad = \text{x ng Insert}$$

Supplementary Table 8. Conventional plasmids			
Vector backbone	Insert	Restriction Sites	Specifications
pTRIPZ	hTspan8-myc	AgeI/MluI	Doxycycline-inducible, 3' myc-tag
pTRIPZ	hCD9-3xHA	AgeI/SbfI/MluI	Doxycycline-inducible, 3' 3xHA-tag
pTRIPZ	hCD81-3xHA	AgeI/SbfI/MluI	Doxycycline-inducible, 3' 3xHA-tag

Plasmids encoding for AP-TGFα, TNFα-AP, AP-IL-6R, and AP-IL-1R2 were kind gifts of D. Floss and I. Lorenzen (University Kiel, Germany).

6.1.2.11 Homologous recombination (Gateway® cloning)

Previously generated Entry-Vectors, containing attL sites, and Destination-Vectors, containing attR sites, were incubated for 1 hour with LR Clonase® II (life technologies, Darmstadt, Germany) at 25°C. The reaction was stopped by adding proteinase K, incubated for 10 min at 37°C, and was then ready-to-use for bacterial transformation. Used Entry-Vectors and Final Vectors are listed in Supplementary Table 9 and Supplementary Table 10, respectively.

Supplementary Table 9. Gateway Entry-Vectors		
Vector backbone	Insert	Restriction Sites
pENTR4	hADAM10	SalI/NotI
pENTR4	hADAM17	NotI/SalI (compatible to XhoI cleavage site)
pENTR4	hCD9	NotI/XhoI
pENTR4	hCD81	NotI/XhoI

Supplementary Table 10. Gateway Final-Vectors		
Destination Vector	Insert	Specifications
pSPICA-C1	hADAM10	3'-fused to *G. princeps* luciferase part 1
pSPICA-C2	hADAM10	3'-fused to *G. princeps* luciferase part 1
pSPICA-C1	hADAM17	3'-fused to *G. princeps* luciferase part 1
pSPICA-C2	hADAM17	3'-fused to *G. princeps* luciferase part 1
pSPICA-C1	hCD9	3'-fused to *G. princeps* luciferase part 1
pSPICA-C2	hCD9	3'-fused to *G. princeps* luciferase part 1
pSPICA-C1	hCD81	3'-fused to *G. princeps* luciferase part 1
pSPICA-C2	hCD81	3'-fused to *G. princeps* luciferase part 1
pSPICA-C1	hTetraspanin8	3'-fused to *G. princeps* luciferase part 1
pSPICA-C2	hTetraspanin8	3'-fused to *G. princeps* luciferase part 1

pDONR233-Tspan8 as well as the pSPICA-C1 and pSPICA-C2 destination vectors were a kind gift from Y. Jacob (Institute Pasteur, Paris, France).

6.1.2.12 Chemical competent bacteria

Bacteria were grown ON in 2ml LB-Medium[23]. 1 ml of the ON culture was transferred to 150 ml fresh medium and was allowed to grow at 37°C with gentle agitation until an OD_{600} of 0.6 was reached. Bacteria were spun down at 5 000 rpm for 10 min and the pellet was resuspended in 15 ml TSB[24]. Bacteria were kept on ice for 10 min. They were then aliquoted and stored at -80°C.

6.1.2.13 Transformation of bacteria

5 µl of a homologous recombination or of a ligation reaction were added to diluted KCM buffer[25] in a total volume of 50 µl and mixed with 50 µl chemically competent *E.coli* DH5α. The mixture was incubated on ice for 30 min, bacteria were heat-shocked for 1 min at 42°C and then left to sit on ice for 1-2 minutes to close the pores. 500 µl LB-Medium was added to the bacterial suspension. The mix was incubated for 1 hour at 37°C with gentle agitation and plated completely or partially on LB-Agar[26] plates containing the appropriate antibiotics using sterile glass beads. Plates were incubated ON at 37°C.

23 LB-Medium (1l): 10 g Tryptone, 5 g yeast extract, 10 g NaCl; adjust to 1 l with ddH_2O and autoclave
24 TSB: 10 g Tryptone, 5 g yeast extract, 10 g NaCl, 5% DMSO, 10 mM $MgCl_2$, 10 mM $MgSO_4$, 10% PEG 4000; adjust to 1 l with ddH_2O and sterilize by filtration
25 KCM buffer (5x): 0.5M KCl, 0.15 M $CaCl_2$, 0.15 $MgCl_2$
26 LB-Agar: 15 g/l Agar in LB-Medium

6.1.2.14 Amplification of plasmids with CopyCutter™ bacteria

For plasmids coding for ADAM17 and ADAM10, CopyCutter™ bacteria (Epicentre, distributed by Biozym, Hessisch Oldendorf, Germany) were used for plasmid amplification. CopyCutter™ bacteria are designed to amplify a significantly lower copy number of vectors. Copy number can be raised by incubation for a short time in the presence of CopyCutter Induction Solution. This technology allows for the amplification of unstable or toxic DNA sequences.

The first steps were as described in 6.1.2.13. A single colony was picked from the plate and used to inoculate an ON culture in 5 ml LB-medium. Bacteria were then again spread on agar-plates and incubated ON. These bacteria were pooled and used to inoculate a new culture in LB-medium with antibiotics and CopyCutter Induction Solution (Biozym Scientific, Hessisch Oldendorf, Germany) that had a starting OD_{600} of 0.2. Cultures were incubated at 37°C under constant agitation for 4 h and plasmid DNA was then isolated with the Nucleobond® XtraMidi kit (Machery-Nagel, Düren, Germany) according to the manufacturer's instructions.

6.1.2.15 Plasmid isolation

For plasmid isolation a single colony was inoculated in 2 ml antibiotic-supplemented LB-medium and incubated ON at 37°C and constant agitation. Bacteria were pelleted, resuspended in SolutionI[27], and lysed in SolutionII[28]. Lysis was stopped by adding SolutionIII[29], samples were centrifuged, DNA precipitated, washed in 70% EtOH, and dried at RT. DNA was dissolved in TE-Buffer by vortexing.

To receive large amounts of plasmid DNA, 100 ml bacterial cultures were inoculated and plasmid DNA was isolated with the Nucleobond® XtraMidi kit (Machery-Nagel, Düren, Germany) according to the manufacturer's instructions.

6.1.2.16 Quantification of nucleic acids and sequencing

DNA concentrations and purity were analyzed spectrophotometrically by a Nano-Drop photometer (distributed by PeqLab, Erlangen, Germany). Sequencing was performed by GATC Biotech (Constance, Germany) using Sanger-sequencing.

27 Solution I: 50 mM Glucose, 25 mM Tris-HCl, 10 mM EDTA, 60 µg/ml RNaseA
28 Solution II: 0.2 mM NaOH, 1% SDS
29 Solution III: 3 M KAc, 11.5 % acetic acid

6.1.3 Supplementary Figures

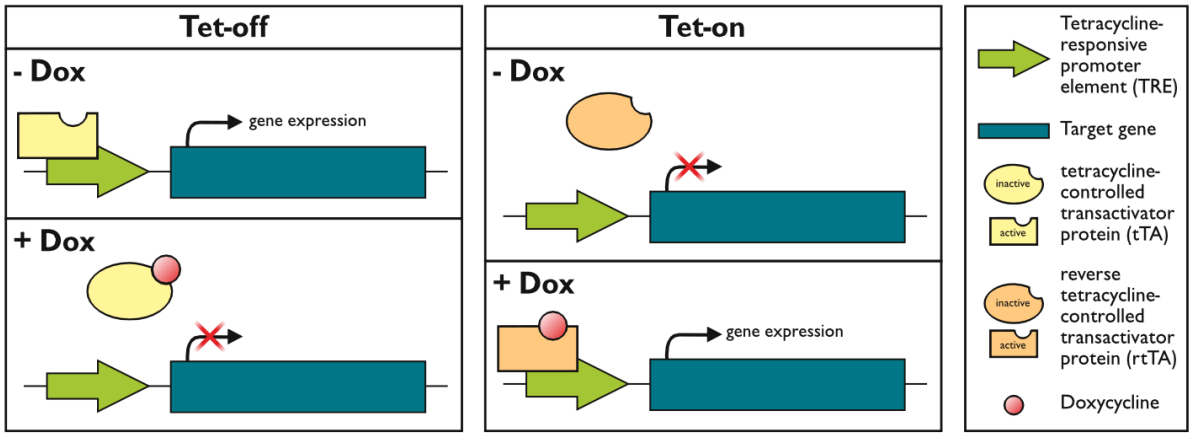

Supplementary Figure 2: Tetracyline regulated Cre system

Schematic of the Tet-off and the Tet-on systems. Expression of the target gene is under the transcriptional control of a tetracycline-responsive promoter element (TRE). The Tet-Off system relies on the activity of a tetracycline-controlled transactivator (tTA) binding to the TRE and activating transcription. In the presence of Tetracycline or doxycycline, a derivative of tetracycline, tTA can not bind and transcription is inactive. Contrary, in the Tet-On system the presence of doxycycline leads to the binding of the reverse tetracycline-controlled transactivator (rtTA) to the TRE and hence transcription of the target gene. The tTA or rtTA expression can be driven by specific promoters to only target select cells or tissues [0]. In our case the target gene under control of the TRE is a Cre-recombinase.

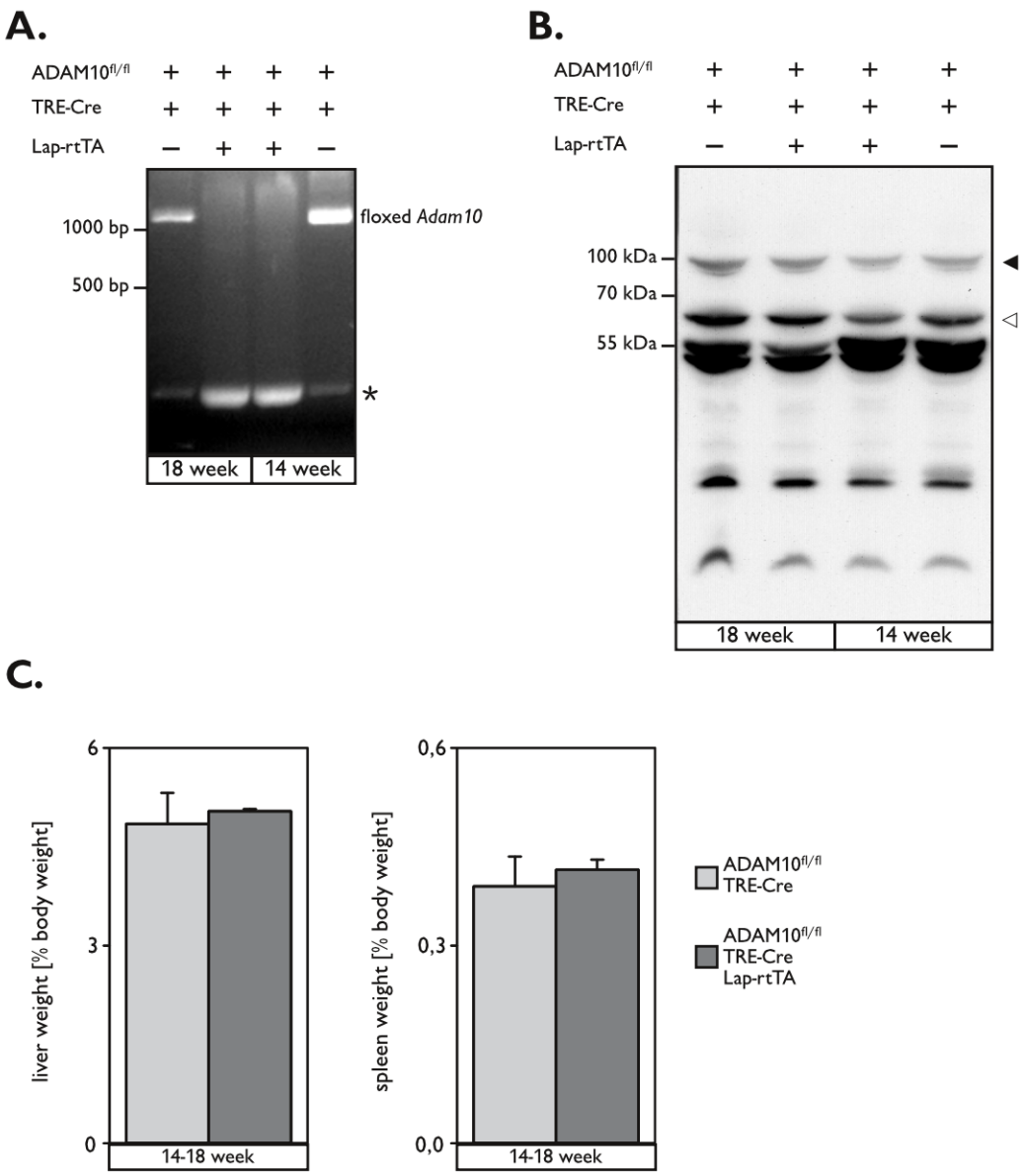

Supplementary Figure 3: No efficient recombination of floxed ADAM10 with the Lap-rtTAxTRE-Cre System

A: Deletion PCR for ADAM10 from genomic DNA from the liver. The band at approximately 2000 bp results from floxed ADAM10. The expected bandsize for ADAM10 that is successfully recombined and therefore has a deletion in Exon2 is between 500 and 750 bp. Asterisk marks low bp band that probably consists of primerdimers. **B:** ADAM10 protein expression does not differ in total liver extracts of ADAM10$^{fl/fl}$ x TRE-Cre mice with or without Lap-rtTA as shown by this Immunoblot. Solid arrowhead marks pro-form of ADAM10. Open arrowhead marks mature form of ADAM10 **C:** Liver weight and spleen weight is not altered in mice carrying the Lap-rtTA transgene compared to their littermate that do not carry that transgene.

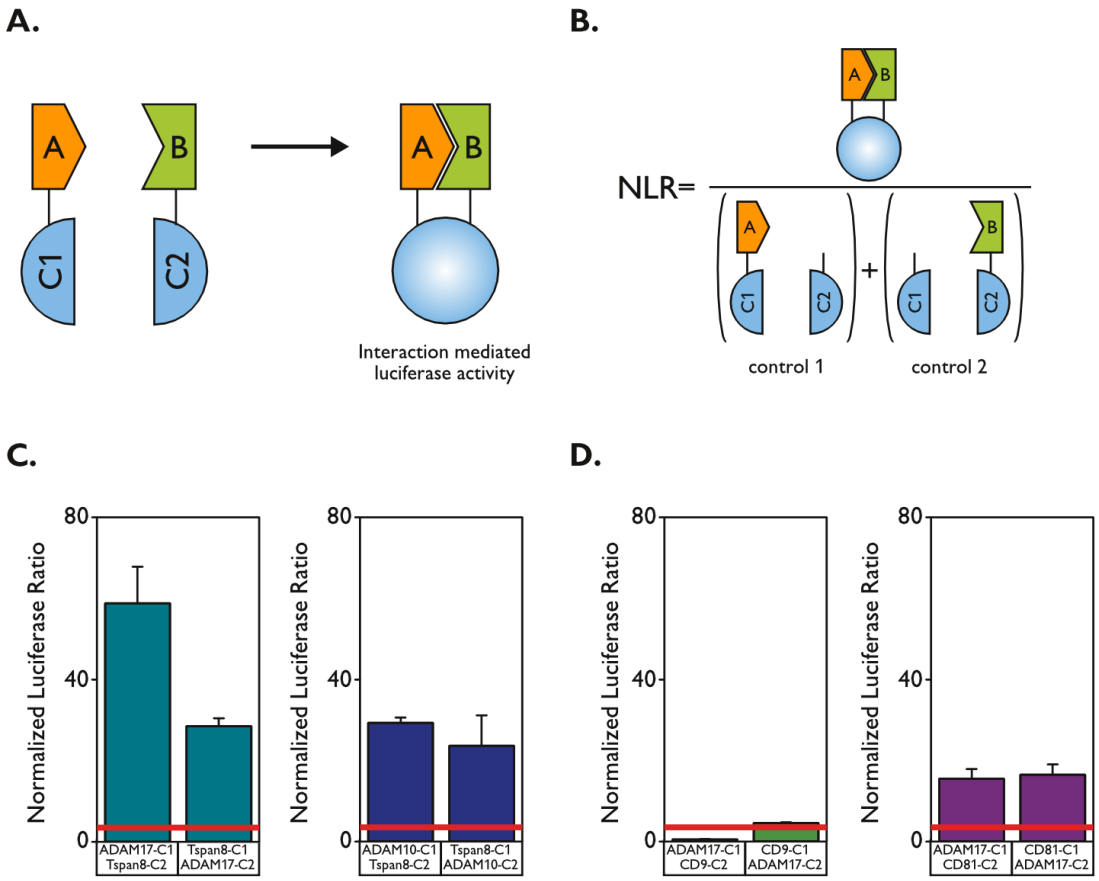

Supplementary Figure 4: Interaction of Tspans and ADAMs

A: Schematic of the luciferase-based protein complementation assay. Both proteins of interest (A+B) are C-terminal tagged with one out of two inactive fragments of *Gaussia princeps* luciferase (C1; C2). If the proteins of interest are in close proximity, the two inactive luciferase fragments can complement each other to a functional enzyme. (modified from [149]) **B:** The normalized luciferase ratio (NLR) for the investigated interaction partners is calculated by dividing the relative light units emitted by cells expressing both proteins of interest by the sum of the luminescence in the controls. (modified from [149]) **C:** Interaction between Tetraspanin8 and the ADAM-family members 10 and 17. The assay was performed with the aforementioned method in Hek293T cells. The depicted results are representative of at least three independent experiments. The default NLR threshold at 3.5 is marked by a red line. (n=3) **D:** Evaluated interaction between Tetraspanins CD9 and CD81 and ADAM17. The assay was performed with the aforementioned method in Hek293T cells. The depicted results are representative of at least three independent experiments. The default NLR threshold at 3.5 is marked by a red line. (n=3)

Data represent the NLR ± standard deviation.

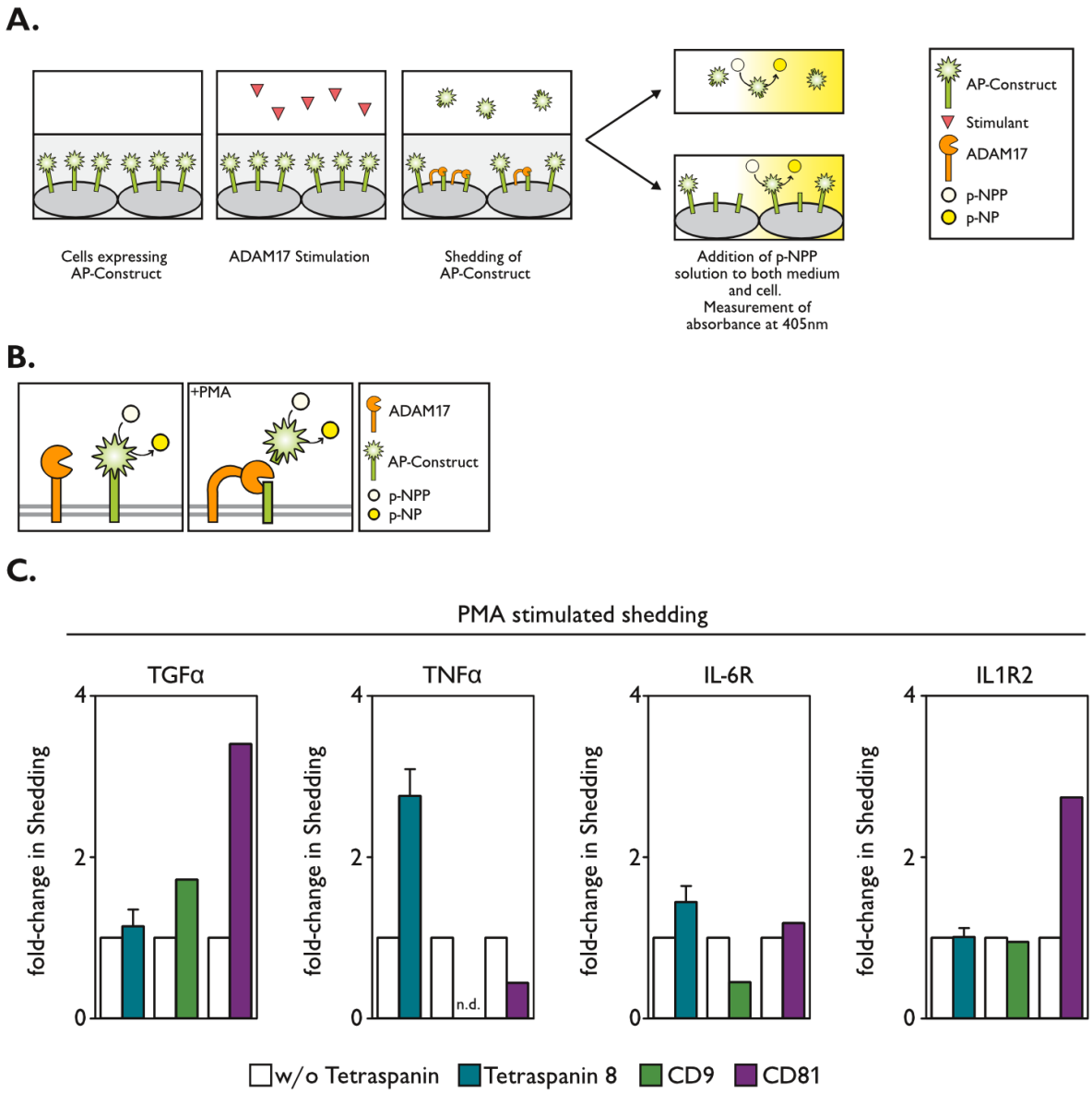

Supplementary Figure 5: Tetraspanins regulate substrate specificity in PMA-stimulated ADAM17-dependent shedding

A: Principle of the alkaline phosphatase (AP)-Shedding assay shown in schematic. Hek293T cells transiently expressing AP-tagged substrates of ADAM17 are stimulated by agents that induce ectodomain shedding by ADAM17. The AP-tagged extracellular domain of the substrate is hence released to the supernatant. Shedding can be quantified by colorimetric measurement of AP activity in the conditioned medium as well as in the remaining cells based on the AP-dependent conversion of *para*-Nitrophenolphosphate (*p*-NPP) to yellow *para*-Nitrophenol (*p*-NP). The relative amount of shed substrate is calculated by dividing the measured absorbance in the conditioned medium by the sum of the measured absorbance in the conditioned medium and the cells. (modified from [150]) **B**: Schematic of experimental setup used in C. Hek293T cells transiently expressing AP-tagged ADAM17 substrates were stimulated with PMA to induces ADAM17-dependent shedding. **C**: Fold change in PMA stimulated shedding in cells expressing specified Tetraspanins compared to cells not expressing these specified Tetraspanins. Values were beforehand normalized to unstimulated cells to account for constitutive shedding. (n.d. = not detected) (n=1-3)

Data represent the mean ± standard error of the mean.

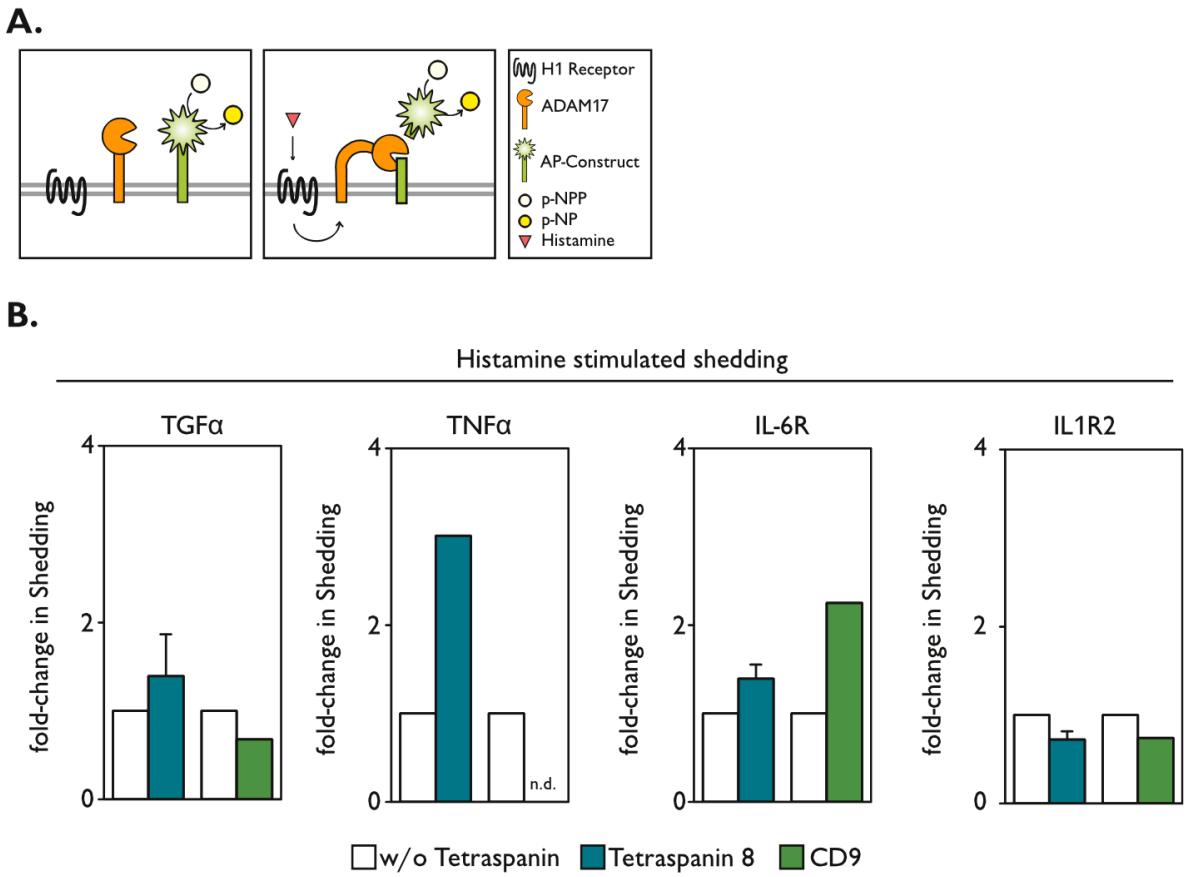

Supplementary Figure 6: Tetraspanins regulate substrate specificity in histamine-stimulated ADAM17-dependent shedding

A: Schematic of experimental setup used in B. Hek293T cells transiently expressing AP-tagged ADAM17 substrates and the Histamine H_1 Receptor were stimulated with Histamine to induces ADAM17-dependent shedding. **B**: Fold change in Histamine stimulated shedding in cells expressing specified Tetraspanins compared to cells not expressing these specified Tetraspanins. Values were beforehand normalized to unstimulated cells to account for constitutive shedding. (n.d. = not detected) (n=1-3)

Data represent the mean ± standard error of the mean.

6.2 Abbreviations

For this work the guidelines and general rules of the International System of Units were adhered to, including the rule that spaces should be used as a thousands separator.

°C	Degree celsius
aa	Amino acid
ADAM	A disintegrin and metalloprotease
ALT	Alanine transaminase
AP	Alkaline Phosphatase
APS	Ammonium persulfate
BMOL	Bipotential murine oval cell line
bp	Basepairs
BSA	Bovine serum albumin
CCL2	Chemokine (C-C motif) ligand 2
CD	Cluster of differentiation
CDE	Choline-deficient, ethionine enriched
cDNA	Complementary deoxyribonucleic acid
CK19	Cytokeratin 19
CM	Conditioned medium
CXCL	(C-X-C- motif) ligand
Cxcr4/7	C-X-C chemokine receptor type 4/7
DMEM	Dulbecco's modified eagle medium
DMSO	Dimethylsulfoxide
DNA	Deoxyribonucleic acid
dNTP	Deoxy nucleoside triphosphate
e	Embryonic day of gestation
ECM	Extracellular matrix
EDTA	Ethylenediaminetetraacetic acid
EGF	Epidermal growth factor
EGFR	Epidermal growth factor receptor
ELISA	Enzyme-linked Immunosorbent Assay
ER	Estrogen receptor
ERK	Extracellular-signal-regulated kinase
EYFP	Enhanced yellow fluorescent protein
FCS	Fetal calf serum
FITC	Fluorescein isothiocyanate
g	Gram
GFP	Green fluorescent protein
h	Hours

H&E	Hematoxylin and Eosin
HGF	Hepatocyte growth factor
HRP	Horseradish peroxidase
HSC	Hepatic stellate cells
ICD	Intracellular domain
iCLIP	Intramembrane-cleaving protease
IGF-II	Insulin-like growth factor-II
IL	Interleukin
IL-1R2	Interleukin-1 receptor 2
IL-1RA	Interleukin-1 receptor antagonist
IL-6	Interleukin-6
IL-6R	Interleukin-6 receptor
IκB	Inhibitor of κB
kDa	kilo Dalton
kg	kilogram
KO	Knock-out
l	Liter
Lap	Liver activator protein
Lgr	Leucine-rich repeat-containing G-protein coupled receptor
LPC	Liver progenitor cell
M	molar
mg	Milligram
min	Minutes
ml	Milliliter
mM	Millimolar
mm	Millimeter
MMP	Matrix metalloproteinase
mRNA	Messenger ribonucleic acid
Mrp2	Multidrug resistence-associated protein 2
MT1-MMP	Membrane type 1 matrix metalloprotease
MTT	3-(4,5-dimethythiazol-2-yl)-2,5-diphenyltetrazolium bromide
NFκB	Nuclear factor κB
NLR	Normalized Luciferase Ratio
nm	Nanometer
OD	Optical density
ON	Over night
p-NP	*para*-Nitrophenol
p-NPP	*para*-Nitrophenolphosphate
panCK	panCytokeratin

PAS	Periodic-acid-Schiff stain
PBS	Phosphate buffer saline
PCR	Polymerase Chain Reaction
PKC	Protein kinase C
PMA	Phorbol 12-myristate 13-acetate
PMSF	Phenylmethylsulfonylfluorid
qRT-PCR	quantitative real-time polymerase chain reaction
RFP	Red fluorescent protein
RH	Relative humidity
RIP	Regulated intramembrane proteolyis
RNA	Ribonucleic acid
rpm	Revolutions per minute
RT	Room temperature
rtTA	Reverse tetracycline-controlled transactivator
SDS	Sodium dodecyl sulfate
SDS-PAGE	Sodium dodecyl sulfate polyacrylamide gel
sec	Seconds
SEM	Standard error of mean
SN	Supernatant
Spp1	Secreted phosphoprotein 1
TEMED	Tetramethylethylenediamine
TGFα/β	Transforming growth factor α/β
TGFβRI/II	Transforming growth factor β Receptor I/II
TIMP	Tissue inhibitor of metalloprotease
TNF	Tumor necrosis factor
Tnfrsf12a	Tumor necrosis factor receptor superfamily 12a
Tnfsf12	Tumor necrosis factor superfamily 12
TRE	Tetracycline-responsive promoter element
Tspan8	Tetraspanin8
tTA	Tetracycline-controlled transactivator
TWEAK	Tumor necrosis factor-like weak inducer of apoptosis
U	Unit
UPL	Univeral probe library
V	Volt
w/v	weight per volume
WT	Wild type
αSMA	Alpha smooth muscle actin
µg	Microgram
µl	Microliter

µm	Micrometer

6.3 List of Figures

6 Appendix

6.4 List of Tables

6.5 Curriculum Vita

Name:	Miryam Müller
Date of Birth:	20.06.1985
Place of Birth:.	Müllheim (Baden)
Citizenship:	German

Education:

1991 – 1995	Elementary school Reinöhlschule (*now* Grundschule Alt-Böckingen), Heilbronn
1995 – 2004	Abitur Robert-Mayer-Gymnasium, Heilbronn
2005 – 2010	Biology Diploma Karlsruhe Institute of Technology
2010	Diploma Thesis (Biology) Department of Experimental Surgery, University Hospital Heidelberg
2011 – 2015	PhD Student Institute of Biochemistry, Christian-Albrechts-University Kiel

Oral Presentations:

XXXIInd Winter School on Proteinases and their Inhibitors, Tiers am Rosengarten, Italy (2015)
A disintegrin and metalloprotease 10 (ADAM10) is a central regulator of murine liver tissue homeostasis.

CHIRI Seminar, Curtin University Perth, Australia (2015)
A disintegrin and metalloproteases in liver disease

Hepatology and Gastrointestinal Research Workshop, Peppers Craigieburn Bowral, Australia (2015)
A disintegrin and metalloprotease 10 (ADAM10) is a central regulator of murine liver tissue homeostasis

Publications:

Schwarz, J., Broder, C., Helmstetter, A., Schmidt, S., Yan, I., Müller, M., Schmidt-Arras, D., Becker-Pauly, C., Koch-Nolte, F., Mittrücker, H., Rabe, B., Rose-John, S. & Chalaris, A. Short-term TNFα shedding is independent of cytoplasmic phosphorylation or furin cleavage of ADAM17. Biochim. Biophys. Acta 1833, 3355-67 (2013).

Schmidt-Arras, D., Müller, M., Stevanovic, M., Horn, S., Schütt, A., Bergmann, J., Wilkens, R.,

Lickert, A. & Rose-John, S. Oncogenic deletion mutants of gp130 signal from intracellular compartments. J. Cell. Sci. 127, 341-53 (2014).

Madhavan, B., Yue, S., Galli, U., Rana, S., Gross, W., Müller, M., Giese, N.A., Kalthoff, H., Becker, T., Büchler, M.W. & Zöller, M. Combined evaluation of a panel of protein and miRNA serum-exosome biomarkers for pancreatic cancer diagnosis increases sensitivity and specificity. Int. J. Cancer 136, 2616-27 (2015).

Müller, M.*, Wetzel, S.*, Köhn, J., Chalupsky, K., Lüllmann-Rauch, R., Barikbin, R., Bergmann, J., Wöhner, B., Zbodakova, O., Leuschner, I. Martin, G., Tiegs, G., Rose-John, S., Sedlacek, R., Tirnitz-Parker, J.E.E., Saftig, P. & Schmidt-Arras, D. A disintegrin and metalloprotease 10 (ADAM10) regulates murine liver progenitor cell activation. *Manuscript submitted*
* Authors contributed equally

6.6 Acknowledgments

First and foremost, I want to thank Dirk for being the best supervisor anyone could hope for. Thank you for letting me grow at my own pace, for being there every step of the PhD-journey in just the way I needed at that moment, for the support and encouragement, and for always having my back. Alles richtig gemacht!

My thanks also goes to Stefan Rose-John for welcoming me at his Institute, for taking on official supervising duties, as well as for the discussions and his input to my work.

Sincere thanks to Thomas Röder for agreeing to be co-reviewer of this thesis.

Thank you Sebastian, for sharing not only the ADAM10 project but also for becoming friends. It wouldn't have been half as fun without you.

Thanks to Paul Saftig for the discussions and the input on the ADAM10 project.

A huge thank you to Elsbeth Schulz for doing all the histological stainings.

To Nina Tirnitz-Parker and Julia Köhn in Australia, thank you for the support with the LPCs, sharing methods and for the warm welcome in your lab. Thanks also to Jully and Frankie. I enjoyed being your “honorary lab member”.

Thanks to Roja Barikbin and Gisa Tiegs in Hamburg for welcoming me in their lab and sharing methods.

Many thanks to Renate Lüllmann-Rauch for the beautiful electron micrographs.

Thanks to Karel Chalupsky and Radislav Sedlacek in Prague for the fruitful cooperation.

I am grateful to the SFB841 and the GRK for funding of the project. Special thanks to Andrea Pfannkuch and Karin Hansen for help with the administrative side.

Many thanks to the staff at the VHH, especially Marika Eschke, for taking such good care of our mice. Also, thank you to the mice.

Thanks to all my favourite bands for providing the soundtrack for my life.

A big thank you to all the people at the Institute for the open and welcoming atmosphere, especially to Petra for her help with all the administrative obstacles and to Steffi for sharing Freezer duty.

I want to thank the whole AG Schmidt-Arras and all our visiting students (in no particular order: Silke, Julia, Juri, Graziella, Marija, Antje, Annett, Colin, Manni, Hanno, Hanna, Lisa, Olivia, Rob, Christopher, Lasse, Birte) for the good times, the supply with self-grown or self-baked goods, for the encouragement and support when things didn't go as planned, for the nice lunches including all the discussions, and for lots of entertainment.

Last but not least I want to thank my family and friends for providing a balance to all the work. Most of all my parents for the constant support and the travels, both literary and literally.